

AD-A253 358



DTIC  
ELECTE  
JUL 30 1992  
S C D

2


**D-<sup>3</sup>HE SPHERICAL TORUS  
FUSION REACTOR SYSTEM STUDY**

By

CPT William A. Macon, Jr., U.S. Army

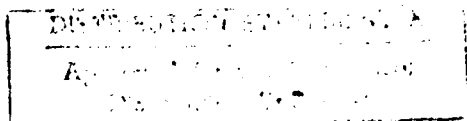
A Thesis Submitted to the Graduate  
Faculty of Rensselaer Polytechnic Institute  
in Partial Fulfillment of the  
Requirements for the Degree of  
MASTER OF SCIENCE

Approved:

  
Don Steiner  
Thesis Adviser

Rensselaer Polytechnic Institute  
Troy, New York

April 1992  
(For Graduation May 1992)



92 7 25 035

92-20521



April 1992

Master of Science Thesis

D-He3 Spherical Torus Fusion Reactor System Study

CPT William A. Macon, Jr., US Army

US Army Student Detachment  
Fort Benjamin Harrison, IN 46216

Thesis submitted to the Graduate Faculty of Rensselaer Polytechnic Institute in  
Partial Fulfillment of the Requirements of Master of Science in Nuclear Engineering

Approved for public release; Distribution is unlimited.

This system study extrapolates present physics knowledge and technology to predict the anticipated characteristics of D-He3 spherical torus fusion reactors and their sensitivity to uncertainties in important parameters. Reference cases for steady-state 1000 MWe reactors operating in H-mode in both the 1st stability regime and the 2nd stability regime were developed and assessed quantitatively. These devices would have a very small aspect ratio ( $A=1.2$ ), a major radius of about 2.0 m, an on-axis magnetic field less than 2 T, a large plasma current (80-120 MA) dominated by the bootstrap effect, and high plasma beta ( $>0.6$ ). The estimated cost of electricity is in the range of 60-90 mills/kW-hr, assuming the use of a direct energy conversion system. The inherent safety and environmental advantages of D-He3 fusion indicate that this reactor concept could be competitive with advanced fission breeder reactors and large-scale solar electric plants by the end of the 21st century if research and development can produce the anticipated physics and technology advances.

Nuclear Science and Technology, Fusion Energy

127

UNCLASSIFIED

UNCLASSIFIED

UNCLASSIFIED

UL

AMERICAN MEDICAL ASSOCIATION  
PUBLISHED WEEKLY  
CHICAGO, ILL., U.S.A.

VOLUME 10  
NUMBER 1  
JANUARY, 1917

CONTENTS

ORIGINAL ARTICLES

1

2

3

4

5

6

7

8

9

10

11

12

13

14

15

16

17

18

19

20

21

22

23

24

25

26

27

28

29

30

## CONTENTS

LIST OF TABLES . . . . .	v
LIST OF FIGURES . . . . .	vi
ACKNOWLEDGEMENT . . . . .	ix
ABSTRACT . . . . .	x
1. Introduction and Historical Review . . . . .	1
1.1 Thesis Objectives . . . . .	1
1.2 D- <sup>3</sup> He Fusion . . . . .	2
1.3 Tokamak Fusion Reactors . . . . .	5
1.4 Spherical Torus Fusion Reactor . . . . .	8
1.5 D- <sup>3</sup> He ST Fusion Reactor . . . . .	9
1.6 Thesis Outline . . . . .	11
2. Spherical Torus Reactor Analysis Code (STORAC) and Assumptions . . . . .	16
2.1 Introduction . . . . .	16
2.2 Review of Original Code . . . . .	16
2.2.1 Architecture of STORAC . . . . .	16
2.2.2 D-T ST Model . . . . .	17
2.2.3 Constraint Equations and Variables . . . . .	19
2.2.4 Summary . . . . .	21
2.3 STORAC Modifications . . . . .	21
2.3.1 D- <sup>3</sup> He ST Model . . . . .	21
2.3.2 Code Revisions . . . . .	22
2.3.3 Summary . . . . .	24
2.4 Assumptions Made for this System Study . . . . .	25
2.4.1 Introduction . . . . .	25
2.4.2 Discussion of Variables . . . . .	26
2.4.3 Discussion of Fixed Parameters . . . . .	28
2.4.4 Summary . . . . .	31

3. Results of D- <sup>3</sup> He ST Reactor Study . . . . .	32
3.1 Introduction . . . . .	32
3.2 1st and 2nd Stability Regime Reference Cases . . . . .	32
3.2.1 Initial Results . . . . .	32
3.2.2 Variation of Edge Safety Factor . . . . .	34
3.2.3 Reference Cases Used for the Study . . . . .	35
3.3 Variation of $\epsilon\beta_p$ . . . . .	36
3.4 Variation of Density and Temperature Profile . . . . .	37
3.5 Variation of the Fuel Ratio . . . . .	38
3.6 Variation of Confinement Time Ratio, $\tau_p/\tau_E$ . . . . .	39
3.7 Variation of Confinement H-factor . . . . .	39
3.8 Variation of Bootstrap Current Fraction . . . . .	40
3.9 Variation of Aspect Ratio . . . . .	40
3.10 Variation of Centerpost Current Density . . . . .	41
3.11 Variation of Thermal Conversion Efficiency . . . . .	42
3.12 Variation of Direct Energy Conversion Efficiency . . . . .	42
3.13 Summary . . . . .	42
4. Discussion and Conclusions . . . . .	67
4.1 Introduction . . . . .	67
4.2 Economic Characteristics . . . . .	68
4.3 Safety and Environmental Characteristics . . . . .	69
4.3.1 Risk of Major Releases of Radioactivity . . . . .	69
4.3.2 Radioactive Waste Burden . . . . .	70
4.3.3 Exposures to Radiation . . . . .	71
4.3.4 Nuclear Weapons Link . . . . .	72
4.4 Conclusion . . . . .	72
APPENDICES . . . . .	75
A. Spherical Torus Physics Model . . . . .	75
A.1 Introduction . . . . .	75
A.2 Plasma Shape and Geometry . . . . .	75
A.3 Plasma Current . . . . .	77

A.4 Bootstrap Current . . . . .	78
A.5 Profile Effects . . . . .	80
A.6 Steady-State Particle Balance . . . . .	82
A.7 Density Limit . . . . .	87
A.8 Beta Limit . . . . .	87
A.9 Global Plasma Power Balance Equations . . . . .	89
B. Reference Cases ST-1B and ST-2B . . . . .	94
C. Edge Safety Factor Scan of ST-2A . . . . .	103
LITERATURE CITED . . . . .	115

DTIC QUALITY INSPECTED 2

Accession For	
DTIC GRAAI	<input checked="" type="checkbox"/>
DTIC TAB	<input type="checkbox"/>
Unannounced	<input type="checkbox"/>
Justification	
By	
Distribution/	
Availability Codes	
Dist	Avail and/or Special
A-1	

## LIST OF TABLES

3.1	Key parameters of the 1st Stability ST, 2nd Stability ST and ARIES-III 2nd Stability Tokamak . . . . .	44
3.2	Key parameters of the 1st Stability ST and 2nd Stability ST reference cases . . . . .	49

## LIST OF FIGURES

1.1	Schematic of a tokamak . . . . .	12
1.2	The JET device. (1) Vacuum vessel (double walled). (2) Material limiter defining the outer plasma edge. (3) Poloidal protective shields to prevent the plasma touching the vessel. (4) Toroidal field magnet of 32 D-shaped coils. (5) Mechanical structure. (6) Outer poloidal field coils. (7) Inner poloidal field coils (primary or magnetizing windings). (8) Iron magnetic circuit (core and eight return sections). (9) Water and electrical connections for the toroidal field coils. (10) Vertical and radial ports in the vacuum vessel for plasma heating systems and diagnostics. . . . .	13
1.3	Plasma cross-sectional shape showing major radius $R$ , horizontal minor radius $a$ , vertical minor radius $b$ , triangularity $\delta = c/a$ , and indentation $d/2a$ . The closed lines depict magnetic flux surfaces. . . . .	14
1.4	Basic ST design configuration, showing unshielded center conductor post and double-null poloidal divertors. . . . .	15
2.1	Schematic of poloidal divertor/direct electrodynamic energy conversion system. . . . .	22
3.1	ST-1A Sensitivity to Variation of Edge Safety Factor: $R_0, B_0, I_P$ , and COE versus $q_\psi$ . . . . .	45
3.2	ST-1A Sensitivity to Variation of Edge Safety Factor: $P_{inj}$ , TF Coil Resistive Power, Recirculating Power Fraction, and Total Cost versus $q_\psi$ . . . . .	46
3.3	ST-2A Sensitivity to Variation of Edge Safety Factor: $R_0, B_0, I_P$ , and COE versus $q_\psi$ . . . . .	47
3.4	ST-2A Sensitivity to Variation of Edge Safety Factor: $P_{inj}$ , TF Coil Resistive Power, Recirculating Power Fraction, and Total Cost versus $q_\psi$ . . . . .	48
3.5	ST-2B Sensitivity to Variation of $\epsilon\beta_p$ : $R_0, B_0, I_P$ , and COE versus $\epsilon\beta_p$ . . . . .	50



3.6	ST-2B Sensitivity to Variation of $\epsilon\beta_p$ : $\beta$ , $P_{inj}$ , TF Coil Resistive Power, and Total Cost versus $\epsilon\beta_p$ . . . . .	51
3.7	ST-2B Sensitivity to Variation of Density and Temperature Profile: $R_0$ , $B_0$ , $I_P$ , and COE versus $\alpha_n$ (where $\alpha_T = 1.5 - \alpha_n$ ) . . . . .	52
3.8	ST-2B Sensitivity to Variation of Density and Temperature Profile: $\langle n_e \rangle$ , $\langle T_e \rangle$ , Recirculating Power Fraction, and Total Cost versus $\alpha_n$ (where $\alpha_T = 1.5 - \alpha_n$ ) . . . . .	53
3.9	ST-2B Sensitivity to Variation of Effective Fuel Ratio: $R_0$ , $B_0$ , $I_P$ , and COE versus $n_3/n_D$ . . . . .	54
3.10	ST-2B Sensitivity to Variation of Effective Fuel Ratio: $\langle n_e \rangle$ , $P_F$ , Neutron Wall Load, and Total Cost versus $n_3/n_D$ . . . . .	55
3.11	ST-2B Sensitivity to Variation of Confinement Time Ratio: $R_0$ , $B_0$ , $I_P$ , and COE versus $\tau_p/\tau_E$ . . . . .	56
3.12	ST-2B Sensitivity to Variation of Confinement H-Factor: $R_0$ , $B_0$ , $I_P$ , and COE versus $f_L$ . . . . .	57
3.13	ST-2B Sensitivity to Variation of Confinement H-Factor: $P_{inj}$ , $\langle T_e \rangle$ , Recirculating Power Fraction, and Total Cost versus $f_L$ . . . . .	58
3.14	ST-2B Sensitivity to Variation of Bootstrap Current Fraction: $R_0$ , $B_0$ , $I_P$ , and COE versus $I_{bs}/I_P$ . . . . .	59
3.15	ST-2B Sensitivity to Variation of Bootstrap Current Fraction: $P_{inj}$ , TF Coil Resistive Power, Recirculating Power Fraction, and Total Cost versus $I_{bs}/I_P$ . . . . .	60
3.16	ST-2B Sensitivity to Variation of Aspect Ratio: $R_0$ , $B_0$ , $I_P$ , and COE versus $R_0/a$ . . . . .	61
3.17	ST-2B Sensitivity to Variation of Aspect Ratio: $\beta$ , TF Coil Resistive Power, Recirculating Power Fraction, and Total Cost versus $R_0/a$ . . . . .	62
3.18	ST-2B Sensitivity to Variation of Centerpost Current Density: $R_0$ , $B_0$ , $I_P$ , and COE versus $J_{cp}$ . . . . .	63
3.19	ST-2B Sensitivity to Variation of Centerpost Current Density: $\beta$ , TF Coil Resistive Power, Recirculating Power Fraction, and Total Cost versus $J_{cp}$ . . . . .	64
3.20	ST-2B Sensitivity to Variation of Thermal Conversion Efficiency: $R_0$ , $B_0$ , $I_P$ , and COE versus $\eta_{th}$ . . . . .	65

3.21	ST-2B Sensitivity to Variation of Direct Energy Conversion Efficiency: $R_0$ , $B_0$ , $I_P$ , and COE versus $\eta_{dec}$ . . . . .	66
------	---	----

## ACKNOWLEDGEMENT

The author wishes to express his gratitude to Don Steiner for the guidance and encouragement received under his supervision. Special thanks are also extended to Martin Peng (Oak Ridge National Laboratory, ORNL) and John Galambos (ORNL) for the technical background and assistance necessary to complete this research, and to Paul Shipe (ORNL) for preparing the plots used in this study. The opportunity to conduct a fusion reactor system study of this scope, which required visits to Oak Ridge and extensive use of a Cray supercomputer, is gratefully acknowledged. Finally, the author is especially grateful to his wife, Dale, for her patience and support during the past two years at Rensselaer Polytechnic Institute.

This research has been sponsored by the Department of Defense and the Department of Energy.

## ABSTRACT

This system study extrapolates present physics knowledge and technology to predict the anticipated characteristics of D-<sup>3</sup>He spherical torus fusion reactors and their sensitivity to uncertainties in important parameters. Reference cases for steady-state 1000 MWe reactors operating in H-mode in both the 1st stability regime and 2nd stability regime were developed and assessed quantitatively. These devices would have a very small aspect ratio ( $A=1.2$ ), a major radius of about 2.0 m, an on-axis magnetic field less than 2 T, a large plasma current (80-120 MA) dominated by the bootstrap effect, and high plasma beta ( $> 0.6$ ). The estimated cost of electricity is in the range of 60-90 mills/kW-hr, assuming the use of a direct energy conversion system. The inherent safety and environmental advantages of D-<sup>3</sup>He fusion indicate that this reactor concept could be competitive with advanced fission breeder reactors and large-scale solar electric plants by the end of the 21st century if research and development can produce the anticipated physics and technology advances.

## CHAPTER 1

### Introduction and Historical Review

#### 1.1 Thesis Objectives

This study investigates the potential of a spherical torus fusion reactor fueled with Deuterium and Helium-3, isotopes of hydrogen and helium, for commercial electric power production. The reactor system study contained in this thesis presupposes that the present knowledge of plasma physics and nuclear fusion technology may be extrapolated to predict the anticipated characteristics of future reactors. The resulting conclusions must be considered speculative because numerous gaps in the physics knowledge and significant technological uncertainties still exist. Nevertheless, the results of this study are extremely useful because they identify critical parameters or assumptions, show which are important physical or technological constraints, and indicate the broad directions in which future research and development should proceed. The inclusion of unit costs allows a quantitative estimate to be made of the economic potential of this fusion reactor concept relative to other energy systems.

The reactor system study presented herein uses parametric investigations to optimize the reactor configuration by allowing a wide range of physical parameters to vary while bounded by physics and engineering constraints. Besides showing sensitivities associated with specific parameters, these studies are valuable in three ways: (1) they evaluate alternative confinement geometries as potential reactor systems, thus aiding the planning of more effective plasma physics research programs; (2) they evaluate the technological and engineering problems involved with the system, thus aiding the planning of more effective fusion technology research programs; and, (3) they evaluate the operational, economic, and environmental advantages of

fusion energy, thus providing justification for more effective fusion research and development programs. An important objective of this reactor study is therefore to quantitatively assess the potential of a D-<sup>3</sup>He spherical torus fusion reactor.

## 1.2 D-<sup>3</sup>He Fusion

Two major motivations for developing fusion energy are the potential to be safer and more environmentally benign than the competition and the potential to secure a virtually unlimited future energy source. For the long term (i.e., 22nd century and beyond), fusion energy systems must demonstrate attractive economic, safety and environmental characteristics comparable with advanced fission breeder reactors and large-scale solar electric plants [1, 2]. Ideally, a purely aneutronic fusion reactor based on the exotic <sup>3</sup>He-<sup>3</sup>He fuel cycle may one day prove to be viable. At present, however, the most promising candidate for an energy source is a nearly aneutronic D-<sup>3</sup>He fusion reactor. Numerous studies of advanced fuel cycles and fusion reactors have been completed [3, 4, 5] and the current ARIES-III study is conducting a detailed analysis of a conceptual D-<sup>3</sup>He fusion reactor based on advanced tokamak parameters [6]. Compared with advanced fission breeder and D-T fusion reactors, a D-<sup>3</sup>He reactor offers substantial advantages which could eventually prove to be competitive.

The most significant advantages of a D-<sup>3</sup>He fuel cycle are reduced neutron activation and tritium handling problems. The basic fusion reaction involved in this fuel cycle is



The important points to note are that both species involved in this reaction are nonradioactive and that 100% of the energy released in this reaction is in the form of nonradioactive charged particles which deposit their energy in the plasma and help maintain the plasma energy balance. This fuel cycle is conditionally aneutronic for

ion temperatures around 50 keV and  $^3\text{He:D}$  fuel ratios greater than 4.0, but this ratio may be too high for plasma ignition and operation. For a more realistic fuel ratio of about 1:1, some neutrons will be produced directly by the  $\text{D(d,n)}^3\text{He}$  reaction and indirectly by the  $\text{D(d,p)T, T(d,n)}^4\text{He}$  and  $\text{D(d,p)T, T(t,2n)}^4\text{He}$  reaction chains, but these account for less than 6% of the total fusion power compared with about 80% for the D-T fuel cycle. The reduced neutron irradiation of the reactor first wall and shield will result in longer component service life and lower activation levels, thus minimizing maintenance problems and shielding requirements. The requirement to produce and store radioactive tritium fuel is eliminated and the net inventory of tritium in the plasma is substantially reduced. This reduces the associated tritium handling problems and reduces the risk of serious accidents involving tritium release.

The disadvantages of the D- $^3\text{He}$  fuel cycle are the significant physics and engineering difficulties which must be overcome to make D- $^3\text{He}$  fusion competitive. Relative to D-T fusion, D- $^3\text{He}$  fusion requires higher operating temperature, better confinement of the plasma, and higher plasma beta. Ignition is an important condition of a self-sustaining fusion reaction, requiring that the charged-particle energy release compensate for the total plasma energy loss (particle and energy transport and radiation losses). Ignition of a D- $^3\text{He}$  plasma in terms of plasma temperature  $T$  (keV), electron density  $n_e$  ( $\text{m}^{-3}$ ), and plasma energy confinement time  $\tau_E$  (s) is optimized at  $Tn_e\tau_E \approx 6 \times 10^{22} \text{keV} \cdot \text{s} \cdot \text{m}^{-3}$  for operating temperature  $T \approx 55$  keV [7]. For D-T ignition, optimization occurs at  $Tn_e\tau_E \approx 3 \times 10^{21} \text{keV} \cdot \text{s} \cdot \text{m}^{-3}$  for operating temperature  $T \approx 15$  keV, substantially lower values which appear to be attainable in the near term. Beta, defined as  $\beta \equiv 2\mu_0 nT/B^2$  (i.e., the ratio of the plasma pressure to the confining magnetic pressure), is an important parameter describing tokamak performance. Beta must be high to make D- $^3\text{He}$  fusion practical since the fusion power density at equivalent beta values is much lower than for D-T [3]. Since power density varies as  $\beta^2$ , higher betas can increase it to be comparable

with D-T. To achieve these conditions and remain economical, however, significant advances in fusion reactor physics and engineering must occur.

An additional obstacle to competitive D- $^3\text{He}$  fusion is that the terrestrial supply of the helium isotope  $^3\text{He}$  is severely limited. While the hydrogen isotope deuterium is found in plentiful supply in nature, terrestrial  $^3\text{He}$  resources are limited to several hundred kilograms. Assuming a consumption rate of about 0.1 kg/MWe-yr, these resources will not sustain long-term commercial power production. Although it may be possible to produce  $^3\text{He}$  as a byproduct in semicatalyzed deuterium fusion reactors [3], in which all the tritium and only part of the  $^3\text{He}$  fuse in the plasma, this method is probably not cost effective. Fortunately, estimates [8] indicate that the regolith of the lunar surface contains about a million tonnes of  $^3\text{He}$  as a result of deposition by the solar wind, and the potential quantity of  $^3\text{He}$  in Jupiter and Saturn is about  $10^{23}$  kilograms. The total energy cost for mining on the moon, degassing, isotropic separation and transportation to earth is estimated [8] to be approximately  $2.4 \times 10^6$  MJ/kg of  $^3\text{He}$ . The thermal energy yield from D- $^3\text{He}$  fusion is about  $6 \times 10^8$  MJ/kg, representing an energy payback of about 250 compared with about 20 for  $^{235}\text{U}$  and about 16 for coal. Although an economic incentive exists, making lunar supplies of  $^3\text{He}$  practical requires a new and expensive industry, dependent upon reliable space travel, a mining operation on the moon and numerous other high-technology advances. Besides the physics and engineering challenges of reaching actual D- $^3\text{He}$  ignition and operation, the supply of  $^3\text{He}$  itself is a significant obstacle to achieving commercial D- $^3\text{He}$  fusion power. Therefore, mining the moon and the outer planets for reactant fuels such as  $^3\text{He}$  would require further investigation as feasible courses of action.



### 1.3 Tokamak Fusion Reactors

The tokamak reactor concept gained recognition at the Novosibirsk Conference in 1968 and since then steady progress has been made toward its development into a viable fusion core for a thermonuclear reactor. Today the tokamak is the most advanced concept for magnetic confinement of a dense, hot plasma. In general, it consists of a toroidal, axisymmetric plasma confined by the combination of a large toroidal magnetic field (typically 5-10 T), a smaller poloidal magnetic field created by a toroidal current (typically 15-25 MA) through the plasma and the superposition of equilibrium and shaping fields created by poloidal field coils external to the plasma. Figure 1.1 shows a schematic of the basic tokamak configuration. The specific position and shape of the plasma cross section is defined by the magnetic fields generated by the poloidal field coils. The solenoidal coil in the center hole of the tokamak functions as a transformer to induce the toroidal current in the plasma. There is a technical limitation to the pulse length, determined by the maximum magnetic flux that can be provided by the transformer action, making the tokamak an inherently pulsed device in the absence of some external current drive mechanism.

The Joint European Torus (JET), the Tokamak Fusion Test Reactor (TFTR) at Princeton, DIII-D in San Diego and JT-60 in Japan are the most advanced operating tokamaks today. The International Thermonuclear Experimental Reactor (ITER) will be the next step in the tokamak program and will build upon the operational experience of these major devices and other tokamak experiments worldwide. These world-class tokamaks are large machines. JET, for example, has a major plasma radius  $R_0=2.96\text{m}$ , a horizontal minor radius  $a=1.25\text{m}$ , and a vertical minor radius  $b=2.10\text{m}$ . Figure 1.2 shows the JET device and identifies its important components, typical of most current tokamaks, and Figure 1.3 shows the basic geometry parameters used to describe tokamak plasmas. The aspect ratio for JET is  $A=2.37$  (an important parameter defined as major radius  $R_0$  divided by minor radius  $a$ ) and

plasma elongation  $\kappa=1.68$  (defined as vertical minor radius  $b$  divided by horizontal minor radius  $a$ ). By comparison, the aspect ratio for TFTR is 2.92, for DIII-D is 3.17 and for JT-60 is 3.0.

Results from tokamak experiments over the past decade have indicated steady-state operation and enhanced confinement of tokamak plasmas may be achievable. Steady-state operation may be possible by noninductive current drive provided by high-energy neutral beam injection (NBI) in the plasma core, radiofrequency electromagnetic waves in the outer regions of the plasma, and bootstrap current (i.e. the current generated by the plasma itself - see A.4) [9, 10]. The advantages of steady-state operation include reduction of thermal fatigue, mechanical fatigue, plasma disruption and reactor down-time. Enhanced confinement of the plasma in the "H-regime" has been obtained in many tokamaks which employ a magnetic separatrix to bound the plasma. A separatrix configuration with a plasma divertor and high magnetic shear at the edge is thought to be highly advantageous for the achievement of high confinement H-mode, which offers improvement over the conventional Goldston L-mode confinement scaling by a factor of two or more [11]. Achieving the H-mode requires a minimum power threshold to be exceeded, resulting in a bifurcation with instantaneous changes occurring in the plasma edge.

For H-mode operation in a separatrix configuration with a poloidal divertor, the effective plasma boundary is defined by the separatrix (also referred to as the plasma X-point). The separatrix surface marks the boundary between the closed magnetic field lines which contain the plasma and the open field lines which leave the vicinity of the plasma and intercept divertor plates. Tokamak plasma turbulence and cross-field transport processes cause the plasma to diffuse across the internal flux surfaces and eventually across the separatrix surface. The plasma then follows the open field lines to actively cooled divertor plates, which absorb the kinetic energy of the impacting plasma particles. The main plasma-wall interaction occurs

at these plates, where the plasma is neutralized and then pumped away through nearby ducts.

Another enhancement of plasma confinement is thought to result from operation in a second stability regime, where higher beta values may be achievable. As the beta values increase, the plasma becomes susceptible to a magnetohydrodynamic (MHD) ballooning instability. Fluid models of these short wavelength, localized instabilities predict that stability is sometimes recovered when the pressure is increased above that corresponding to the first onset of instability. It is theoretically possible to optimize the current profile in such a way that ballooning instabilities are not excited at any beta [11]. It has also been shown numerically that indentation of the small-side major radius may result in stability against these MHD modes even for high beta values and may provide an access path to the second stability regime [12].

Despite the enhancement of reactor performance resulting from steady-state, H-mode operation in the second stability regime, the attainment of beta values and plasma confinement good enough to achieve cost effective D-<sup>3</sup>He fusion may be constrained by a practical lower limit on the aspect ratio for the basic tokamak. The conventional wisdom of tokamak operation and prudent engineering suggests the inclusion of a solenoid for current-drive start-up, thick nuclear shields inboard to the plasma for the protection of superconducting magnet coils and insulators, and a separate first wall and vacuum boundary. These factors limit the major radius and aspect ratio, which leads to modest values of plasma beta (typically around 5-10% for aspect ratios of around 3, and perhaps greater than 20% in the 2nd stability regime) and require high on-axis toroidal magnetic fields for plasma confinement [13]. Plasma beta limits and confinement may be enhanced with high plasma elongation [14], but to achieve plasma elongation of even 1.6 with mild triangularity for tokamaks with  $A \sim 3$ , large external shaping fields (quadrupole and hexapole fields)

are required [15]. The high capital cost, complexity, and maintenance problems associated with a large fusion power core and superconducting magnets would tend to make the conventional tokamak reactor design an unlikely concept for practical D-<sup>3</sup>He fusion.

#### 1.4 Spherical Torus Fusion Reactor

Reactor studies conducted at Oak Ridge National Laboratory in 1985 indicate performance improvements for tokamaks with very low aspect ratio operating at low on-axis magnetic field. Plasmas with a very low aspect ratio ( $A < 2$ ) display a naturally elongated ( $\kappa > 2$ ) D-shaped plasma cross section, high toroidal beta ( $\beta > 20\%$ ), and other desirable features [13, 16]. Since the magnetic field lines in a very low aspect ratio plasma have a high pitch, the plasma equilibrium becomes highly paramagnetic and essentially force-free with a large plasma current density nearly parallel to the magnetic field. This leads to a strongly enhanced toroidal field on-axis, and, combined with a dominating poloidal field at the outboard region of the plasma, creates a nearly omnigeneous region which is nearly free of locally trapped particles, contributing to the kinetic stability of the plasma and reduced neoclassical transport. To achieve a very low aspect ratio, inboard components such as the solenoid, shield, and organic insulator are eliminated and only a cooled, normal conductor that carries current to produce the toroidal magnetic field is retained. The plasma major radius is significantly reduced and the resulting plasma looks much like a sphere with a small hole through its center, hence the name "spherical torus." Figure 1.4 shows the basic design configuration of a spherical torus (ST) reactor. The features of a spherical torus place it in a unique physics regime which may permit compact fusion at low magnetic field and modest cost.

Several subsequent studies of ST reactors have investigated ignition assessments and engineering feasibility [17, 18, 19]. These studies indicate ST reactors

can be exceptionally small in unit size and highly cost-effective, but are somewhat limited by the fact that no experimental data base for very low aspect tokamaks exist. Assumptions regarding plasma confinement and performance are extrapolated from the current physics data base, accumulated from experiments on JET, TFTR, DIII-D, JT-60 and other research reactors ( $A > 2.3$ ), which may or may not be valid at very low aspect ratio ( $A < 2$ ). Recently, the START (Small Tight Aspect Ratio Tokamak) experiment in operation at Culham Laboratory has formed hot plasmas at aspect ratios around 1.3 which exhibit good positional and MHD stability, and exhibit many typical tokamak characteristics [20, 21]. Oak Ridge National Laboratory is conducting an assessment now, and preparing to produce a conceptual design, for a hydrogen-fueled steady-state spherical tokamak (TST) intended to clarify the potential of the TST as a near-term, low-cost toroidal device to generate critical data for the next phase of magnetic fusion energy development [22]. As experimental data from ST reactors become available to verify stability and equilibrium calculations and to define physics scalings appropriate at very low aspect ratio, more credible ST reactor studies can be conducted.

### 1.5 D-<sup>3</sup>He ST Fusion Reactor

Except for one ST reactor study investigating the ignition and burn criteria for a D-<sup>3</sup>He tokamak [19], all ST reactor research has been oriented toward D-T fuel cycles. The current ARIES-III study of a conceptual D-<sup>3</sup>He tokamak reactor assumes advanced tokamak parameters and advanced physics performance, but at aspect ratio around 3.0. This presented an opportunity to investigate the competitive potential of a D-<sup>3</sup>He ST fusion reactor, which was the basis for this thesis. If compact D-<sup>3</sup>He fusion at low field and modest cost appears viable, then the possibility may exist for competitive fusion power.

Previous D-T ST reactor studies conducted at Oak Ridge National Laboratory

(ORNL) used a computer code called STORAC (Spherical TORus Reactor Analysis Code), run on the Cray computers at the National Energy Research Supercomputer Center. This code is a variant of TETRA (Tokamak Engineering Test Reactor Analysis), an earlier reactor analysis code developed at ORNL which calculates tokamak performance, cost, and configuration as a function of plasma and engineering parameters [23]. STORAC assumes a 0-dimensional, profile averaged global physics model which uses conventional tokamak modeling algorithms modified for the ST and adopts many of the ITER scalings for nominal ST modeling (e.g. energy confinement laws, etc.). The code is organized in a standard equation solver format, consisting of a numerical software package which iterates a prescribed set of variables in order to satisfy a prescribed set of constraints, and optionally maximizes or minimizes a given figure of merit. The costs accounting used in STORAC combines methods used in TETRA and the GENEROMAK method [24]. A standard cost accounting system [25] is used, which follows that used in the reporting of power reactor costs, updated to 1990 dollars. STORAC is benchmarked with ARIES-I and ITER computer models and extrapolates to very low aspect ratio using a modified model.

Using STORAC as the start point, the research for this thesis involved essentially five steps. They were: (1) learning the architecture of the existing code and how to run the code; (2) modifying parts of the code to convert from a D-T fuel cycle to a D-<sup>3</sup>He fuel cycle; (3) debugging the modified code and clarifying assumptions; (4) running the new code to establish credible reference cases; and, (5) performing sensitivity studies for several key parameters of the reference cases. From the sensitivity studies, conclusions regarding the potential of a D-<sup>3</sup>He ST fusion reactor have been made.

## 1.6 Thesis Outline

This thesis is arranged in four chapters with three appendices. Chapter 2 reviews the modifications made to STORAC and the basic assumptions adopted for this study. Chapter 3 discusses the reference cases and the results of the sensitivity studies. Chapter 4 discusses the economic, safety and environmental assessment of the reference cases and presents the conclusions of this study. Appendix A reviews the spherical torus physics model used in STORAC. (For the reader unfamiliar with fusion reactor physics, a brief review of the material contained in Appendix A would be beneficial before proceeding to the next chapter.) Appendix B contains the details of the reference cases used in the study. Appendix C contains a copy of all the output plots for the edge safety factor scan of the ST-2A 2nd stability regime reference case, which is representative of the output plots produced for all the other sensitivity studies.

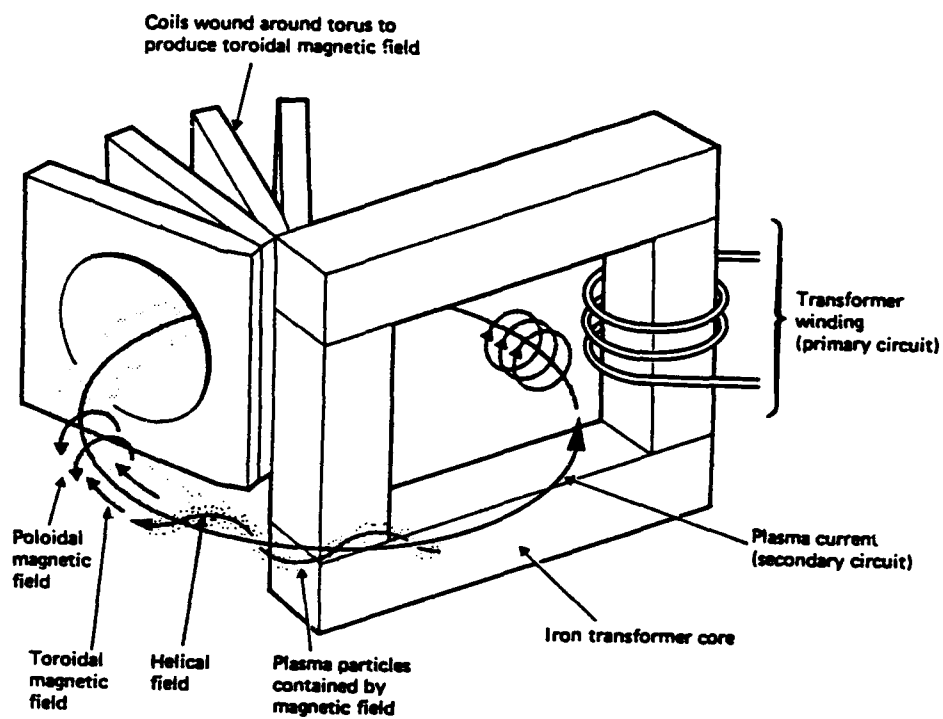


Figure 1.1: Schematic of a tokamak



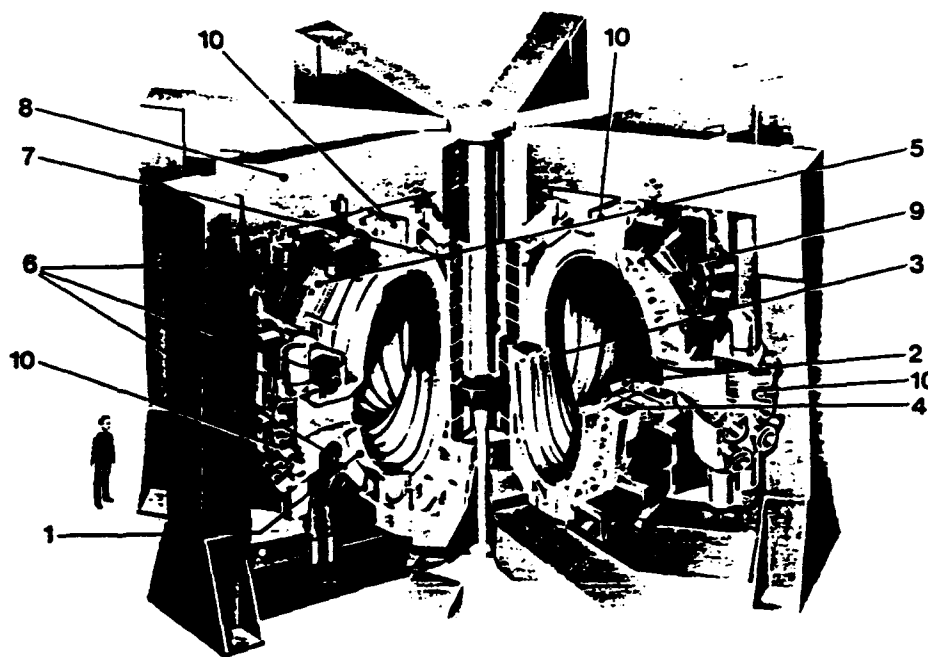


Figure 1.2: The JET device. (1) Vacuum vessel (double walled). (2) Material limiter defining the outer plasma edge. (3) Poloidal protective shields to prevent the plasma touching the vessel. (4) Toroidal field magnet of 32 D-shaped coils. (5) Mechanical structure. (6) Outer poloidal field coils. (7) Inner poloidal field coils (primary or magnetizing windings). (8) Iron magnetic circuit (core and eight return sections). (9) Water and electrical connections for the toroidal field coils. (10) Vertical and radial ports in the vacuum vessel for plasma heating systems and diagnostics.

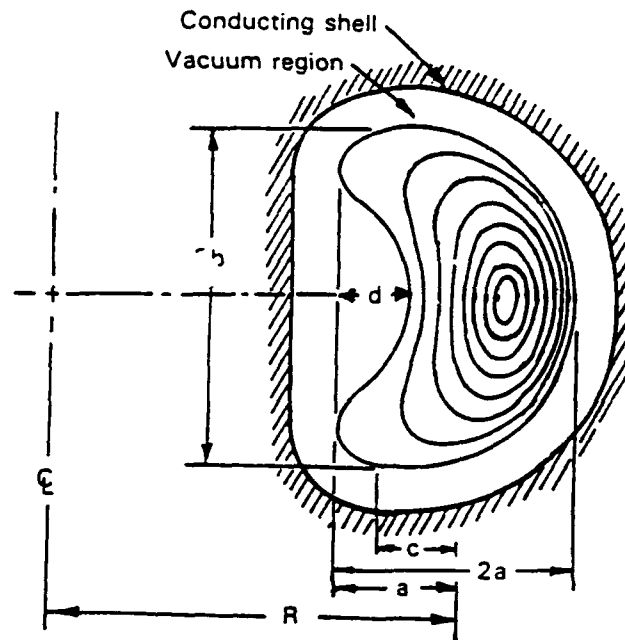


Figure 1.3: Plasma cross-sectional shape showing major radius  $R$ , horizontal minor radius  $a$ , vertical minor radius  $b$ , triangularity  $\delta = c/a$ , and indentation  $d/2a$ . The closed lines depict magnetic flux surfaces.

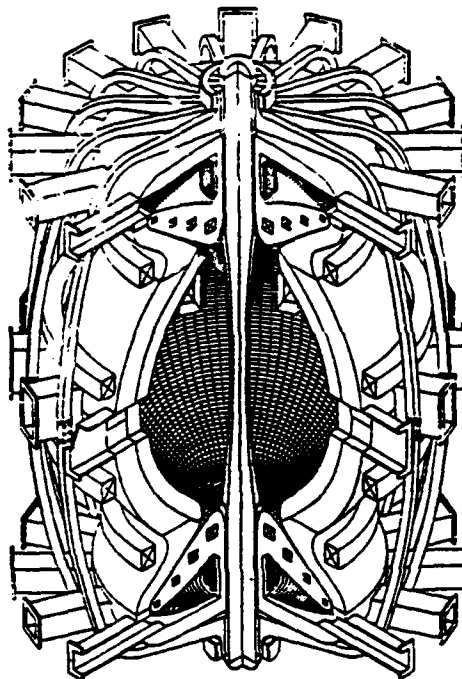


Figure 1.4: Basic ST design configuration, showing unshielded center conductor post and double-null poloidal divertors.

## **CHAPTER 2**

### **Spherical Torus Reactor Analysis Code (STORAC) and Assumptions**

#### **2.1 Introduction**

This chapter describes the computer model used and provides justification for the assumptions adopted for this study. Section 2.2 reviews the basic architecture and operation of the original code. Section 2.3 describes the fundamental modifications made to the code. Section 2.4 reviews the assumptions adopted, which includes justification for why certain constraints and variables were selected. Many of these modifications and assumptions were developed over time, based on several debugging problems and preliminary results showing fundamental flaws in original assumptions. The modifications and assumptions described here represent those ultimately adopted for this study.

#### **2.2 Review of Original Code**

##### **2.2.1 Architecture of STORAC**

The Spherical Torus Reactor Analysis Code (STORAC) consists of a series of modules, each describing a reactor system or component, controlled by a driver or optimizer routine. It contains a numerical software package which can iterate a prescribed set of variables to satisfy a prescribed set of constraints. Tokamak reactors are complex devices consisting of many nonlinear interactions, many of which are described in Appendix A. STORAC uses the generalized nonlinear programming subroutine VMCON [26] as an optimizer. This option requires: (1) iterating more variables than constraints being considered; (2) incorporating upper and lower bounds on all variables being iterated; and, (3) specifying a prescribed figure of merit to be minimized or maximized. For example, using cost of electricity (COE)

as the figure of merit, VMCON is able to find the device configuration providing minimum COE which satisfies the prescribed physics and engineering constraints. Other figure of merit options include construction cost, aspect ratio and plasma major radius. Some of the constraints available are formulated as inequalities, which provides additional flexibility as VMCON iterates to find a self consistent set of device parameters. An option to use a nonlinear equation solver without optimization is also available, which is useful for performing benchmark comparisons using fixed parameters.

When STORAC runs in the optimization mode, it reads in an input file identifying which constraints are to be used, which variables are to be used, which figure of merit is to be used, and initial values for the various device parameters. If a parameter is not identified as a variable, it remains fixed. The code runs through its calculations using the given parameters. The VMCON subroutine then calculates the least value of a function of several variables subject to linear and nonlinear equality and inequality constraints. Variables are then incremented upward or downward within their bounds in such a way that the figure of merit moves closer to optimization. The code continues to iterate in this manner until all prescribed constraints are met to within a given error tolerance, such as  $10^{-4}$ . When optimization is complete, the code produces an output file listing the final values of the variables, the residual error of the constraints, and the calculated reactor parameters which include system costs, physics parameter values and engineering parameter values.

### 2.2.2 D-T ST Model

Before addressing the modifications made to STORAC for this study, it is important to understand the D-T ST configuration which the original code models. Basically, the D-T fusion reaction at optimum operating conditions releases about 20% of its 17.6 MeV reaction energy in the form of 3.5 MeV alpha particles and

about 80% in the form of 14.1 MeV neutrons. Other fusion reactions are negligible at this temperature and are generally ignored. The charged alpha particles accumulate as "plasma ash" and the fast neutrons escape to be moderated in a lithium blanket surrounding the vacuum vessel and first wall and then stopped in a steel shield surrounding the blanket. The lithium blanket is important for breeding tritium for later use as fuel. The heat energy deposited by the fast neutrons in the blanket and shield is removed by a coolant fluid and converted to electricity in a basic Rankine cycle employing heat exchangers, turbine/generators, condensers and pumps. Radiation losses from the fast alpha particles are small, making a negligible contribution to the overall heat energy deposited in the blanket/shield structure and available for conversion to electricity. The unshielded center conducting post is also heated by the fast neutrons and must be cooled to keep its maximum temperature below a threshold for material melting or excessive resistive losses.

The D-T ST plasma is modelled relatively simply by assuming the D-T fuel ratio and alpha ash fraction and optimizing the plasma electron density and operating temperature for a specified geometry. (Many other parameters must also be assumed or specified, but these four are illustrative of how the code operates.) The neutron fusion power resulting from the D-T reaction is converted to electricity with an efficiency of about 35-40%. The net electric power produced by the reactor equals the gross electric power minus the resistive losses in the TF magnet coils (i.e, the center conducting post and TF coil return legs), plasma heating and current drive power requirements, and miscellaneous power requirements for pumps, tritium handling systems, etc. Neutral beam injection is generally used as the external current drive method, assuming a deuterium/tritium beam interacting with the D-T plasma background. For a given energy beam, STORAC calculates the current drive efficiency as well as the number of beam-plasma fusion reactions and the beam beta. Based on the plasma physics calculations for the given parameters,

STORAC performs engineering calculations to determine dimensions of the reactor vessel, CENTERPOST, and the toroidal field (TF) and poloidal field (PF) magnet coils required for the plasma configuration. Capital costs for the reactor components are then calculated and, finally, the cost of electricity is determined.

### 2.2.3 Constraint Equations and Variables

As STORAC iterates to optimize a prescribed figure of merit, certain constraints are necessary to insure a self consistent solution. Constraint equations which must be satisfied include: the plasma beta equation, which relates beta to the plasma parameters (see A.8); the global plasma power balance, which relates power sources to power losses (see A.9); the beam ion density, used only with the NBI option; magnetic field at the coil, which insures that the field at the coil is consistent with the field at the plasma; the radial build, which matches the inboard component radial build to the plasma major radius; and the centerpost temperature, which insures that the correct resistivity is used. Optional inequality constraints related to the plasma parameters include: the density limit (see A.7); the Troyon beta limit, a parameter useful in first stability regime calculations, and the  $\epsilon\beta_p$  limit, a parameter useful in second stability regime calculations (see A.8); the volt seconds limit, which is used for pulsed operation; the edge q, which establishes a minimum edge safety factor for the plasma (see A.3); and neutral beam energy, where beam decay lengths to plasma center equals a prescribed input value. Optional inequality constraints related to overall device operational considerations include: the neutron wall load, which limits the amount of radiation damage to the first wall, blanket and shield; the divertor heat load, which limits the amount of erosion damage to divertor plates by charged particles; the fusion power limit; the net electric power limit; and the peak centerpost temperature.

Numerous physics and engineering parameters can be specified as variables,

with prescribed upper and lower bounds. Physics parameters include: aspect ratio  $A = R_0/a$ ; plasma major radius  $R_0$ ; edge safety factor  $q_\psi$ ; toroidal magnetic field on-axis  $B_0$ ; plasma beta  $\beta$ ; electron density  $n_e$ ; plasma temperature  $T_e$ ; neutral beam density  $n_{beam}$ ; neutral beam energy  $E_{beam}$ ; confinement H-factor; and several inequality variables for use with the physics constraints. Engineering parameters include: centerpost current density; centerpost average temperature; centerpost coolant velocity; centerpost coolant fraction, the area of coolant versus cross sectional area of the centerpost; TF coil thickness; TF coil current density; and several inequality variables for use with the operational constraints.

Initial values are given to all parameters prescribed as variables as well as all fixed parameters. Fixed parameters include: D-T fuel ratio; alpha ash fraction; plasma elongation and triangularity, which either assume a fixed scaling dependent upon inverse aspect ratio (see A.2) or are specified explicitly; Troyon beta scaling coefficient and maximum  $\epsilon\beta_p$ ; energy confinement time scaling (14 different scaling options available); divertor shape, either single null or double null; divertor model, either conventional or expanded gaseous divertor; plasma scrape-off layer width and length; required net electric power; neutral beam ion mass; neutral beam width; permitted neutral beam e-decay lengths to plasma center; bootstrap current fraction; angle of incidence of field line on divertor plate; first wall, blanket and shield thicknesses; centerpost and TF coil resistivities; number of TF coils and PF coil groups; coolant inlet temperature and thermal conductivity; thermal to electric conversion efficiency; and unit costs and other cost information such as plant capacity factor, inflation rate, level of safety assurance, etc. This list of parameters is only representative of the many parameters required to run the code, but is indicative of the complexity of a tokamak fusion device. It is important to note that initial values used to start the code should be reasonably close to a working solution, or else the physics and engineering calculations may be inconsistent and the code will not



execute. For this reason, it is best to start with a case that works and modify the input file to get a desired output.

#### 2.2.4 Summary

Although this review of the original code is brief, it provides a basic description of how STORAC runs, what it is trying to model, and some of the constraints and variables available for modelling a reactor configuration. A complete description of the code and its operation is beyond the scope of this thesis, which is not meant to be a STORAC user manual. By understanding what the original code does, one will better understand what the modified code does and why the changes were made.

### 2.3 STORAC Modifications

#### 2.3.1 D-<sup>3</sup>He ST Model

Identifying the general features of the D-<sup>3</sup>He ST configuration was necessary before any changes could be made to STORAC. How would the D-<sup>3</sup>He ST be different from the D-T ST, assuming advanced physics parameters? Conceptually, it would operate at low field in steady-state, with high beta in the second stability regime, and have a significant plasma current dominated by the bootstrap effect and supplemented by NBI current drive. Tritium fuel would not be required, eliminating the need for a lithium breeder blanket and allowing the device to be more compact. A direct energy convertor/expanded gaseous divertor system would provide conversion of charged particle fusion power to electricity, offering potentially greater efficiency than the standard Rankine cycle, as well as provide plasma ash exhaust and impurity control. Figure 2.1 shows a schematic of a conceptual double-null poloidal divertor/direct electrodynamic energy convertor system [6], which would consist of chambers above and below the core plasma into which the scrape-off layer plasma would be diverted, collecting ions on one divertor plate and electrons on the other.

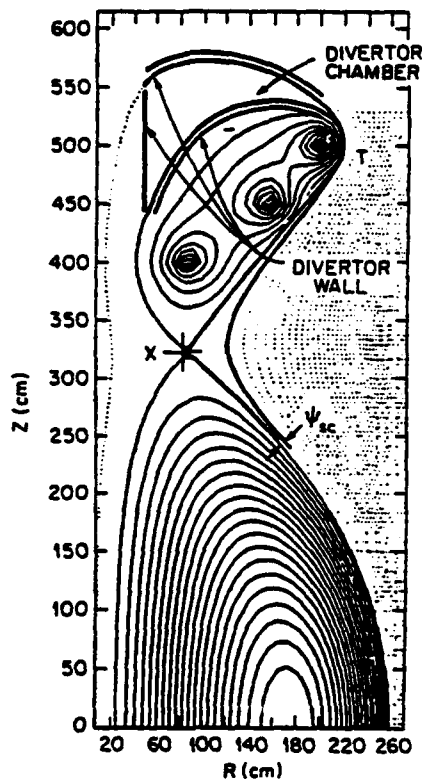


Figure 2.1: Schematic of poloidal divertor/direct electrodynamic energy conversion system.

However, in the D-<sup>3</sup>He reactions only about 50% of the total charged-particle energy release is subject to direct conversion due to radiation and high particle transport to the walls [7], so a conventional thermal energy conversion system would still be necessary to remove a significant fraction of heat energy and convert it to electricity.

### 2.3.2 Code Revisions

The first significant modification required to transform STORAC from a D-T model to a D-<sup>3</sup>He model was to incorporate a routine to solve for the steady-state particle balance and add routines for additional fusion reaction rates (see A.6). A new calculation was added to solve for the deuterium density  $n_D$  as a function of particle balance, charge balance and fuel ratio  $n_3/n_D$  and then determine remaining particle densities as a function of  $n_D$ . At the optimum D-<sup>3</sup>He operating temperature

in the 50-80 keV range, the D-T reaction rate is still higher than for D- $^3\text{He}$  and significant for determining neutron fusion power, the two D-D reaction rates are low but important for establishing an accurate plasma composition, and the T-T reaction rate is significantly lower but accounts for some removal of radioactive tritium from the plasma. Including the obvious D- $^3\text{He}$  reaction rate, these other four reactions are important and were all considered in the steady-state particle balance. The original code simply assumed fractional densities of deuterium, tritium and alpha particles relative to the plasma electron density. With the addition of  $^3\text{He}$  and protons to the plasma background, and with five different fusion reactions occurring simultaneously, no simple scaling would be appropriate.

The new particle balance required new variables and routines to be defined and old ones deleted or changed, throughout most of the subroutines in the code. A new variable for particle confinement time  $\tau_p$  required a new constraint equation to be satisfied for a self consistent solution. The simple D-T scalings for charged fusion power and neutron fusion power (20% and 80% of total fusion power, respectively) had to be generalized with new calculations for charged fusion power, neutron fusion power and additional fast particle losses fusion power. The D-T scaling for fast alpha beta had to be replaced with a calculation for a more general fast particle beta, accounting for all fast particles produced by the five fusion reactions and their different energies. The calculations for fast alpha energy transferred to electrons and ions were also replaced with new calculations for general fast particle energy transferred to the electrons and ions. The NBI calculations had to be modified to account for a D- $^3\text{He}$  background, essentially by replacing tritium entries with  $^3\text{He}$  where appropriate. Since the operating plasma densities for D- $^3\text{He}$  tend to be higher than D-T, requiring beam energies of about 5 MeV or more for current drive, the NBI calculations had to be modified to correct a fitting factor scaled for beam energies of about 1 MeV. The beam fusion calculations also had to be modified to

account for a D-<sup>3</sup>He background and new beam fusion equations added to account for the additional reactions.

The next significant modification to STORAC was to the heating power and gross electric power calculations. Since <sup>3</sup>He has charge  $Z=2$ , the electron density is a larger fraction of the total charged particle density than in a D-T plasma. This effect, coupled with the higher operating temperatures for D-<sup>3</sup>He, means radiation power losses play a larger role in the overall power balance than they do in the D-T plasma. Bremsstrahlung and synchrotron radiation losses from the core and edge plasma (see A.9) were already calculated, but neglected from the equations used to determine heat energy deposited in the centerpost and shield since their contribution was negligible compared to the D-T neutron energy. These equations were modified to include both neutron and radiation energy deposited in the centerpost and shield. The inclusion of a direct energy convertor required an additional calculation to convert charged particle power to the divertor into electricity with a prescribed DEC efficiency. The remaining power to the divertor would then appear as heat energy to the divertor plates, to be included in the heat energy sum. The total heat energy deposited to the shield and divertor plates would then be converted to electricity with a prescribed thermal efficiency. Thus, the gross electric power would be a sum of the electricity generated by the DEC and the turbine/generators.

### 2.3.3 Summary

Adding the steady-state particle balance routine to the code, with its associated modifications to other variables and routines, and modifying the gross electric power calculations to account for direct energy conversion represented the significant modifications to STORAC. Most of these changes were obvious from the start, while others became evident once the code was running and producing output of dubious

quality. To list here each individual code change made to STORAC would be unnecessarily tedious. (The individual code changes are documented in the STORAC files.) What is important to understand here are the fundamental modifications to STORAC that were necessary for modelling the new D-<sup>3</sup>He ST configuration.

## 2.4 Assumptions Made for this System Study

### 2.4.1 Introduction

With the code modifications to STORAC in place, the task of establishing reference cases for further study required a number of assumptions oriented toward specific objectives. Since the stated purpose of this study was to investigate the potential of the steady-state D-<sup>3</sup>He ST for commercial electric power production, the reference cases should seek to minimize the cost of electricity for a typical 1000 MWe fusion reactor. One case should assume operation in the first stability regime and one case should aggressively assume operation in the theoretical second stability regime. Both cases should assume advanced, though reasonable, physics and engineering parameters. Once these two reference cases are established, sensitivity studies can investigate the effect of varying the values of important parameters.

The reference cases for this study both used 13 constraint equations and 21 variables to arrive at a self consistent successful optimization. The following constraints were used to develop these cases: plasma beta; global plasma power balance; neutral beam ion density; field at coil; centerpost temperature; particle confinement time; net electric power limit; and neutral beam energy. The following inequality constraints were used to develop the reference cases: density limit; Troyon beta limit;  $\epsilon\beta_p$  limit; and edge safety factor  $q$ . The following variables are used: aspect ratio,  $A=R_0/a$ ; toroidal magnetic field,  $B_0$ ; plasma major radius,  $R_0$ ; average electron temperature,  $\langle T_e \rangle$ ; plasma beta,  $\beta$ ; average electron density,  $\langle n_e \rangle$ ; neutral beam density fraction,  $n_{beam}/\langle n_e \rangle$ ; confinement H-factor,  $f_L$ ; current drive power used for

additional heating; neutral beam energy,  $E_{beam}$ ; centerpost radius; centerpost current density,  $J_{cp}$ ; centerpost average temperature; centerpost coolant velocity; average radius of centerpost coolant channel; centerpost coolant fraction; and TF coil current density. Four other variables were used for the inequality constraints. The figure of merit to be minimized was cost of electricity. The residual error tolerance for the VMCON optimizer was  $10^{-4}$ .

#### 2.4.2 Discussion of Variables

The basic geometry of the plasma and the reactor required to maintain it is dependent upon the aspect ratio and plasma major radius. The aspect ratio was allowed to vary between a lower limit of 1.2 [18] and an upper limit of 2.0, representing the full operational regime of ST plasmas. The plasma major radius was allowed to vary over a broad range of 1-4 meters. These limits would allow for optimization at whatever plasma size is required for a 1000 MWe reactor, although both aspect ratio and major radius tend to be as low as possible for cost effective performance.

The plasma performance is dependent upon operating temperature and density, as well as the beta value required for stable confinement and the confinement H-factor required for power balance. Since D-<sup>3</sup>He fusion peaks at temperatures of about 55 keV, the electron temperature was given a reasonable range of 40-80 keV. Density was assumed to vary between  $10^{20} - 10^{21} m^{-3}$ , with the Borass density limit (see A.6) expected to be within this range and the density to be at or slightly below this limit for maximum fusion power density. Since strong paramagnetism introduces an important uncertainty in the application of the Troyon beta limit [16], the plasma beta was given a broad range of 0.20-2.0, with the upper limit set high enough to allow for possible beta values greater than 1.0 for operation in the second stability regime [27]. The confinement H-factor was also given a broad range of 1-10

to allow for whatever H-mode enhancement was required for global plasma power balance (see A.9). All of these bounds were broad enough so as to not constrain an optimization unnecessarily.

The magnetic confinement of the plasma is dependent on the magnet coil configuration surrounding the reactor vessel. The toroidal magnetic field on-axis was allowed a range of 1-4 Tesla, with the field strength expected to fall in the 2-3 T range for the assumed reactor configuration [27]. To produce the required magnetic field on-axis, strong electric currents must pass through the centerpost and TF coil legs. The allowable current density through the centerpost is limited by temperature and material stress constraints (however, only the temperature constraint is used in the current model). Since the maximum allowable current density determines the minimum radius of the centerpost, to which the aspect ratio is very sensitive, the centerpost parameters are critical. Assuming an unshielded centerpost could be made of a single dispersion strengthened copper conductor cooled by high-velocity pressurized water, the maximum current density is estimated to be about 75 MA/m<sup>2</sup> without causing the peak copper temperature to exceed 250°C [18]. Thus, the centerpost current density was given an upper bound of 75 MA/m<sup>2</sup>, the average temperature was given the upper bound of 125°C, and the centerpost radius was allowed a range of 0.1-1.0 m. The coolant velocity of high-speed pressurized water was assumed to have an upper bound of 20 m/s [17], which neglects the corrosive effects of high velocity coolant. The average radius of the coolant channels was allowed a range of 0.001-0.010 m and the coolant fraction of the centerpost was allowed a range of 0.1-0.4, where the number of coolant channels is calculated to equal the coolant area divided by the average coolant channel area. For the conventional copper TF coil legs, which do not involve such critical parameters, the current density was allowed a range of 1-10 MA/m<sup>2</sup>. The dimensions of the TF coils are then determined by dividing the required current by the current density to get

the cross sectional area, which is then multiplied by the required TF leg length to give the volume of the TF coil legs. STORAC optimizes to find the best balance between the cost of the centerpost and TF coil magnet assembly (volume  $\times$  unit costs) and resistive power losses, based on all prescribed parameters.

The noninductive current drive provided by NBI requires high energy neutral beams to generate an ion current equal to the injected beam current multiplied by the average number of times the fast ions circulate the torus before being thermalized [11]. Counteracting this current is a reverse electron current due to friction with the bulk electrons, which forms a component of the plasma current. This generated current is dependent upon the density and energy of the neutral beam. STORAC determines the beam density and energy required for current drive. The beam density as a fraction of the electron density was allowed a range of  $10^{-5} - 10^{-2}$  and the beam energy was allowed a range of  $1-10^5$  keV to allow full flexibility in meeting current drive requirements. The neutral beam power used for additional plasma heating (if required) was allowed a range of 1-100 MW.

The remaining four variables were used for the density limit, Troyon beta limit,  $\epsilon\beta_p$  limit, and minimum edge q inequality constraint equations, with their respective 'f-values' allowed a range of 0.0-1.0. These variables would allow the average electron density, plasma beta and  $\epsilon\beta_p$  values to be at or below their upper limits and for the edge q value to be at or above its lower limit. This would allow for considerable flexibility during optimization since each and every constraint would not have to be at an extreme.

### 2.4.3 Discussion of Fixed Parameters

This intent of this section is to identify most of the fixed parameters used to establish the reference cases, with some justification for why they were chosen. Many of the parameters used as defaults in the physics model are described in Appendix



A and will be summarized here. Other physics and engineering parameters critical for this study will also be described in this section.

Plasma shape and geometry (see A.2) assumed plasma elongation and triangularity to scale as a function of inverse aspect ratio. This study also assumed a plasma scrape-off layer thickness of 0.04 m, a first wall thickness of 0.02 m, and a shield thickness of 0.50 m. Since no blanket is required, the blanket thickness was set equal to zero. The vertical gap between the shield and TF coils was assumed to be 0.163 m. A double-null, expanded gaseous divertor concept was assumed, in which a simple divertor heat load calculation is employed (i.e., the divertor power is assumed to be uniformly distributed about the divertor area by the action of copious amounts of neutral particle interactions). The increase in the vertical build to accommodate this divertor concept was then accounted for in the vertical build.

Other shape and geometry parameters were related to the magnet parameters. The conventional copper TF coil legs were assumed to have a resistivity of  $2.5 \times 10^{-8}$  Ohm-m and the strengthened copper centerpost was assumed to have a resistivity of  $3.0 \times 10^{-8}$  Ohm-m. The reactor is assumed to be built on top of or adjacent to its power supplies, with a bus length of 10 m for each leg and the bussing current density assumed to be  $1.25 \times 10^6$  A/m<sup>2</sup>. Two superconducting PF coil groups are assumed, with the PF coils assumed to be external to the TF coils.

The assumed plasma current scaling (see A.3) is based on a double-null divertor scaling. The minimum edge  $q$  was scaled as a function of inverse aspect ratio. The maximum bootstrap current fraction (see A.4) was assumed to be 0.9. NBI provides the remaining noninductive current drive, which provides the seed current for the bootstrap effect and profile control for the plasma current. The beam width was assumed to be 0.31 m and the neutral beam wall plug to injector efficiency was assumed to be 0.5. The permitted neutral beam e-decay length to plasma center ratio was assumed to be 3.0 (i.e.,  $n_{beam}(0) = e^{-3}n_{beam}$ ).

Other miscellaneous physics parameters are identified in Appendix A. The density and temperature profile exponents (see A.5) were assumed to be 0.5 and 1.0, respectively. The ion and electron temperatures were assumed to be equal. The particle confinement time to energy confinement time ratio (see A.6) was assumed to be 3.0. The effective helium-3 to deuterium fuel ratio (see A.6) was assumed to be 1.0. Tritium recycling was assumed. The trapping fractions of the fast charged particles resulting from fusion reactions (see A.6) were assumed to be 1.0, with the exception that 0.9 was assumed for the 14.7 MeV protons. The 1990 ITER H-mode power scaling (see A.9) was assumed for the energy confinement time. The reactor wall reflectivity (see A.9) was assumed to be 0.9, representative of a hot stainless steel vacuum chamber at 400°C [28].

Among the remaining engineering parameters, the average thermal energy conversion efficiency was assumed to be 40% (typical of most power plants) and the direct electrodynamic conversion efficiency was assumed to be 50% [6]. The level of safety assurance (LSA) was assumed to be 2, which assumes large-scale passive protection in the event of an accident [1]. The plant operating life and capacity factor were assumed to be 30 years and 0.75, respectively. The cost accounting remained the same as established in the original code [24, 25], except for two modifications [27]. The unit cost for the divertor system was assumed to be \$1 million/m<sup>2</sup> to account for the additional complexity of the direct energy conversion system and the unit cost for the NBI system was assumed to be \$5/watt to account for high energy beam systems (greater than 1 MeV).

The reference cases for the first and second stability regimes (see A.8) assumed the same parameters except three. For the first stability regime reference case, the Troyon coefficient for the beta limit was assumed to be 3.3 for steady-state operation, the  $\epsilon\beta_p$  limit was assumed to be 0.6, and the central safety factor  $q(0)$  was assumed to be 1.0. For the second stability regime reference case, the Troyon beta limit was

not used, the  $\epsilon\beta_p$  limit was assumed to be 1.0, and  $q(0)$  was assumed to be 2.0 [27]. All other parameters discussed previously remained the same.

#### 2.4.4 Summary

Having decided upon which constraint equations and variables to use, with appropriate bounds and initial values, the task of establishing reference cases was reduced to running the code to get a successful optimization and checking that the output variable values, when re-entered as initial values in the input file, converged to a self-consistent solution. Based upon all assumptions made, there should be only one solution for each reference case. Any change to the input file, such as assuming a thermal conversion efficiency of only 35% rather than 40%, would specify a different reactor and result in a different solution. For the most part, the assumptions defined here were agreed upon [27] throughout the period of code modification and debugging.

## CHAPTER 3

### Results of D-<sup>3</sup>He ST Reactor Study

#### 3.1 Introduction

This chapter discusses the reference cases which resulted from the assumptions described in the previous chapter and the results of several parametric investigations. Section 3.2 discusses the reference cases, both the initial results and the final reference cases selected for further study. Section 3.3 investigates the sensitivity of the 2nd stability reference case to  $\epsilon\beta_p$ , which was given a range of 0.5-1.5. This is primarily to demonstrate a linkage between the 1st and 2nd stability regimes. With a linkage between the two reference cases established, further investigations can focus on just one reference case, that being the more optimistic 2nd stability case. The remaining sections investigate the sensitivity of the 2nd stability reference case to the following nine parameters: (1) temperature and density profile factors; (2) ratio of particle confinement time to energy confinement time; (3) fuel ratio; (4) confinement H-factor; (5) bootstrap current fraction; (6) aspect ratio; (7) centerpost current density; (8) thermal conversion efficiency; and, (9) DEC conversion efficiency. Reactor performance based upon the varying parameter values is then quantitatively evaluated relative to the 2nd stability reference case.

#### 3.2 1st and 2nd Stability Regime Reference Cases

##### 3.2.1 Initial Results

Based upon the basic assumptions adopted for this study, STORAC produced successful optimizations for a 1st stability regime ST reactor ( $\epsilon\beta_p = 0.6$ ) and a 2nd stability regime ST reactor ( $\epsilon\beta_p = 1.0$ ). These two cases have been designated ST-1A and ST-2A, respectively. Table 3.1 lists the key parameters of these two cases.

This table also lists the key parameters for ARIES-III [29], a conceptual D-<sup>3</sup>He 2nd stability regime tokamak reactor, as a benchmark comparison. Although the ARIES-III results are about as speculative as the results of this study, considerable expertise has been committed to the ARIES program and the ARIES-III results provide a useful benchmark for evaluating the relative potential of the D-<sup>3</sup>He ST reactor.

The bottom line comparison of these results indicate that the estimated unit cost of electricity (COE) in mill/kWh (mills per kilowatt-hour; 1000 mills = \$1) is 116.5 for ST-1A, 88.5 for ST-2A, and 74.3 for ARIES-III. Costs are in 1990 dollars for all three cases. Comparable COE estimates [30] for an advanced pressurized water reactor (APWR) and a solar photovoltaic electric plant are 40-50 mill/kWh and 200-300 mill/kWh, respectively. Thus, the D-<sup>3</sup>He fusion reactors do not appear to be as economically competitive as advanced fission breeder reactors (assuming COE comparable with APWR), but they do appear to fall within the broad COE range expected for future energy systems.

Comparison of ST-1A, ST-2A and ARIES-III results indicate significantly lower toroidal magnetic fields on-axis for the ST reactors, as expected. However, the higher peak magnetic fields required at the TF coil for the ST reactors are characteristic of very low aspect ratio geometry. This may be seen in the following equation, where the magnetic field at the plasma axis is

$$B_0 = B_c \frac{R_0 - a_0 - s}{R_c}$$

where  $s$  is the distance between the plasma and magnet coil necessary to house the first wall and shield. The higher fields required at the TF coil lead to higher resistive power losses in the copper magnets, resulting in larger recirculating power fractions and higher COE. Ideally, the reference cases for the ST should have recirculating power fractions comparable with ARIES-III, where 20-30% represents a reasonable range. Power losses much greater than 300-400 MWe for a 1000 MWe commercial

power plant simply are not attractive to the electric utilities.

A few other points are worth noting from Table 3.1. First, the neutron wall load is much lower for ARIES-III than for the ST reactors, since the first wall surface area for ARIES-III is larger (1394 m<sup>2</sup> versus less than 400 m<sup>2</sup> for the ST reactors). Second, the total magnet costs are also lower for ARIES-III than for the ST reactors, since the ST reactors use normal copper magnets and more than 60% of the total magnet costs are for the PF magnet assemblies, which are necessary for the stronger vertical fields required for ST confinement. Third, the NBI beam energy for ARIES-III appears to be very large, but the models used in both ARIES and STORAC are very speculative. The beam energies and power requirements are useful for cost estimates, but further conclusions should be reserved until better models become available. Lastly, the Lawson parameter  $n\tau_E$  (which defines the breakeven condition for a fusion plasma) for both ST-1A and ST-2A is about  $1.8 \times 10^{21} \text{ s/m}^3$ , which appears to be well within the ignition regime. Previous studies [19] indicate D-<sup>3</sup>He ignition in a spherical torus could be achieved with wall reflectivities below 80% and at  $n\tau_E \leq 10^{21} \text{ s/m}^3$ , without strong plasma shaping or  $\epsilon\beta_p > 0.6$ .

### 3.2.2 Variation of Edge Safety Factor

The parameter with perhaps the most significant effect on reactor performance was the edge safety factor, defined as  $q_\psi = aB_0/R_0B_p$ . The edge safety factor scaling used for the q-limit constraint equation is aspect ratio dependent (see A.3), which may or may not be valid for very low aspect ratio. Theoretically, a high-q reactor seems advantageous with regard to decreasing the statistical probability of plasma disruptions [9]. Disruptions due to MHD instabilities can lead to the sudden loss of plasma confinement, an operational transient which could result in an accident. In addition to increased risk of disruptions, plasma confinement and stability also tend to deteriorate with low-q operation. Although  $q_\psi \sim 3$  appears to be the lower limit

for safe operation, the practical lower limit is probably higher and only detailed MHD calculations for a specific reactor configuration could determine what the actual  $q$ -limit should be.

Reducing the edge safety factor reduces the on-axis toroidal magnetic field and the required peak field at the TF coil, leading to lower resistive power losses and lower COE. Figures 3.1 through 3.4 show various effects on reactor performance as  $q_\psi$  is reduced from 7.68 to 3.5 for ST-1A and ST-2A, respectively. As seen in the figures, there is a linear reduction in the on-axis magnetic field  $B_0$  with lower  $q_\psi$  values, leading to smaller major radius values and much smaller TF coil resistive power losses. The required injection power also shows a linear decrease with lower  $q$  values. The lower recirculating power fractions associated with lower  $q_\psi$  values mean less fusion power is required to meet the net electric power constraint, resulting in more compact reactors and lower costs.

### 3.2.3 Reference Cases Used for the Study

Based on the results of low- $q$  effects on reactor performance, new reference cases for the study were established which attempt to strike a balance between the physics advantages of high- $q$  operation (i.e., reduced risk of disruptions) and the engineering advantages of low- $q$  operation (i.e., reduced resistive power losses and lower COE). An edge safety factor  $q_\psi = 5$  was selected as a reasonable value on which to base further parametric investigations [27]. Since high  $\beta$  limits and good energy confinement are strongly correlated to large plasma current, which leads to operation at low  $q$ , values of  $q_\psi \leq 5$  may be attainable. Table 3.2 lists the key parameters of these two reference cases, designated ST-1B and ST-2B, respectively. Appendix B contains a complete output listing of all parameters for these two reference cases.

The cost of electricity for both ST-1B and ST-2B (88.9 and 73.7 mill/kWh, respectively) are comparable with ARIES-III, due to the reductions in reactor size,

magnetic fields and recirculating power fractions associated with a lower q-value. The use of superconducting magnets and lower PF field requirements in ARIES-III tends to offset the cost of high field operation, which the ST reactors must compensate for with better plasma performance at very low aspect ratio. The higher beta values permit lower field requirements and higher operating temperatures and densities, which lead to fusion power densities high enough to make ST reactors competitive with advanced tokamaks. Both reference cases have a major radius of about 2 m and an on-axis magnetic field of less than 2 T. Despite the relative 'compactness' of these two cases ( $R_0 \sim 2$  m), these are not small machines; the radial build for both cases is about 5 m and the vertical build is more than 8 m - roughly 30' in diameter and 50' high. The total capital cost for both cases is estimated at about \$5 billion, which would be a significant investment for any electric power utility.

As indicated in Chapter 2, all assumptions used to develop these reference cases are based upon reasonable extrapolations of physics knowledge and engineering technology. Specific details will have to be resolved, regardless of any assumptions adopted for this study. Although the specific cost accounting used in STORAC may be different from that used in the ARIES-III study (unit costs assumed for ARIES appear to be lower than those assumed for this study), a useful benchmark comparison can be made between the ST reference cases and ARIES-III. Therefore, these reference cases describe reasonably well the anticipated characteristics of future D-<sup>3</sup>He ST reactors, upon which useful parametric investigations may be conducted.

### 3.3 Variation of $\epsilon\beta_p$

Although it has been observed that gross plasma confinement in 1st stability regime tokamaks deteriorates for  $\epsilon\beta_p > 0.6$ , practical limits on  $\epsilon\beta_p$  values for operation in the 2nd stability regime are still undefined. Values approaching unity



are believed to be reasonable, but ARIES-III assumes  $\epsilon\beta_p = 1.803$ , suggesting that higher values may be attainable. Figures 3.5 and 3.6 show the effect on the ST-2B reactor performance for  $\epsilon\beta_p$  values over the range 0.5-1.5. As seen in these figures, reactor performance generally improves with higher  $\epsilon\beta_p$ . It is interesting to note that the parameters at  $\epsilon\beta_p = 0.6$  match those for the ST-1B reference case, demonstrating a linkage between ST-1B and ST-2B as  $\epsilon\beta_p$  varies from 0.6 to 1.0.

The linkage between the two reference cases indicates an operating path may exist between high beta operation in the 1st stability regime and operation in the theoretical 2nd stability regime with beta values approaching or exceeding unity. This is important when considering what the access path might be from ignition to steady-state operation in the 2nd stability regime. While reactor performance increases significantly as  $\epsilon\beta_p$  increases from 0.5 to 1.0, higher values produce only slightly better performance overall, as seen in the COE curve.

### 3.4 Variation of Density and Temperature Profile

The nominal values adopted for the density profile factor ( $\alpha_n = 0.5$ ) and the temperature profile factor ( $\alpha_T = 1.0$ ) represent reasonable estimates for initial study (see A.5). These would have to be refined through detailed MHD analysis to ensure that the plasma pressure profile, defined by the density and temperature profiles, is consistent with the current density profile, which was not included in the model used for this study. The radial plasma pressure is proportional to density and temperature:

$$p(\rho) \propto n(\rho)T(\rho) = \langle n \rangle \langle T \rangle (1 + \alpha_n)(1 + \alpha_T)(1 - \rho^2)^{\alpha_n + \alpha_T}$$

Assuming the pressure profile defined in the reference case to be valid, it must remain constant as the density and temperature profiles vary, so that MHD equilibrium and stability is maintained.

The assumed pressure profile can remain relatively constant by making the simplified assumption that  $\alpha_n + \alpha_T$  remains constant. Figures 3.7 and 3.8 show the effect on reactor performance for  $\alpha_n$  values over the range 0.1-1.3, where  $\alpha_T = 1.5 - \alpha_n$ . These figures show slight improvement in reactor performance with more peaked density profiles and flatter temperature profiles. This indicates there is some flexibility in the pressure profile without a significant impact on COE. If technology can be developed to form and sustain peaked density profiles (see A.5), this may be very useful for overall profile control (i.e., selecting the best combination of density and temperature profiles for optimum MHD equilibrium and stability).

### 3.5 Variation of the Fuel Ratio

The nominal value for the fuel ratio,  $n_3/n_D = 1.0$ , represents an apparent optimum for D-<sup>3</sup>He fusion. However, since the maximum fusion power density is virtually independent of the fuel ratio (see A.6), reactor performance sensitivity to variations may be oriented towards other important design parameters. Figures 3.9 and 3.10 show the effect on reactor performance for  $n_3/n_D$  values over the range 0.5-2.0. The neutron wall load curve clearly indicates the lower irradiation levels associated with <sup>3</sup>He-rich fuel ratios. It is worth noting that the <sup>3</sup>He/D injection rate ratio is almost identical to the effective fuel ratio in all fuel cycles considered here (i.e., these plasmas are loss dominated rather than fusion dominated [4]).

These figures indicate reactor performance is minimized for fuel ratios around 0.75, with improved performance for both higher and lower fuel ratios, but do not address plasma ignition. Increase of the fuel ratio much beyond 2.0 reduces the neutron wall load somewhat, but leads out of the ignition domain [4]. It is worth noting here that the shielding requirement does not reduce linearly, but roughly logarithmically, with the neutron wall loading. Decrease of the fuel ratio beyond 0.5 simply increases the neutron wall load to unacceptably high levels, regardless of

ignition requirements.

### 3.6 Variation of Confinement Time Ratio, $\tau_p/\tau_E$

The nominal value for the ratio of particle confinement time to energy confinement time,  $\tau_p/\tau_E \simeq 3.0$ , represents a reasonable estimate for initial study (see A.6). (ARIES-III, by comparison, assumes  $\tau_p/\tau_E \simeq 2.0$ ). Actual particle transport phenomena in any given reactor configuration could be different, and means to actively manipulate conductive power losses are not well understood. Figure 3.11 shows the effect on reactor performance for  $\tau_p/\tau_E$  values over the range 1.5-5.0. These figures indicate only minor effects on performance over the expected range  $2 < \tau_p/\tau_E < 4$ . This confirms the expectation that ST reactors operating at high beta are more robust to uncertainties in particle confinement and ash buildup effects, as well as synchrotron radiation effects [19]. This is related to the relatively lower radiation power losses at higher beta levels, which reduces the impact of ash buildup.

### 3.7 Variation of Confinement H-factor

The 1990 ITER H-mode power scaling used for this study determines the confinement time enhancement factor required for global power balance (see A.9). The required H-factor for ST-2B was 3.633, which represents an optimistic value. Actual confinement may be better, but worse confinement should be anticipated. Figures 3.12 and 3.13 show the effect on reactor performance for decreasing H-factor values over the range 3.63-3.0. These figures show a sharp decline in performance as confinement worsens and erratic behavior for values below 3.3. Injection power requirements and TF coil resistive losses both increase for operation at lower H-factors, which drives up the recirculating power fraction and COE.

### 3.8 Variation of Bootstrap Current Fraction

The assumed bootstrap current fraction,  $I_{bs}/I_P = 0.90$ , represents an optimistic maximum value. At least 5-10% of the plasma current should be externally driven to provide the seed current for the bootstrap effect and to provide current density profile control. The bootstrap current fraction for the ST-2B configuration may be less than 90%, based upon its actual pressure profile and particle diffusion effects. Figures 3.14 and 3.15 show the effect on reactor performance for decreasing values of the bootstrap current fraction over the range 0.90-0.60. These figures show a linear decline in performance proportional to the bootstrap current fraction. As more power is required for current drive, the recirculating power fraction and COE increase. The plasma temperature also increases, and possible limitations on temperature (or temperature gradient) may impose a minimum acceptable bootstrap current fraction necessary for safe operation. If a peaked density profile and a relatively flat temperature profile can be formed, as previously discussed, then high bootstrap current fractions (80-90%) at acceptable operating temperatures might be possible.

### 3.9 Variation of Aspect Ratio

The aspect ratio lower limit of 1.2 adopted for the study represents an artificially imposed bound, allowing enough room for an adequate centerpost and to accommodate for engineering difficulties. Theoretically, this limit could be lower. However, unforeseen physics and engineering constraints could impose a higher bound. Figures 3.15 and 3.16 show the effect on reactor performance for aspect ratios over the range 1.16-1.30.

The most significant effect indicated by these figures is the linear increase in magnetic field strength and TF coil resistive power proportional to aspect ratio. The COE curve generally shows a linear increase, but the total capital cost curve shows

only a marginal decrease at lower aspect ratio and a linear increase with higher aspect ratio values. The plasma beta curve reflects the higher beta levels at lower aspect ratio, as usually observed, but shows a leveling off at aspect ratios below 1.2. The maximum current density in the centerpost tends to limit any increases in reactor performance at these very low aspect ratios, but is not so critical at higher aspect ratios.

### 3.10 Variation of Centerpost Current Density

The maximum current density  $J_{cp}$  in a single dispersion strengthened copper conductor centerpost is estimated to be 75 MA/m<sup>2</sup>, which was the value adopted for the study. Whether such a component can be manufactured to this specification or greater, capable of withstanding high stresses and neutron irradiation over its lifetime, is uncertain. Even if the technological uncertainties can be resolved, such a component might not be cost effective relative to a centerpost with a lower current density.

Figures 3.18 and 3.19 show the effect on reactor performance for centerpost current density values over the range 55-85 MA/m<sup>2</sup>. These figures generally show a linear improvement in performance proportional to the current density. If current densities less than 75 MA/m<sup>2</sup> are required, the impact on COE is not very significant. The increases in reactor performance for current densities greater than 75 MA/m<sup>2</sup> are minimal, which is probably due to the aspect ratio lower bound of 1.2. High centerpost current densities and very low aspect ratios are inextricably linked, as also observed in the previous section. Further studies should consider these two parameters together for more meaningful results.

### 3.11 Variation of Thermal Conversion Efficiency

The 40% thermal conversion efficiency assumed for the study represents a reasonable value, based upon industry experience. The thermal conversion efficiency is an average based upon the heat energy removal from the shield and divertor plates. The efficiency could be higher in the shield (ARIES-III assumes 44%), but high efficiency in the divertor plates might not be attainable. Figure 3.20 shows the effect on reactor performance for average thermal conversion efficiency values over the range 30-45%. These figures show a linear improvement in performance proportional to efficiency, which is to be expected. Actually, this variation shows a larger impact on COE than many of the "physics uncertainty" variations discussed previously.

### 3.12 Variation of Direct Energy Conversion Efficiency

A preliminary estimate of the efficiency of a direct electrodynamic convertor is 50%, which was the value adopted for the study. Details of the particle drifts and distribution functions within the DEC need to be resolved, but the basic design appears feasible. Figure 3.21 shows the effect on reactor performance for DEC efficiency values over the range 40-60%. These figures also show a linear improvement in performance proportional to efficiency. However, comparing the COE curves in Figures 3.20 and 3.21, the sensitivity to DEC efficiency is not as great as that to thermal efficiency. Thus, a conceptual direct electrodynamic convertor with an efficiency of only 40% would not degrade reactor performance significantly.

### 3.13 Summary

These parametric investigations have shown the sensitivity of reactor performance to several key design parameters. The ST fusion reactor appears to be very sensitive to the edge safety factor limit, the  $\epsilon\beta_p$  limit, the confinement H-factor, and

the bootstrap current fraction. It appears to be more robust with regard to the other parameters studied, permitting considerable flexibility without significantly affecting reactor performance.

Parameter	ST-1A	ST-2A	ARIES-III
Aspect ratio, $A = R_0/a$	1.20	1.20	3.00
Major radius, $R_0$ (m)	2.676	2.344	7.500
Minor radius, $a$ (m)	2.230	1.953	2.500
Plasma vertical elongation, $\kappa_X = b/a$	2.665	2.665	1.842
Plasma triangularity, $\delta_X$	0.766	0.766	0.814
Edge safety factor, $q$	7.681	7.681	6.850
Troyon coefficient, $g_f$	2.84	4.74	15.10
Plasma toroidal beta, $\beta$	0.593	0.988	0.239
$\epsilon\beta_p$	0.60	1.00	1.803
Electron n-temperature, $[T_e]$ (keV)	66.12	71.10	53.29
Average electron density, $\langle n_e \rangle (10^{20}/m^3)$	4.331	4.658	3.272
Average ion density, $\langle n_i \rangle (10^{20}/m^3)$	3.193	3.463	2.075
Fuel ratio, $n_{He}/n_D$	1.00	1.00	1.07
Density profile factor, $\alpha_n$	0.50	0.50	0.140
Temperature profile factor, $\alpha_T$	1.00	1.00	0.792
Plasma effective charge, $Z_{eff}$	2.217	2.232	1.998
Lawson parameter, $n\tau_E (10^{21}s/m^3)$	1.88	1.81	2.45
Particle confinement time, $\tau_p$ (s)	13.03	11.67	22.55
Ratio $\tau_p/\tau_E$	3.0	3.0	2.0
ITER90 H-factor, $f_L$	2.099	3.014	2.086
On-axis toroidal magnetic field, $B_0$ (T)	2.624	2.200	7.575
Peak TF-coil magnetic field, $B_c$ (T)	18.19	15.59	13.971
Plasma toroidal current, $I_P$ (MA)	122.0	89.54	29.88
Bootstrap current fraction, $I_{BS}/I_P$	0.90	0.90	0.911
NBI beam energy, $E_{beam}$ (MeV)	5.29	4.93	18.40
Current drive efficiency, $\gamma (10^{20}A/W - m^2)$	2.336	2.458	1.066
Absorbed current-drive power, $P_{CD}$ (MW)	68.10	40.97	116.93
Total fusion power, $P_F$ (MW)	3261	2759	2682
Plasma Q-value, $Q_P = P_F/P_{CD}$	47.88	67.34	15.59
Radiation power loss, $P_{rad}$ (MW)	1835	1490	1967
Neutron power, $P_n$ (MW)	210	177	109
Neutron wall loading ( $MW/m^2$ )	0.441	0.483	0.079
Gross electric power (MWe)	1844	1571	1319
Net electric power output (MWe)	1000	1000	1000
Recirculating power fraction	0.460	0.360	0.242
Thermal conversion efficiency, $\eta_{th}$	0.40	0.40	0.44
Magnet costs (\$M)	668	368	253
Current drive costs (\$M)	380	244	478
First-wall/shield costs (\$M)	138	108	181
Total cost (\$B)	7.20	5.30	3.63
Cost of electricity, COE (mill/kWh)	116.5	88.5	74.3

Table 3.1: Key parameters of the 1st Stability ST, 2nd Stability ST and ARIES-III 2nd Stability Tokamak



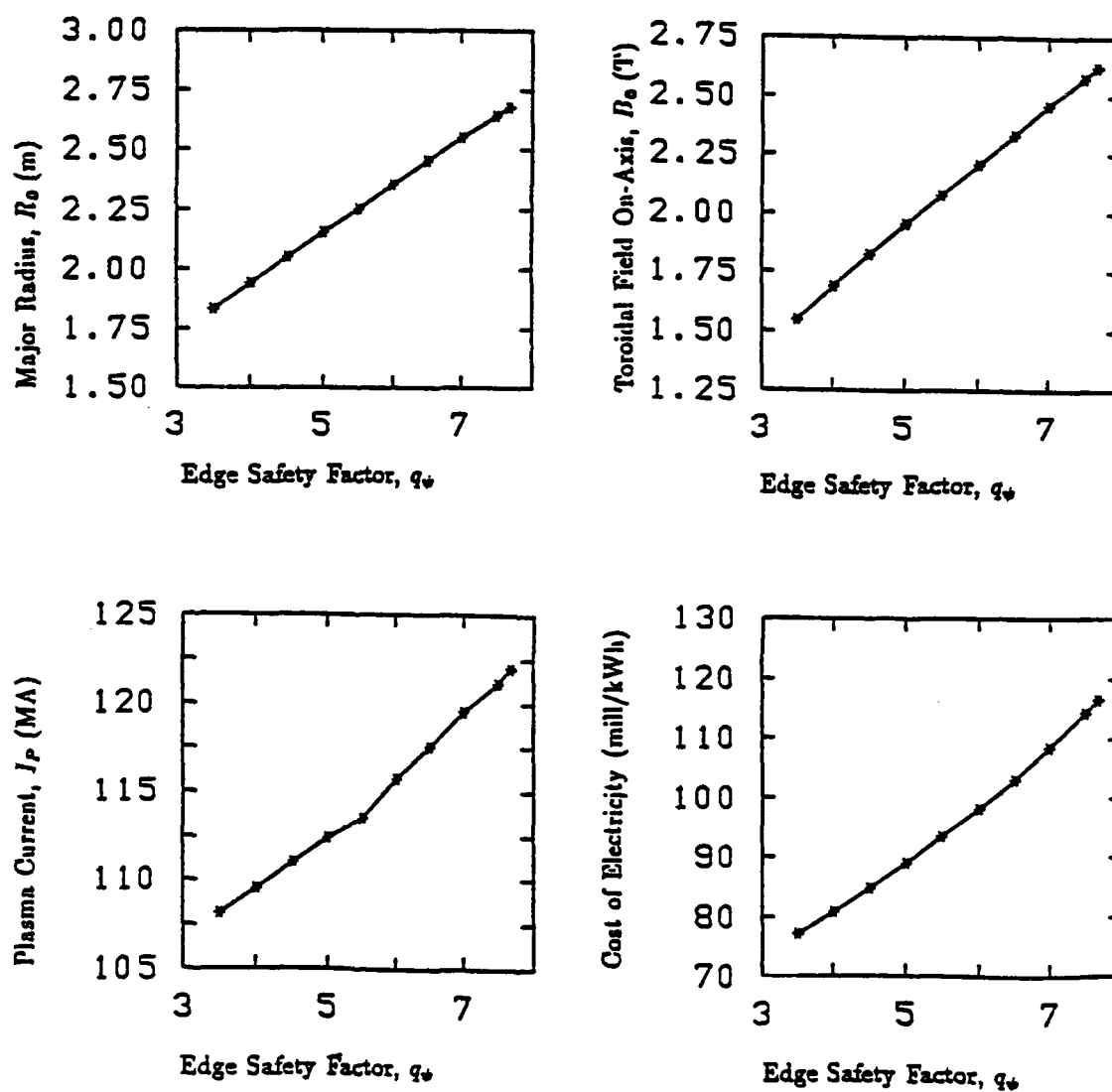


Figure 3.1: ST-1A Sensitivity to Variation of Edge Safety Factor:  $R_0$ ,  $B_0$ ,  $I_P$ , and COE versus  $q_\psi$

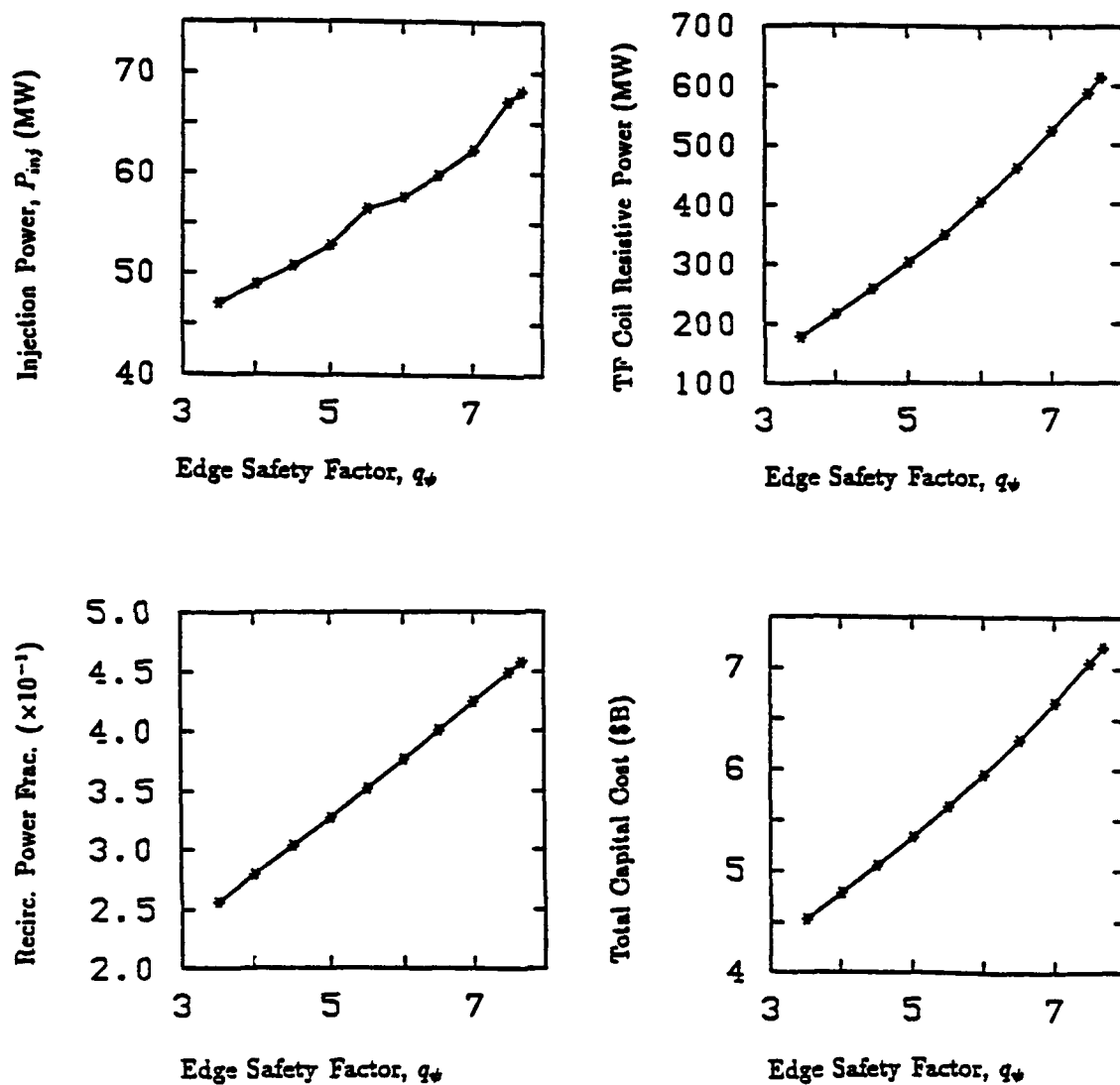


Figure 3.2: ST-1A Sensitivity to Variation of Edge Safety Factor:  $P_{inj}$ , TF Coil Resistive Power, Recirculating Power Fraction, and Total Cost versus  $q_\psi$

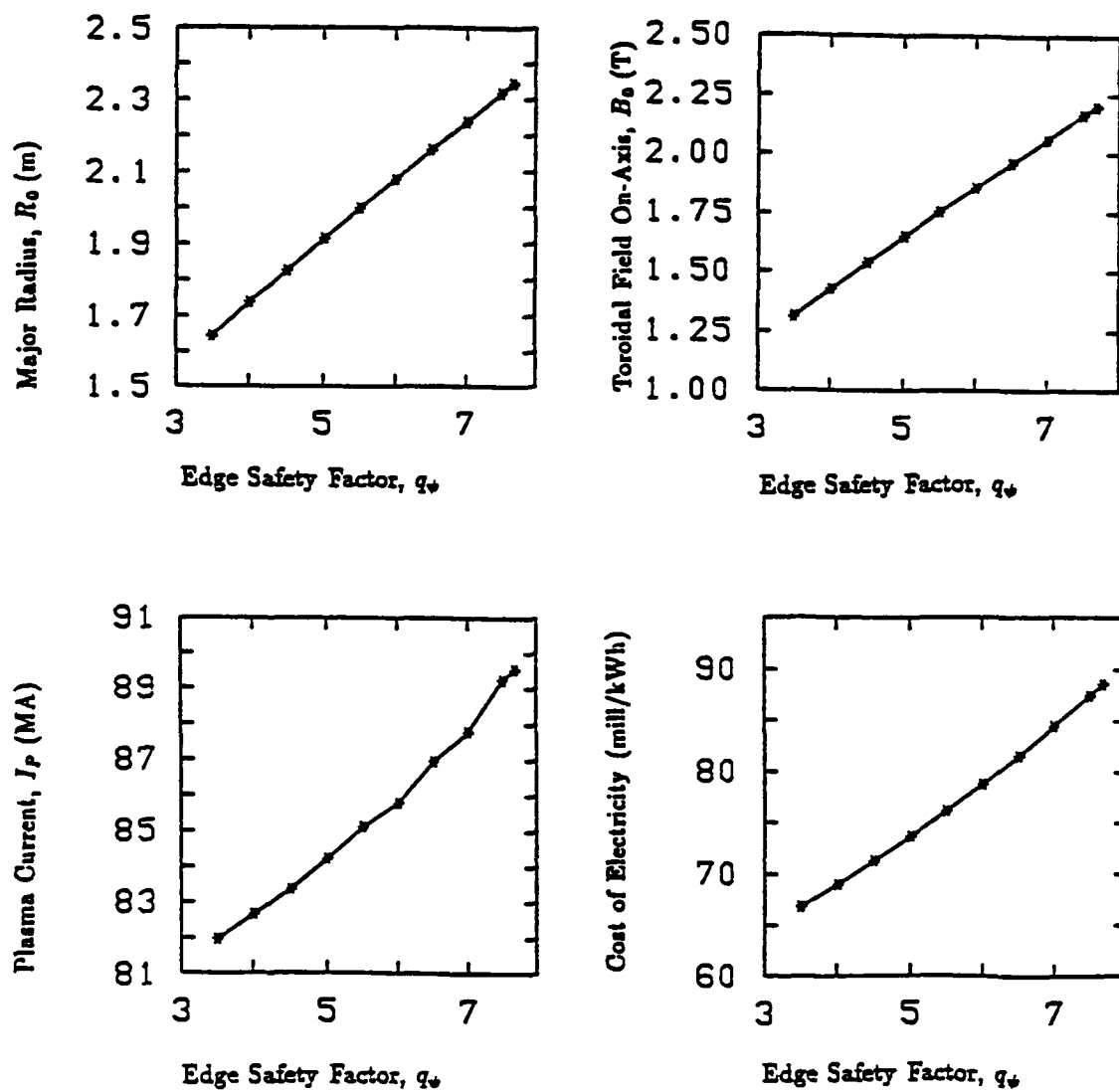


Figure 3.3: ST-2A Sensitivity to Variation of Edge Safety Factor:  $R_0$ ,  $B_0$ ,  $I_P$ , and COE versus  $q_\psi$

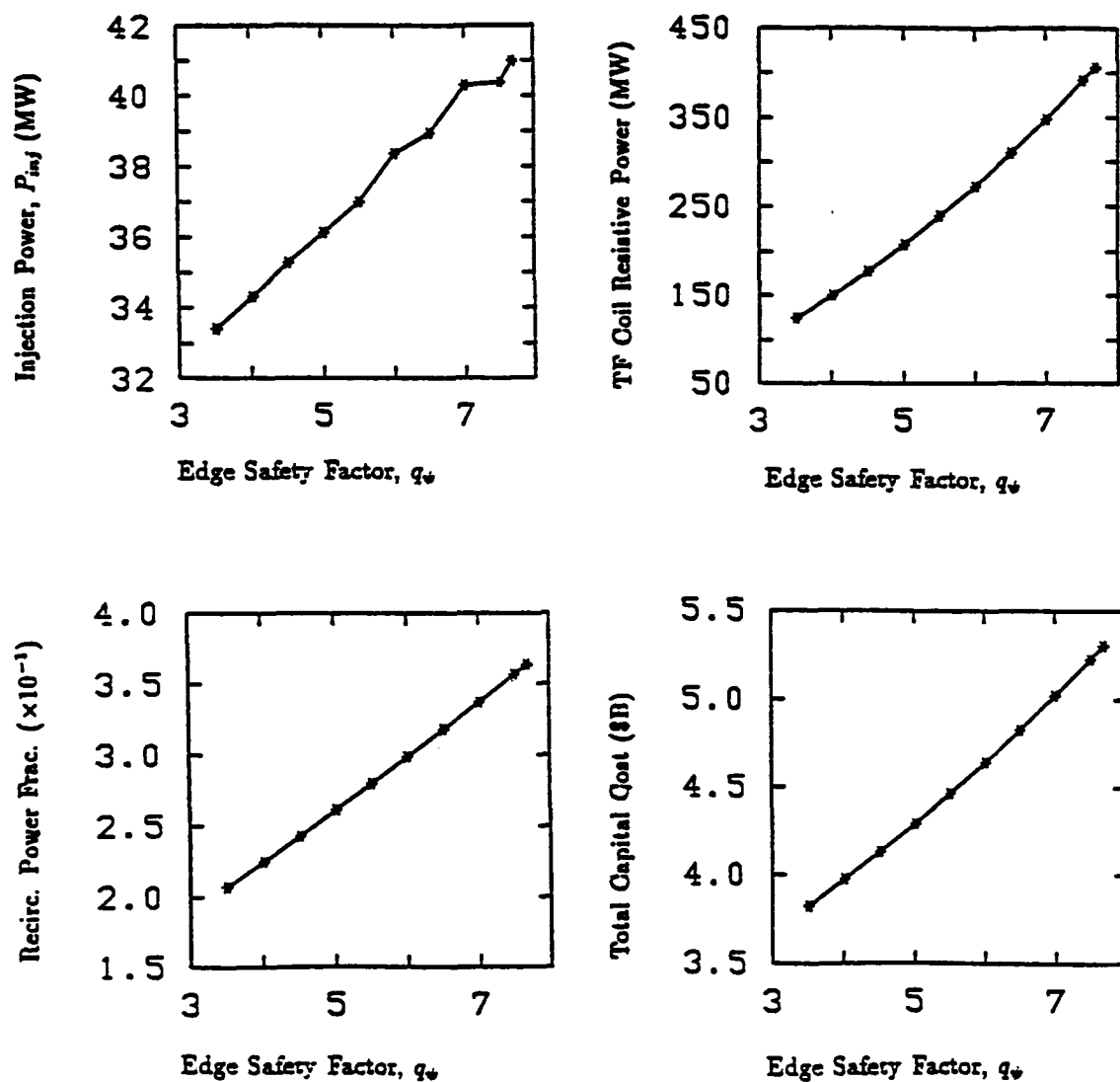


Figure 3.4: ST-2A Sensitivity to Variation of Edge Safety Factor:  $P_{inj}$ , TF Coil Resistive Power, Recirculating Power Fraction, and Total Cost versus  $q_\psi$

Parameter	ST-1B	ST-2B
Aspect ratio, $A = R_0/a$	1.20	1.20
Major radius, $R_0$ (m)	2.154	1.912
Minor radius, $a$ (m)	1.795	1.594
Plasma vertical elongation, $\kappa_X = b/a$	2.665	2.665
Plasma triangularity, $\delta_X$	0.766	0.766
Edge safety factor, $q$	5.0	5.0
Troyon coefficient, $g_f$	2.06	3.43
Plasma toroidal beta, $\beta$	0.660	1.100
$\epsilon\beta_p$	0.60	1.00
Electron n-temperature, $[T_e]$ (keV)	71.85	75.52
Average electron density, $\langle n_e \rangle (10^{20}/m^3)$	5.086	5.640
Average ion density, $\langle n_i \rangle (10^{20}/m^3)$	3.776	4.223
Fuel ratio, $n_{He}/n_D$	1.00	1.00
Density profile factor, $\alpha_n$	0.50	0.50
Temperature profile factor, $\alpha_T$	1.00	1.00
Plasma effective charge, $Z_{eff}$	2.228	2.244
Lawson parameter, $n\tau_E (10^{21}s/m^3)$	1.77	1.76
Particle confinement time, $\tau_p$ (s)	10.46	9.37
Ratio $\tau_p/\tau_E$	3.0	3.0
ITER90 H-factor, $f_L$	2.582	3.633
On-axis toroidal magnetic field, $B_0$ (T)	1.955	1.649
Peak TF-coil magnetic field, $B_c$ (T)	14.09	12.19
Plasma toroidal current, $I_P$ (MA)	112.4	84.18
Bootstrap current fraction, $I_{BS}/I_P$	0.90	0.90
NBI beam energy, $E_{beam}$ (MeV)	5.026	4.995
Current drive efficiency, $\gamma (10^{20}A/W - m^2)$	2.489	2.587
Absorbed current-drive power, $P_{CD}$ (MW)	52.85	36.09
Fusion power, $P_F$ (MW)	2585	2348
Plasma Q-value, $Q_P = P_F/P_{CD}$	48.92	65.06
Radiation power loss, $P_{rad}$ (MW)	1384	1231
Neutron power, $P_n$ (MW)	165	150
Neutron wall loading ( $MW/m^2$ )	0.535	0.616
Gross electric power (MWe)	1488	1353
Net electric power output (MWe)	1000	1000
Recirculating power fraction	0.330	0.260
Thermal conversion efficiency, $\eta_{th}$	0.40	0.40
Magnet costs (\$M)	398	231
Current drive costs (\$M)	304	220
First-wall/shield costs (\$M)	92	74
Total cost (\$B)	5.33	4.29
Cost of electricity, COE (mill/kWh)	88.9	73.7

Table 3.2: Key parameters of the 1st Stability ST and 2nd Stability ST reference cases

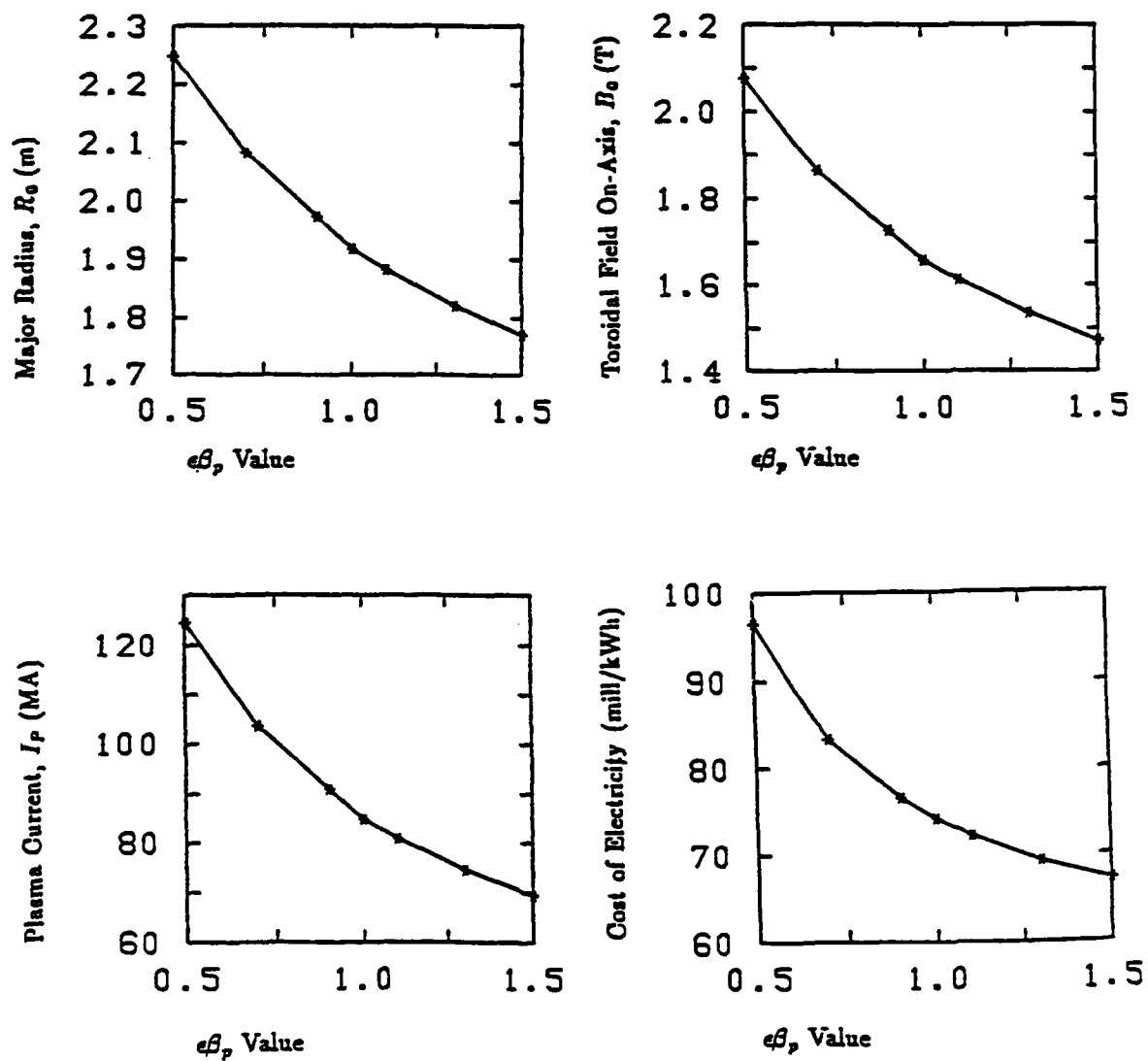


Figure 3.5: ST-2B Sensitivity to Variation of  $\epsilon\beta_p$ :  $R_0$ ,  $B_0$ ,  $I_P$ , and COE versus  $\epsilon\beta_p$

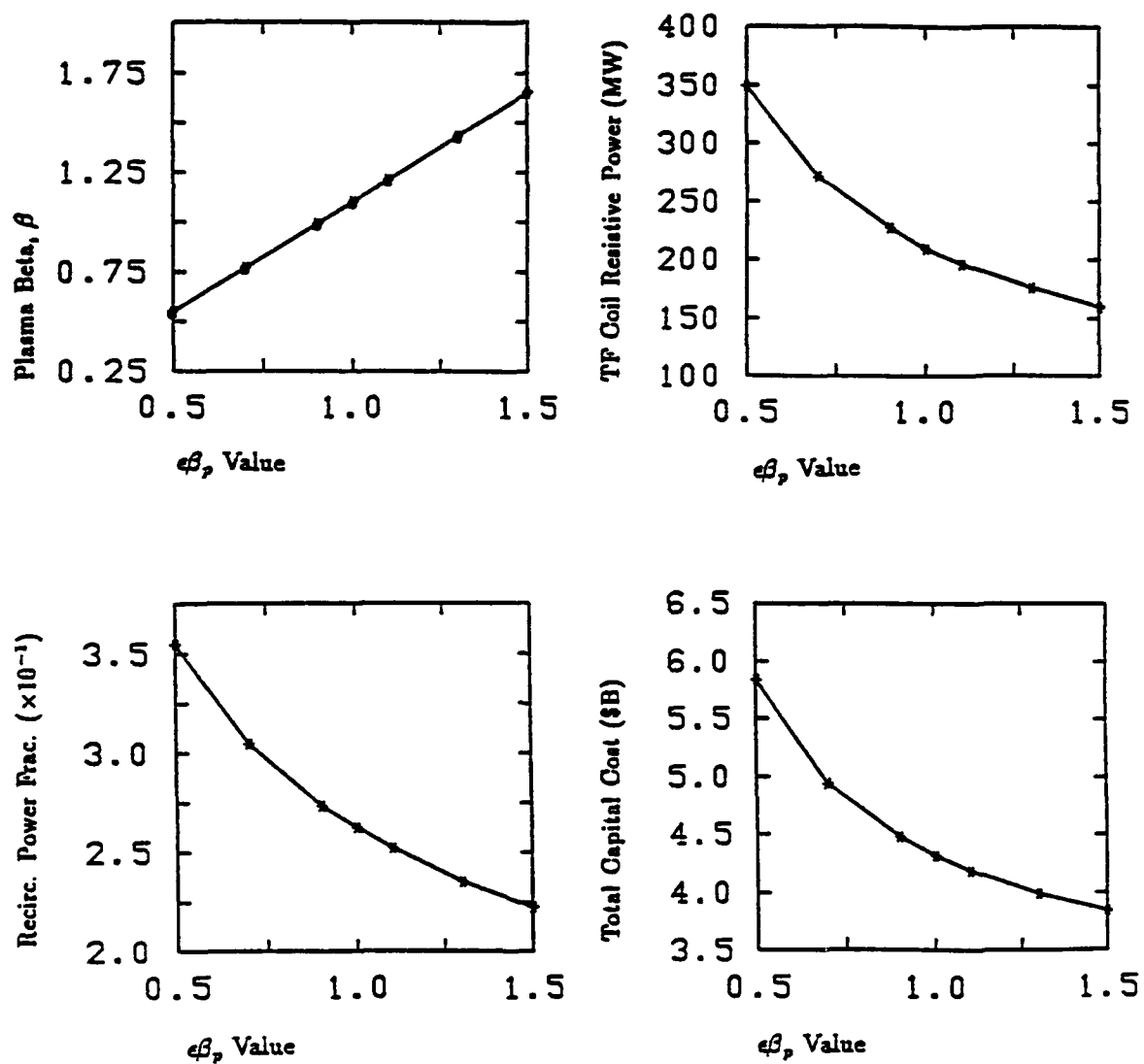


Figure 3.6: ST-2B Sensitivity to Variation of  $\epsilon\beta_p$ :  $\beta$ ,  $P_{inj}$ , TF Coil Resistive Power, and Total Cost versus  $\epsilon\beta_p$

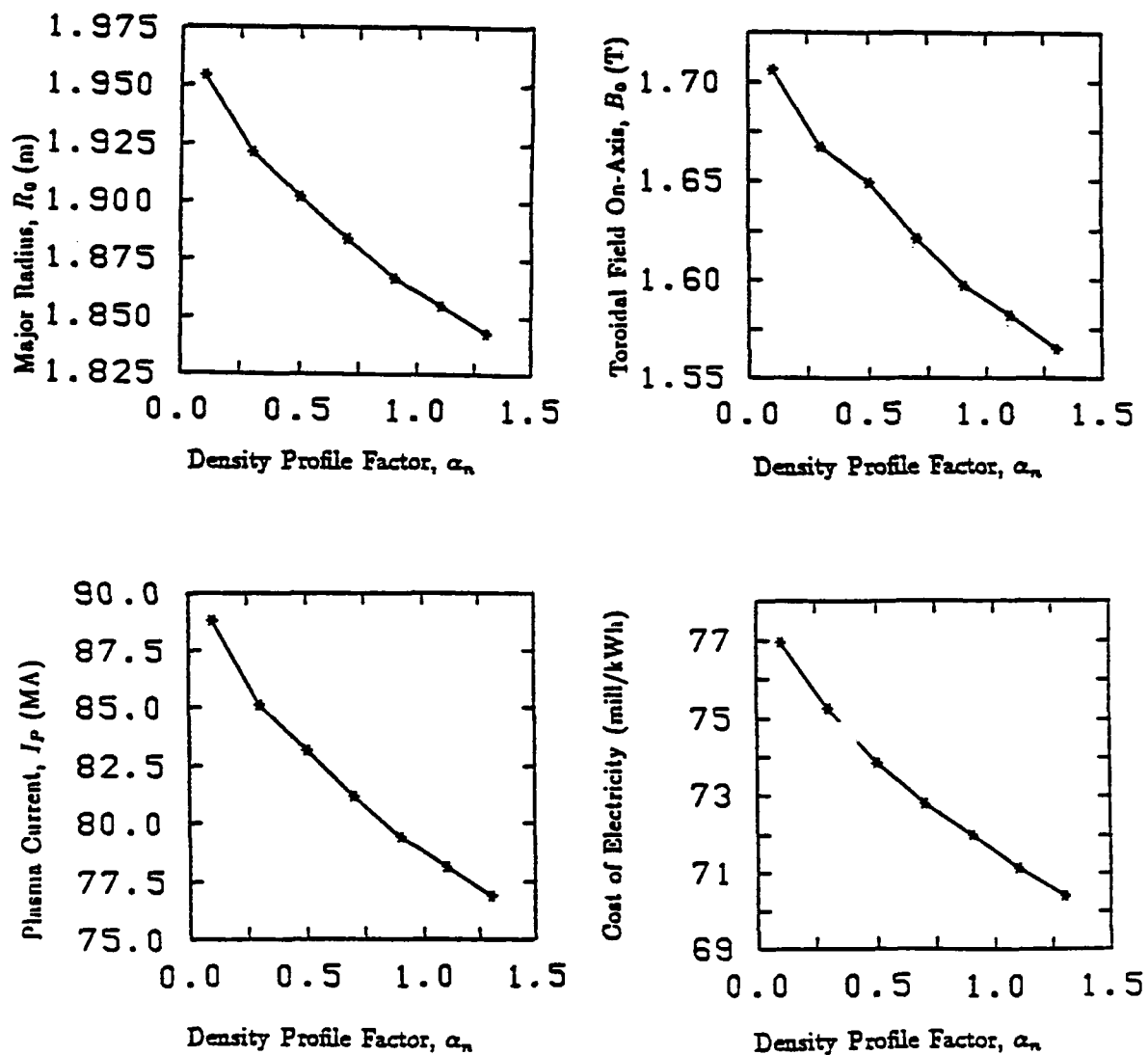


Figure 3.7: ST-2B Sensitivity to Variation of Density and Temperature Profile:  $R_0$ ,  $B_0$ ,  $I_P$ , and COE versus  $\alpha_n$  (where  $\alpha_T = 1.5 - \alpha_n$ )



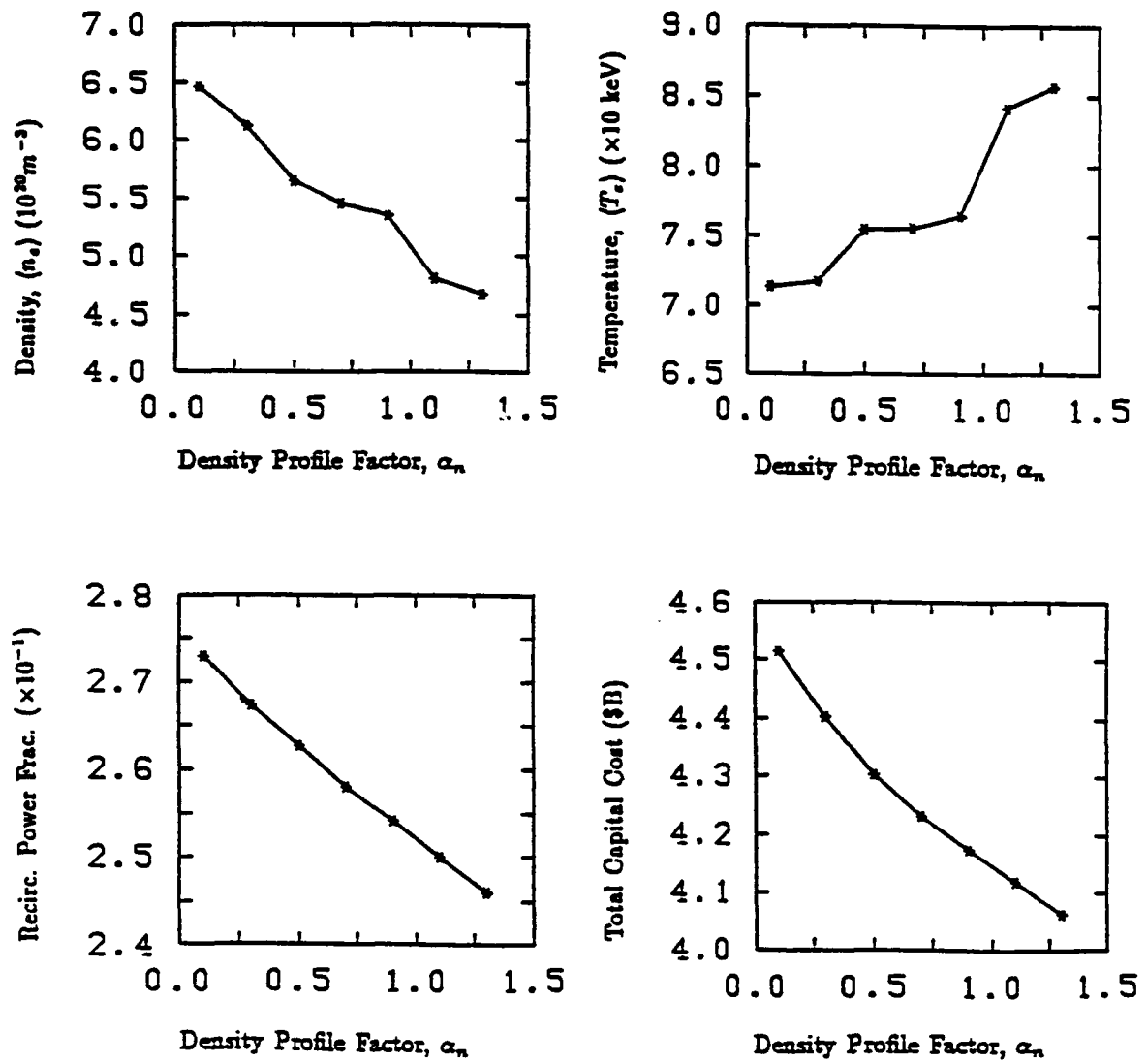


Figure 3.8: ST-2B Sensitivity to Variation of Density and Temperature Profile:  $\langle n_e \rangle$ ,  $\langle T_e \rangle$ , Recirculating Power Fraction, and Total Cost versus  $\alpha_n$  (where  $\alpha_t = 1.5 - \alpha_n$ )

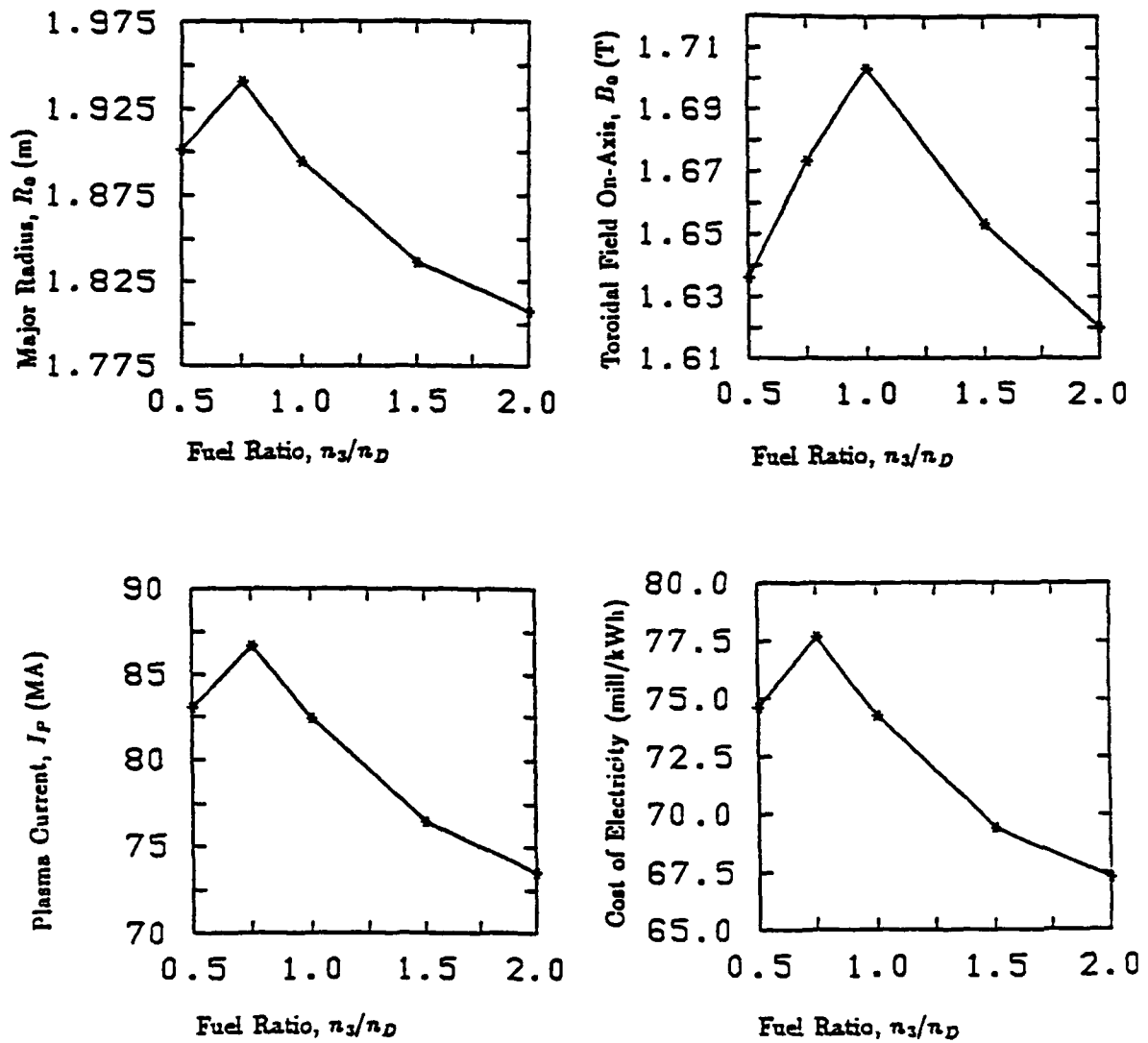


Figure 3.9: ST-2B Sensitivity to Variation of Effective Fuel Ratio:  $R_0$ ,  $B_0$ ,  $I_P$ , and COE versus  $n_3/n_D$

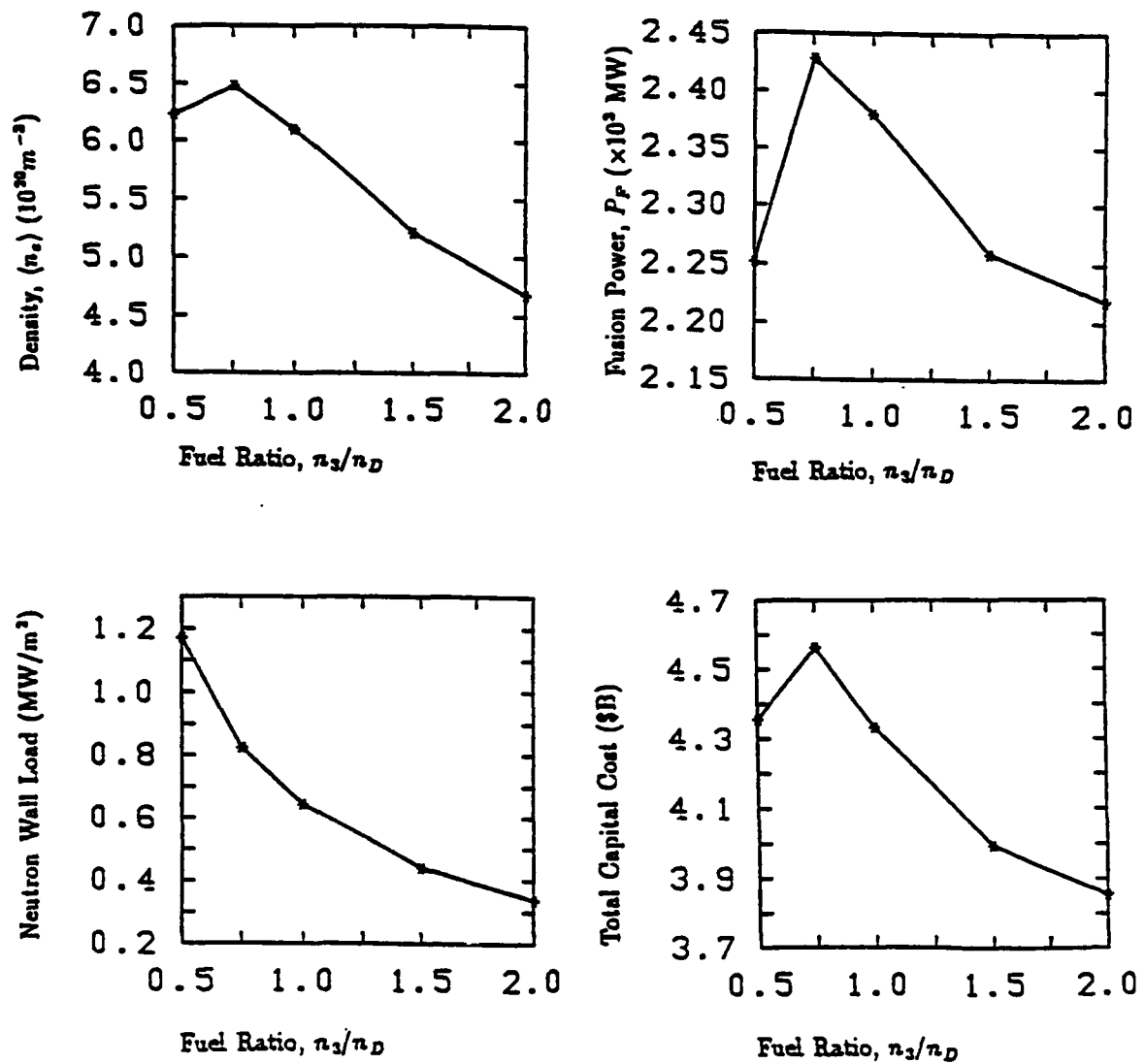


Figure 3.10: ST-2B Sensitivity to Variation of Effective Fuel Ratio:  $\langle n_e \rangle$ ,  $P_F$ , Neutron Wall Load, and Total Cost versus  $n_3/n_D$

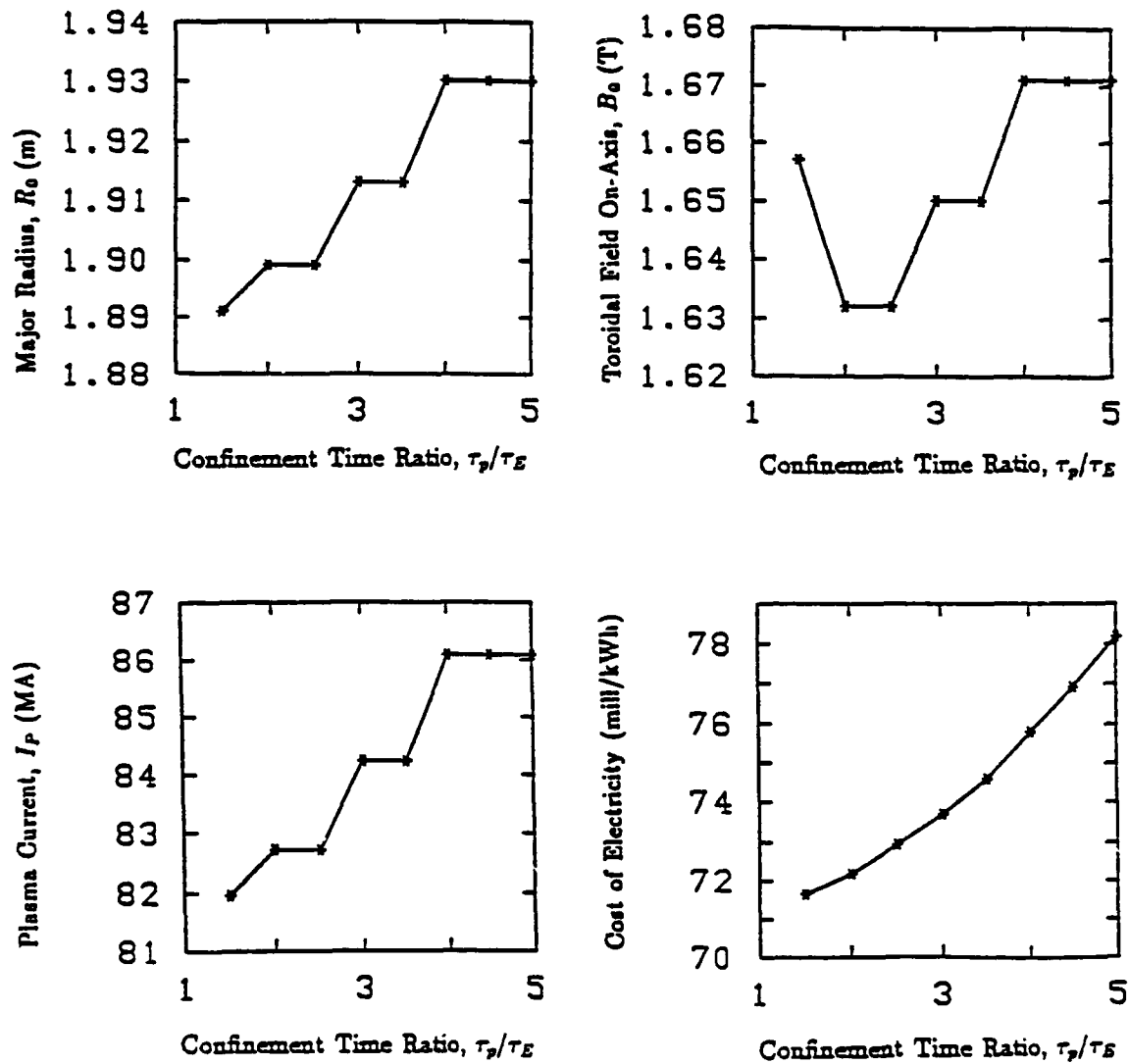


Figure 3.11: ST-2B Sensitivity to Variation of Confinement Time Ratio:  $R_0$ ,  $B_0$ ,  $I_P$ , and COE versus  $\tau_p/\tau_E$

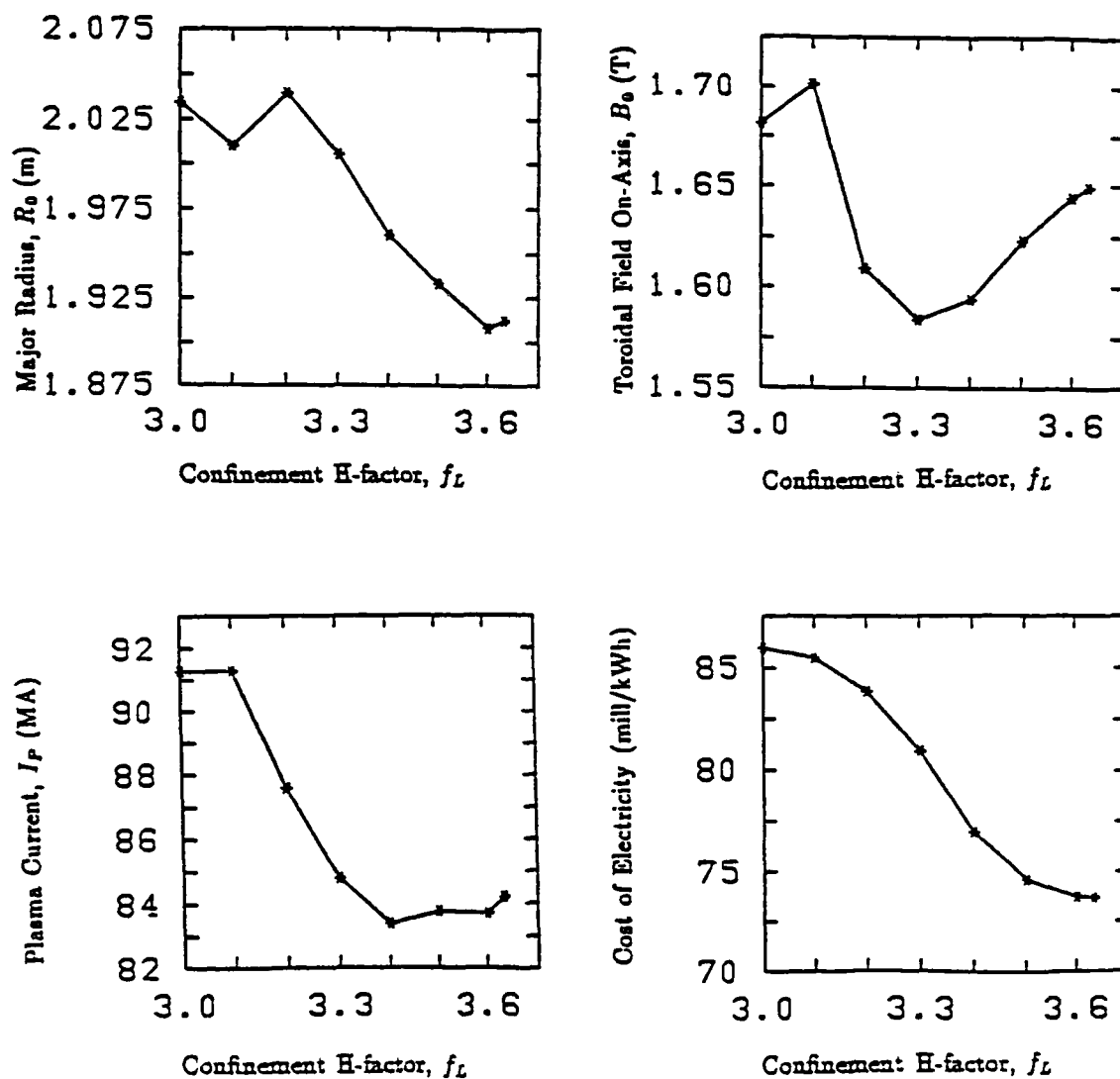


Figure 3.12: ST-2B Sensitivity to Variation of Confinement H-Factor:  $R_0$ ,  $B_0$ ,  $I_P$ , and COE versus  $f_L$

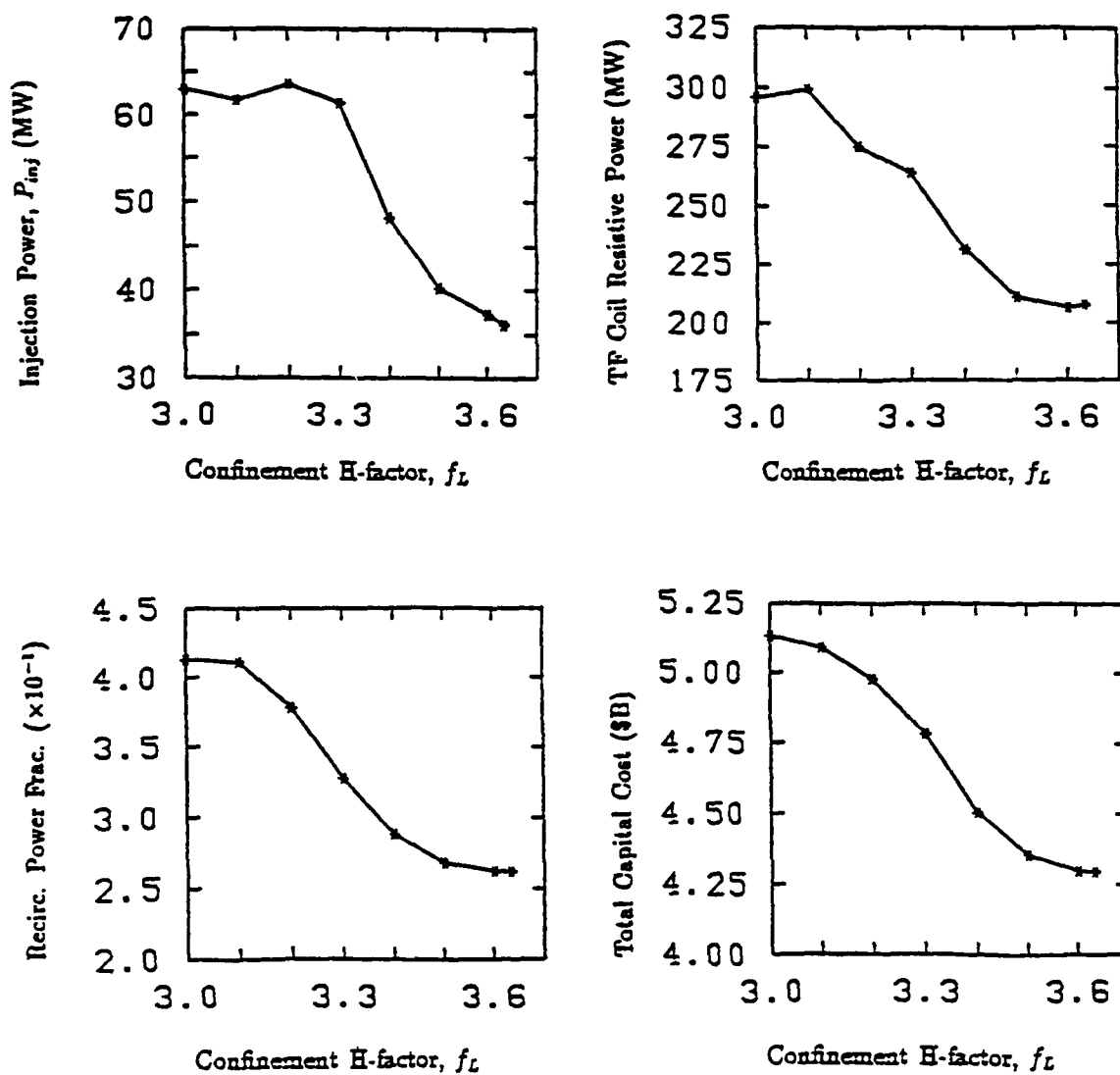


Figure 3.13: ST-2B Sensitivity to Variation of Confinement H-Factor:  $P_{inj}$ ,  $\langle T_e \rangle$ , Recirculating Power Fraction, and Total Cost versus  $f_L$

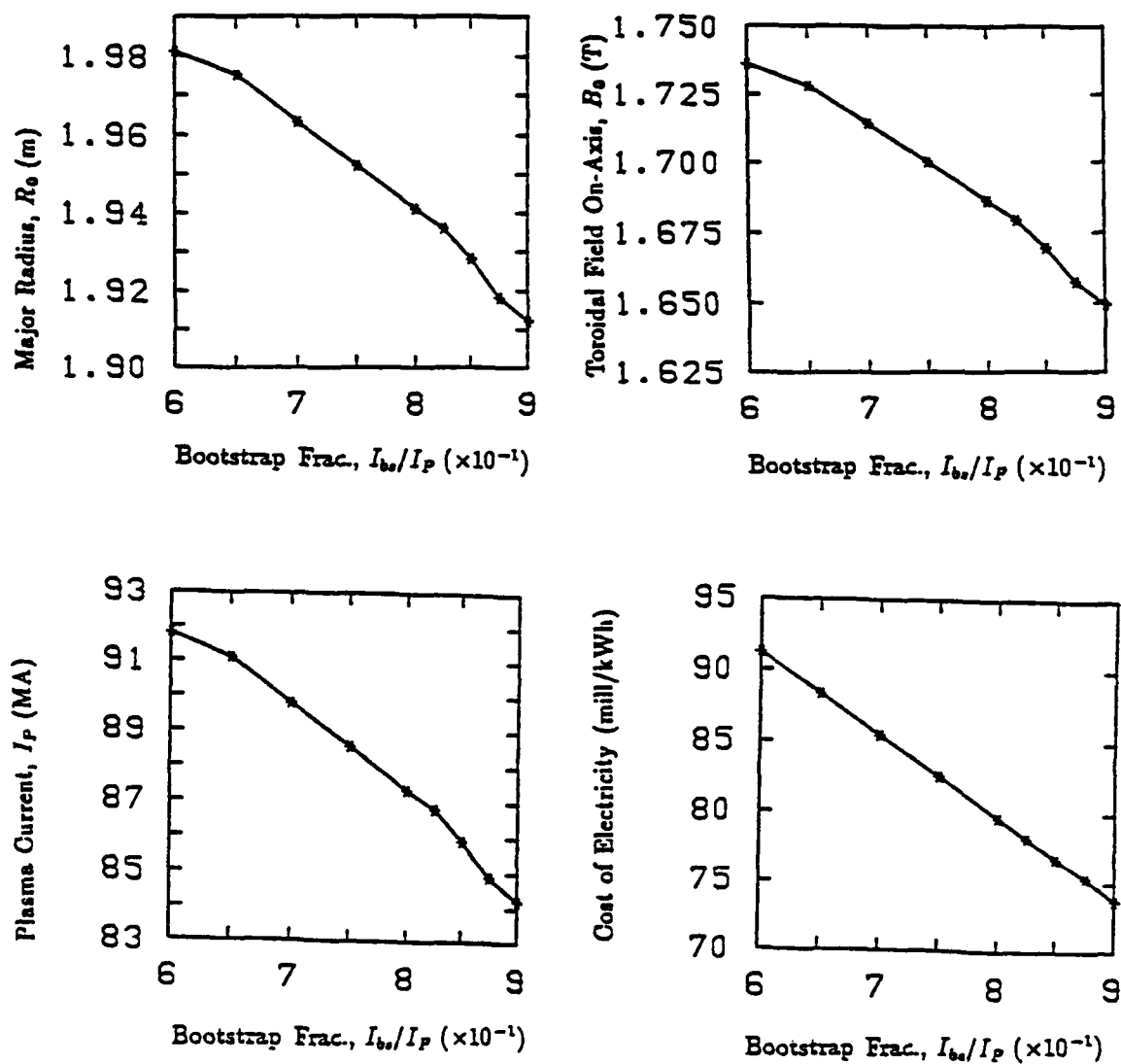


Figure 3.14: ST-2B Sensitivity to Variation of Bootstrap Current Fraction:  $R_0$ ,  $B_0$ ,  $I_P$ , and COE versus  $I_{bs}/I_P$

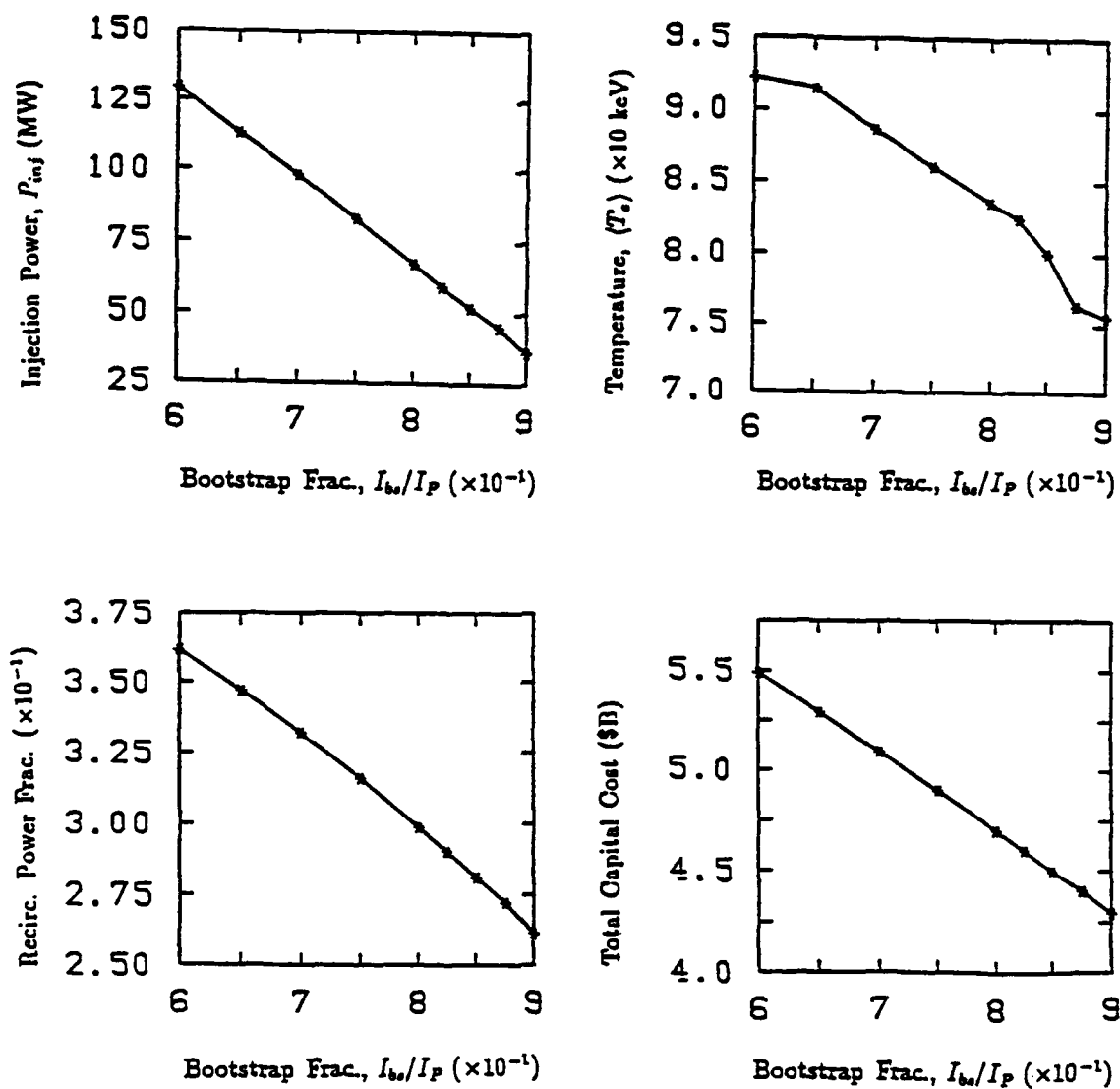


Figure 3.15: ST-2B Sensitivity to Variation of Bootstrap Current Fraction:  $P_{inj}$ , TF Coil Resistive Power, Recirculating Power Fraction, and Total Cost versus  $I_{bs}/I_P$



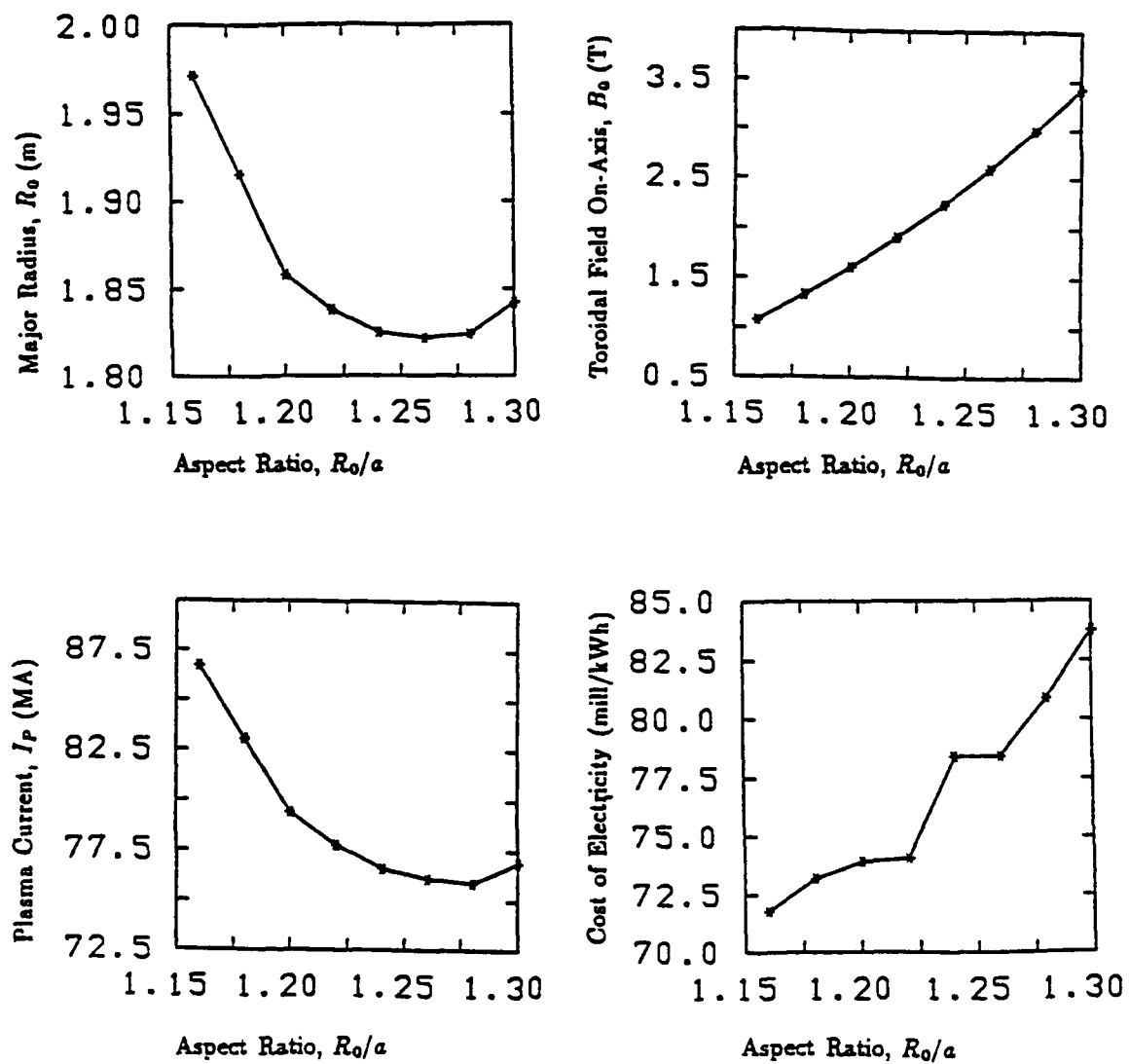


Figure 3.16: ST-2B Sensitivity to Variation of Aspect Ratio:  $R_0$ ,  $B_0$ ,  $I_P$ , and COE versus  $R_0/a$

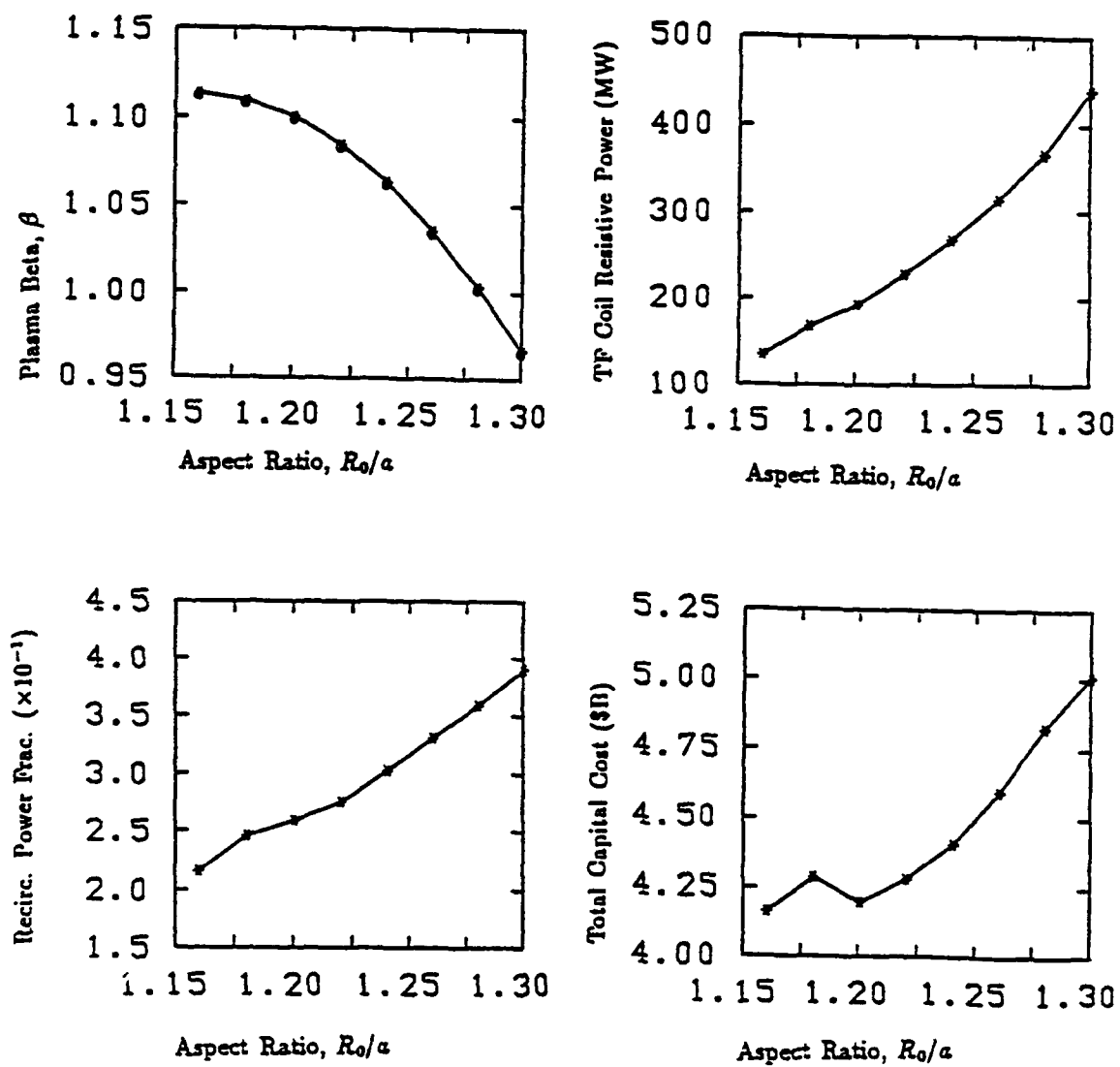


Figure 3.17: ST-2B Sensitivity to Variation of Aspect Ratio:  $\beta$ , TF Coil Resistive Power, Recirculating Power Fraction, and Total Cost versus  $R_0/a$

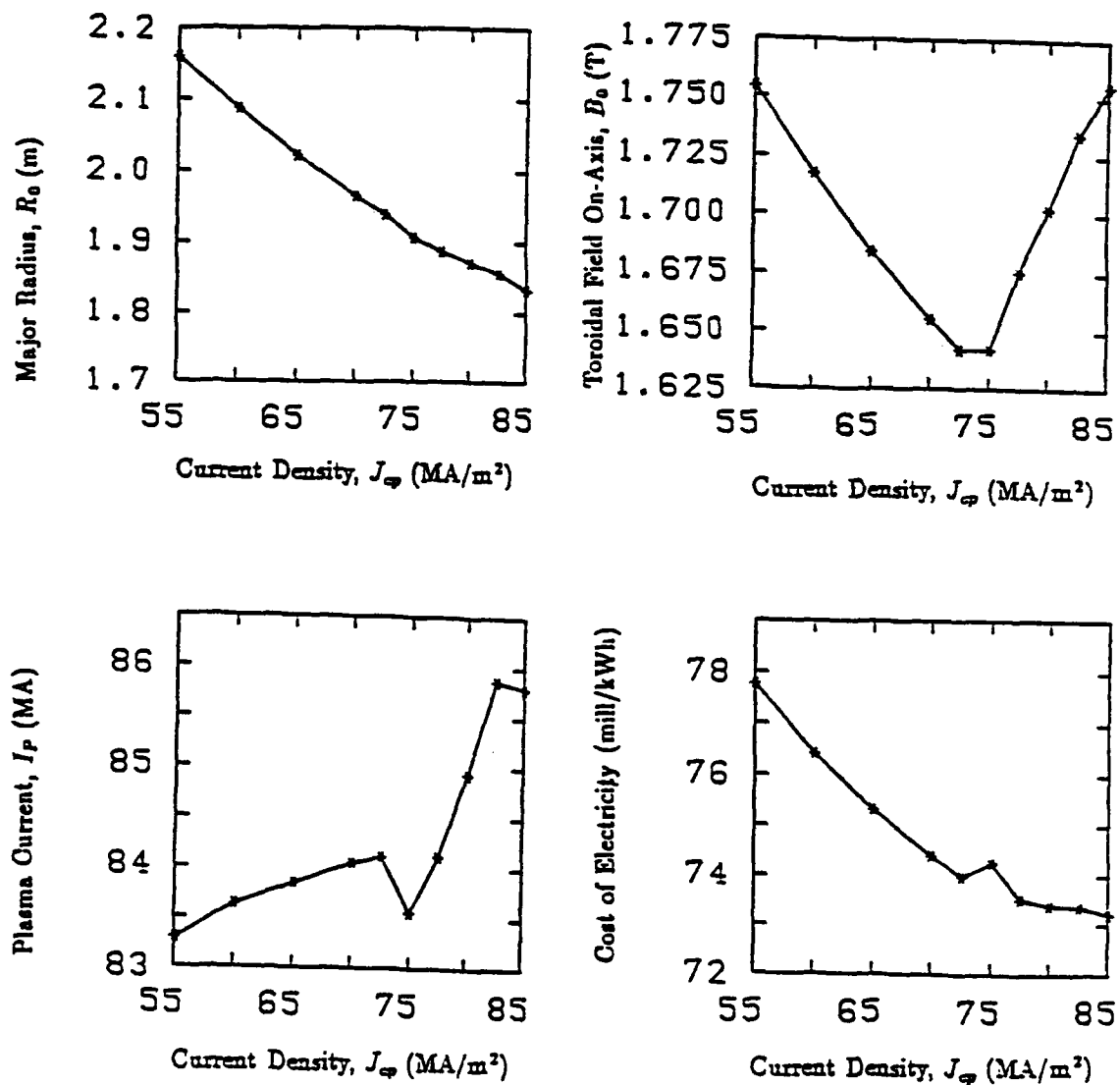


Figure 3.18: ST-2B Sensitivity to Variation of Centerpost Current Density:  $R_0$ ,  $B_0$ ,  $I_P$ , and COE versus  $J_{cp}$

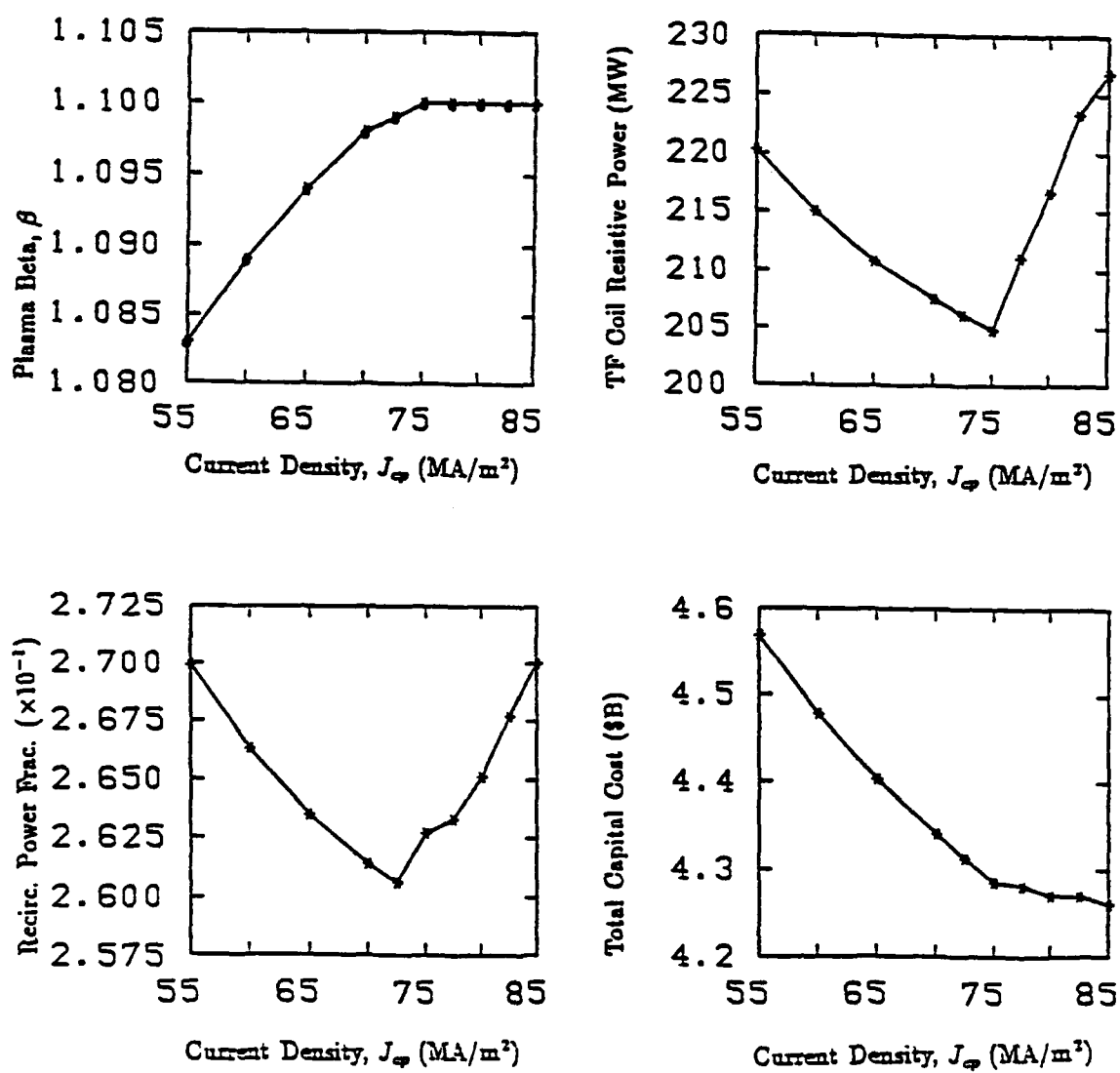


Figure 3.19: ST-2B Sensitivity to Variation of Centerpost Current Density:  $\beta$ , TF Coil Resistive Power, Recirculating Power Fraction, and Total Cost versus  $J_{cp}$

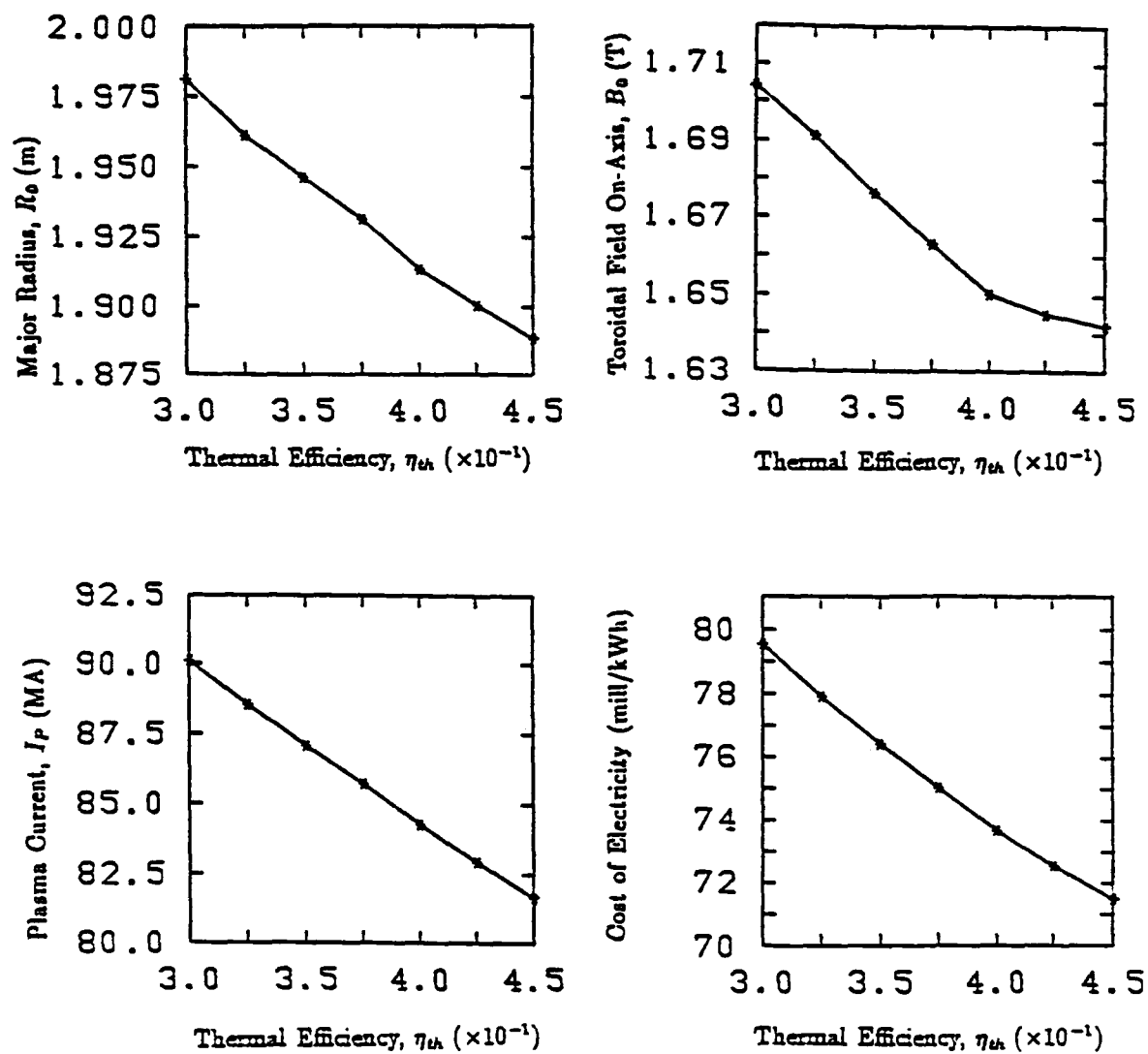


Figure 3.20: ST-2B Sensitivity to Variation of Thermal Conversion Efficiency:  $R_0$ ,  $B_0$ ,  $I_P$ , and COE versus  $\eta_{th}$

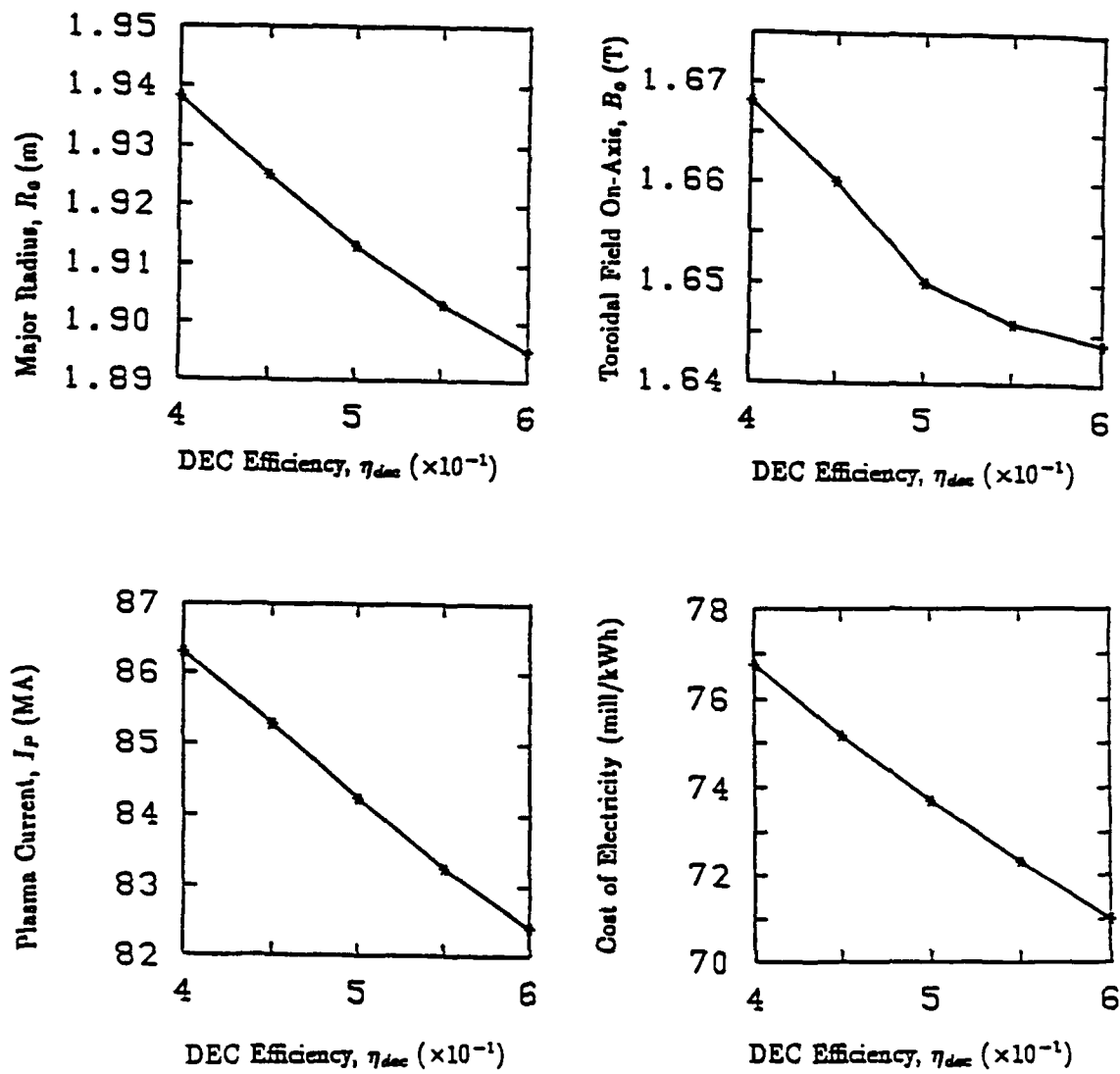


Figure 3.21: ST-2B Sensitivity to Variation of Direct Energy Conversion Efficiency:  $R_0$ ,  $B_0$ ,  $I_P$ , and COE versus  $\eta_{dec}$

## CHAPTER 4

### Discussion and Conclusions

#### 4.1 Introduction

Based on the ST-2B reference case used for the study, compact ( $R_0 < 2\text{m}$ ) D- $^3\text{He}$  fusion at low field ( $B_0 < 2\text{T}$ ) and modest cost (COE  $\sim 74$  mill/kWh, comparable to ARIES-III) appears viable. The assumptions adopted for the study represent reasonable extrapolations of physics and technology, which might be attainable by the time a D- $^3\text{He}$  ST demonstration plant could become operational ( $\sim 2050?$ ). The parametric investigations discussed in Chapter 3 describe the reactor performance sensitivities to several key parameters. The supporting database for those parameters can be refined as future experiments resolve physics issues and technological advances occur.

Assuming the ST-2B reference case represents the anticipated parameters of a D- $^3\text{He}$  ST fusion reactor, it is useful to assess its economic, safety and environmental characteristics. Among the specific reference cases examined by the Senior Committee on Environmental, Safety, and Economic Aspects of Magnetic Fusion Energy (ESECOM) [1], the D- $^3\text{He}$  tokamak was one of the most potentially attractive, but technological uncertainties and lack of design detail made its feasibility uncertain. The ESECOM analysis emphasized future development of reactor designs combining high levels of safety assurance, high mass power density, direct energy conversion, and design simplicity for reliability and ease of maintenance necessary to realize the possibility of cost-competitive electricity. The D- $^3\text{He}$  ST meets these challenges head-on. With such well-defined criteria available, the potential advantages of the ST-2B reference case may be assessed realistically and quantitatively.

## 4.2 Economic Characteristics

The COE of the ST-2B does not appear to be economically competitive with advanced fission breeder reactors, but does appear to be economically competitive with large-scale solar electric plants, as discussed in Chapter 3 (see 3.2.1). There are many uncertainties involved in the COE estimate for ST-2B. The uncertainties with the largest effects on ESECOM's estimates of COE were associated with achieving the assumed plasma beta and current-drive efficiency and with attaining plant reliability and maintainability characteristics compatible with reasonable capacity factors. These are crucial issues for the D-<sup>3</sup>He ST, too.

The design characteristics [1] offering the most important potential benefits for fusion COE are: (1) compactness, which reduces the capital cost of the fusion power core and the sensitivity of COE to plasma performance, and may ease maintenance; (2) high level of public safety assurance based on low radioactive inventories and passive mechanisms for preventing releases, which should reduce costs for active safety systems and nuclear-grade components as well as facilitating siting and licensing; and, (3) advanced energy conversion systems, which should be able to reduce balance of plant (BOP) costs and may increase capacity factors.

The ST-2B reference case combines all three features mentioned above in one design (ARIES-III is not compact and does not use advanced energy conversion). If design simplification can reduce the number of plant components and design ruggedness can enhance critical design margins and extend plant life (> 60 years), then additional reductions in the COE estimate may be possible for ST-2B. These favorable features might be able to offset some physics and technology shortcomings, and permit a D-<sup>3</sup>He ST fusion reactor to remain economically competitive. Additionally, it might be possible to design smaller modular reactors (100-500 MWe), where the potential for mass production could lower the capital cost per kilowatt capacity. A low initial capital cost would then permit the spread of nuclear energy to developing



countries and smaller communities of developed countries.

### 4.3 Safety and Environmental Characteristics

The inherent advantages of the D-<sup>3</sup>He fuel cycle (i.e., reduced neutron activation and tritium handling problems relative to the D-T fuel cycle) significantly reduces the safety and environmental risks normally associated with D-T fusion and advanced fission reactors. ESECOM's analysis of safety and environmental characteristics assessed the following areas: (1) possibilities and consequences of major releases of radioactivity from reactor accidents; (2) magnitude of the radioactive waste burden; (3) occupational and public exposures to radiation in routine operation; and, (4) unwanted links to nuclear weaponry. The next few sections assess these characteristics qualitatively and quantitatively for the ST-2B reference case.

#### 4.3.1 Risk of Major Releases of Radioactivity

The probability and consequences of major radioactivity releases during accidents for any nuclear power plant must be covered by design and demonstrated during the licensing procedure. The largest quantities of radioactivity are generally in the form of neutron activation products, most of which are embedded in solid reactor materials. Since the neutron wall load for ST-2B is about 0.6 MW/m<sup>2</sup>, which is about 25% that of a D-T tokamak, activation products in the reactor structure would accumulate more slowly. The steady-state inventory of radioactive tritium in the ST-2B plasma is less than 1 g and the total inventory in the tritium handling system is probably much less than 1 kg, but this is notably less than the anticipated tritium inventories for D-T reactors (up to 5 kg). Such a low tritium inventory in ST-2B represents a radioactive hazard an order of magnitude less than a D-T reactor and many orders of magnitude less than the fuel inventory hazard in a fission reactor.

Prominent features of fusion in general with regard to safety are the expected self-termination of the fusion process under accidental conditions and the fact that a recriticality problem does not exist. Nevertheless, the critical safety issues of concern regarding fusion reactors are [31]: (1) loss of cooling accidents; (2) loss of vacuum accidents; (3) tritium system failure; and, (4) magnet system failure. Without elaborating on the details of these issues, if an accident in ST-2B occurs, the total radioactivity release to the environment in the form of tritium and activation products can be kept below regulatory limits [31].

The ST-2B reference case was assumed to have a level of safety assurance (LSA) of 2. In a level 2 reactor, safety is assured by passive mechanisms of release limitation as long as severe reconfiguration of large-scale geometry is avoided, and escalation to fatality-producing reconfigurations from less severe initiating events can plausibly be precluded by passive design features [1]. The quantitative threshold for avoidance of early fatalities off-site is a critical whole-body dose of 200 rem at the plant boundary, assumed to be 1 km from the point of the release. Level 2 is probably a conservative assumption, considering the low level of radioactivity in ST-2B. It may be possible to warrant the classification of ST-2B as Level 1, where safety is assured by passive mechanisms of release limitation no matter what the accident sequence. For either classification, however, the passive safety features and the reduced probability of a severe accident (both in terms of public safety and investment protection) should significantly ease the siting and licensing process for a D-<sup>3</sup>He ST power plant.

#### **4.3.2 Radioactive Waste Burden**

The only radioactive wastes associated with ST-2B are those components which will contain neutron activation products, primarily the center conducting post and the first wall/shield. The fully exposed centerpost will receive neutron

damage and require replacement at regular intervals, perhaps every few years [18]. The activated centerpost, however, contains no sensitive or toxic fissile material, requires little processing, and is self-contained in a modest volume ( $\sim 10.3m^3$ ). Despite the low neutron wall load, the first wall and shield will probably accumulate a high level of radioactivity over their effective lifetimes, which will be longer for ST-2B than for D-T reactors. Two separate studies [24, 32] indicate that if low activation components are used for the first wall and shield, the criteria for Class A disposal according to 10CFR61 would be satisfied. Class A refers to minimal restriction surface storage. Components made of conventional materials such as Type 316 stainless steel and Fe1422 steel would require Class C (restricted) surface storage. In either case, these wastes would qualify for shallow burial under the current regulatory philosophy. There would be no high-level waste, such as the spent fuel elements from fission reactors, that requires deep geological disposal. The overall reduced level and volume of radioactive waste for ST-2B would permit on-site disposal until deactivation to acceptable levels, presenting minimal risk to the public and environment at minimal cost.

#### 4.3.3 Exposures to Radiation

The normal operation of nuclear power plants entail small emissions of radioactivity to the environment and some exposure of the public to radiation, as well as routine exposure of workers to radiation at plant sites. For ST-2B, radioactivity release to the environment in the form of tritium,  $^{14}C$ , and other activation products would be negligible during normal operation, well below regulatory limits. Radiological exposure of workers normally reaches its highest levels during reactor maintenance and repair. With higher capacity factors and reduced activation of components, radiological exposure of workers should be significantly lower than for

advanced fission and D-T fusion reactors. If low activation SiC composites or Al-Mg-Si alloys with impurities  $< 1$  ppm could be used as structural materials, then limited contact maintenance outside the shield may be permissible [33]. Unfortunately, the materials community cannot identify with confidence any ceramic or alloy that meets all the diverse requirements as a structural material for a fusion reactor (i.e., fabricability, mechanical strength, chemical compatibility, cost, etc.) [34].

#### 4.3.4 Nuclear Weapons Link

In general, fusion energy systems are less likely than fission energy systems to contribute to the acquisition of nuclear weapons capabilities by subnational groups because tritium is not a limiting constraint on thermonuclear weapon construction the way fissile materials are a constraint on fission weapon construction [1]. Since the tritium inventory in ST-2B is very small, even this link to nuclear weapons is tenuous. In contrast, the relative weapons potential of an advanced fission breeder reactor is very high and represents a risk to international security. It may be advantageous, however, to allow tritium to decay to  $^3\text{He}$  before it is reinjected into the plasma (as assumed for this study) at the expense of tritium storage requirements which safeguard against weapons proliferation. In general, though, a D- $^3\text{He}$  ST fusion reactor presents minimal risk and may be freely promoted throughout the world as a relatively safe power source with an unlimited fuel supply.

#### 4.4 Conclusion

The anticipated D- $^3\text{He}$  spherical torus fusion reactor demonstrates attractive economic, safety and environmental characteristics which should justify its continued research and development (R&D). This conclusion is based on assumptions about

plasma performance and engineering characteristics that are optimistic but defensible extrapolations from current experience and application of a computer model to quantitatively assess the performance of a reference case configuration. Overall, the D-<sup>3</sup>He ST reactor appears to be competitive with advanced fission breeder reactors and large-scale solar electric plants as a future energy source for the long term.

The physics and engineering extrapolations adopted for this system study highlight a number of outstanding issues which need to be resolved through continued R&D of ST reactors. These include: (1) tokamak-like confinement at very low aspect ratio; (2) stable  $\epsilon\beta_p$  of order unity; (3) plasma stability at low edge  $q$ ; (4) bootstrap current fraction of order unity; (5) power and particle control using expanded poloidal divertors with gaseous targets; (6) particle drifts and distribution functions within a direct electrodynamic convertor; (7) high energy neutral beam current drive at high plasma densities; (8) high-speed fuel pellet injection at high plasma densities and temperatures; (9) low-activation structural materials; and, (10) <sup>3</sup>He mining on the moon. These issues represent significant challenges which must be overcome before a D-<sup>3</sup>He ST reactor can be designed with confidence.

Two other aspects of D-<sup>3</sup>He ST reactor operation which will have to be addressed are plasma ignition and response to transients. This study only assumed steady-state operation at high plasma temperature. If reaching the steady-state condition requires a D-T ignition plasma, with its adverse neutron activation and tritium handling problems, then the inherent advantage of the D-<sup>3</sup>He fuel cycle will be compromised. If the D-<sup>3</sup>He plasma can be heated directly to the ignition regime with auxiliary power only, perhaps with a deuterium-rich ignition plasma [28], then D-T assisted start-up could be avoided. Operational transients, due either to minor plasma disruptions or changing load demands from the electric utility grid, require flexible response from the reactor configuration. R&D efforts must resolve what the design margins should be relative to the optimum steady-state configuration and

their impacts on COE. Since the reactor performance is highly non-linear, R&D efforts must also resolve how operators will be able to monitor and control reactor performance during transient scenarios. These are complex issues that may only be resolved through operational experience from large steady-state experiments.

## APPENDIX A

### Spherical Torus Physics Model

#### A.1 Introduction

The Spherical TORus Reactor Analysis Code (STORAC) uses a profile-averaged global model, which closely follows the method for zero-dimensional International Thermonuclear Reactor (ITER) scoping studies [35], with the exception of the particle transport effect on energy confinement. The model described here is the one used for this study, which incorporates the changes identified in Chapter 2. Meter-kilogram-second units are used throughout with the exception of kilo-electron-volts for plasma temperatures and megawatts per cubic meter for power densities, unless otherwise noted.

#### A.2 Plasma Shape and Geometry

Free-boundary magnetohydrodynamic (MHD) equilibrium calculations show that as the aspect ratio is reduced to around 1.5 for spherical torus plasmas, plasma elongation of  $\kappa \simeq 2$  occurs naturally without a significant shaping field [16]. Enhanced elongation (relative to that of tokamaks with conventional aspect ratios around 3) is a natural feature of the spherical torus. MHD calculations also show that shaping the plasma by giving it a triangularity  $\delta$  produces a stabilizing effect. The STORAC scalings for the plasma separatrix elongation and triangularity given by [19] are:

$$\kappa = 2.1(1.0 + 0.44\epsilon^{2.1})$$

$$\delta = 0.53(1.0 + 0.77\epsilon^{3.0})$$

where  $\epsilon$  is the inverse aspect ratio,  $a/R_0$ . This represents about 25% higher elongation than the natural elongation, but within acceptable limits. If the plasma is

further elongated above a critical elongation it becomes unstable to a global, mainly vertical instability [11]. For a spherical torus reactor with aspect ratio around 1.2,  $\epsilon = 0.71$ ,  $\kappa = 2.73$  and  $\delta = 0.77$ . The elongation scaling used here also fits for an ARIES-I reactor and the ITER.

The plasma surface area  $A_p$ , approximated by a revolution of two arcs which intersect the plasma x-points (assuming a double-null divertor configuration) and the plasma midplane outer radius and inner radius, is:

$$A_p = 4\pi[r_{co}\{(R + a - r_{co})\sin^{-1}(b/r_{co}) + b\} + r_{ci}\{(R - a + r_{ci})\sin^{-1}(b/r_{ci}) - b\}]$$

where  $b = \kappa a$  and the radii of curvature of the outer and inner arcs are

$$r_{co} = a \left( 1 + \frac{(\kappa^2 + \delta^2 - 1)}{2(1 + \delta)} \right)$$

$$r_{ci} = a \left( 1 + \frac{(\kappa^2 + \delta^2 - 1)}{2(1 - \delta)} \right)$$

The plasma volume  $V_p$  is the volume between these two swept arcs (ITER method),

$$V_p = V_{out} - V_{in}$$

where

$$V_{out} = -\frac{2\pi b^3}{3} + 2\pi b(r_{c1}^2 + R_1^2) + 2\pi r_{c1}\{b\sqrt{R_1^2 - b^2} + R_1^2 \sin^{-1}(b/R_1)\}$$

$$V_{in} = -\frac{2\pi b^3}{3} + 2\pi b(r_{c2}^2 + R_2^2) + 2\pi r_{c2}\{b\sqrt{R_2^2 - b^2} + R_2^2 \sin^{-1}(b/R_2)\}$$

$$r_{c1} = \frac{(R + a)^2 - (R - \delta a)^2 - b^2}{2a(1 + \delta)}$$

$$r_{c2} = \frac{(R - a)^2 - (R - \delta a)^2 - b^2}{2a(1 - \delta)}$$

$$R_1 = R + a - r_{c1}$$

$$R_2 = r_{c2} - R + a$$



### A.3 Plasma Current

The plasma current ( $I_P$ ) scaling used for a spherical torus is a function of the edge safety factor ( $q_\psi$ ), toroidal magnetic field on-axis ( $B_0$ ), and plasma geometry. In any toroidal plasma with a finite aspect ratio, the exact relationship among  $q_\psi$ ,  $I_P$ ,  $B_0$ ,  $R$ , and  $a$  is complex. For  $A < \kappa^2/(1 + \delta) + \delta$ , which is normally the case for spherical torus plasmas, the plasma current scaling given by [19] is

$$I_P(MA) = \frac{5a(m)B_p(T)\kappa}{\pi} \left( \frac{\sin^{-1}(E_1)}{E_1} + \frac{\sin^{-1}(E_2)}{E_2} \right)$$

where the relationship between the average poloidal field at the plasma edge ( $B_p$ ) and the toroidal magnetic field on axis ( $B_0$ ) is

$$B_p(T) = \frac{B_0(T)}{2\pi q_\psi} (F_1 + F_2)$$

$$F_1 = f_1 \left( g - h_1 \ln \left( \frac{1 + y_1}{1 - y_1} \right) \right) \quad F_2 = f_2 [g + 2h_2 \tan^{-1}(y_2)]$$

$$f_1 = \frac{d_1(1 + \delta)\epsilon}{(1 + \epsilon)(c_1\epsilon - 1)} \quad f_2 = \frac{d_2(1 - \delta)\epsilon}{(1 - \epsilon)(c_2\epsilon + 1)}$$

$$g = \epsilon\kappa/(1 - \epsilon\delta)$$

$$h_1 = \frac{1 + (1 - c_1)\epsilon/2}{\sqrt{(1 + \epsilon)(c_1\epsilon - 1)}} \quad h_2 = \frac{1 + (c_2 - 1)\epsilon/2}{\sqrt{(1 - \epsilon)(c_2\epsilon + 1)}}$$

$$y_1 = \sqrt{\frac{c_1\epsilon - 1}{1 + \epsilon}} \frac{1 + \delta}{\kappa} \quad y_2 = \sqrt{\frac{c_2\epsilon + 1}{1 - \epsilon}} \frac{1 - \delta}{\kappa}$$

$$E_1 = \frac{2\kappa}{d_1(1 + \delta)} \quad E_2 = \frac{2\kappa}{d_2(1 - \delta)}$$

$$c_1 = \kappa^2/(1 + \delta) + \delta \quad c_2 = \kappa^2/(1 - \delta) - \delta$$

$$d_1 = \left( \frac{\kappa}{1 + \delta} \right)^2 + 1 \quad d_2 = \left( \frac{\kappa}{1 - \delta} \right)^2 + 1$$

The edge safety factor is an important parameter which is related to the fluid stability of the plasma-field configuration. It is defined as  $q_\psi = aB_0/R_0B_p$ , which represents the number of rotations a magnetic field line makes in the toroidal direction per rotation in the poloidal rotation (i.e., the helical twisting of the field lines

around the torus). For a given machine,  $q_\psi$  is a decreasing function of the plasma current and is a convenient parameter to use because it presents a lower limit below which the MHD stability of the plasma is compromised. Safe operation for tokamaks is normally obtained for  $q_\psi > 3.0$  [36]. The default scaling assumed in STORAC for the edge safety factor limit given by [19] is

$$q_\psi = 3.0(1 + 2.6\epsilon^{2.8})$$

For an aspect ratio of 1.2,  $q_\psi \geq 7.68$ . The parameter  $q_\psi$  itself is not derived in the STORAC calculations; it is either input as a fixed value or iterated as a program variable to be greater than or equal to the assumed  $q_\psi$  limit.

It is also desirable to have a simple formula for the safety factor which can be used to calculate the energy confinement time  $\tau_E$  for various scalings. The edge safety factor is typically evaluated on the surface which contains 95% of the total flux enclosed by the separatrix. For a spherical torus, the assumed MHD  $q$ -value at 95% flux is

$$q_\psi(95\%) = q_\psi \times 1.3(1.0 - \epsilon)^{0.6}$$

For an aspect ratio around 1.2,  $q_\psi(95\%) \simeq 3.41$ . Plasma confinement tends to deteriorate with low- $q$  operation [35], and a value of  $q_\psi(95\%) - q(0)$  larger than 2 is assumed to provide sufficient global shear for stability of kink modes in ITER-like reactors. Since the scalings used here are aspect ratio dependent, and may not be appropriate at very low aspect ratio, low- $q$  confinement effects in a spherical torus are unknown. Optimistically, lower values of  $q_\psi$  and  $q_\psi(95\%) - q(0)$  sufficient for stability might be possible.

#### A.4 Bootstrap Current

It is predicted theoretically [37] that radial diffusion induces a current in the toroidal direction and that the current becomes large in the trapped particle region. In a plasma with a finite pressure gradient and an applied magnetic field, the

superposition of the Larmor orbits of the plasma particles creates a diamagnetic 'bootstrap' current perpendicular to both the magnetic field and the pressure gradient. For an axially symmetric and collision free system, the steady-state current density due to the net electron flow derived in [38] is

$$J_{bs} \approx -\frac{\epsilon^{1/2}}{B_p} \frac{\partial p}{\partial r}$$

where  $\epsilon$  is the inverse aspect ratio. In a tokamak plasma, the radial pressure gradient generates a substantial current parallel to the helical magnetic field. A large bootstrap current is also expected to be generated in the core plasma with central pellet deposition and heating, and in the edge plasma in the H-regime [11]. A completely bootstrapped device is not possible, however, and a small "seed" current must still be driven in the center of the plasma, where the pressure gradient is negligible. The seed current is then amplified by the bootstrap effect in the plasma.

An empirical fit for the bootstrap current fraction assumed for ITER [35] is

$$I_{bs}/I = C_{bs}(\epsilon^{0.5}\beta_p)^{1.3}$$

where

$$C_{bs} = 1.32 - 0.235[q_\psi(95\%)/q(0)] + 0.0185[q_\psi(95\%)/q(0)]^2$$

$$\beta_p = \frac{\langle p \rangle}{B_p^2/2\mu_0} = \beta \left( \frac{B_0}{B_p} \right)^2$$

$$B_p = \frac{I_p}{5\langle a \rangle}$$

and

$$\langle a \rangle = [V/(2\pi^2 R_0)]^{1/2}$$

is the effective plasma radius.

This empirical scaling is probably inappropriate for very low aspect ratios (relative to ITER). Therefore, the maximum bootstrap current fraction is optimistically assumed to be 90% of the total plasma current (ARIES-III assumes 91.1%).

It may be possible to achieve such a large bootstrap contribution by varying the various plasma profiles and geometries, as indicated by the pressure gradient and  $I_p$  dependence shown in the previous equations. To benefit substantially from bootstrap current generation, a peaked density profile provided by central fueling of the plasma may be desirable.

### A.5 Profile Effects

STORAC uses a profile-averaged global model to evaluate tokamak performance. A zero-dimensional analysis considers only relationships between averaged quantities and ignores any dependence on poloidal coordinates. Poloidal sections of constant density and temperature are represented by a family of concentric and similar ellipses given by [36] as

$$\frac{x^2}{a^2} + \frac{y^2}{b^2} = \rho^2$$

where  $a$  and  $b$  are the horizontal and vertical minor radii of the plasma poloidal cross section, respectively, and  $\rho$  is a nondimensional radial coordinate equal to 1 at the plasma boundary. The radial plasma profiles of density and temperature are assumed to be of a parabolic form

$$X(\rho) = X_0 [1 - \rho^2]^{\alpha_X}$$

where  $X = n, T$ . The average density, average temperature and density-weighted temperature are

$$\langle n \rangle = \frac{1}{V} \int_V n dV = \frac{n_0}{1 + \alpha_n}$$

$$\langle T \rangle = \frac{1}{V} \int_V T dV = \frac{T_0}{1 + \alpha_T}$$

and

$$[T] = \frac{\int_V n T dV}{\int_V n dV} = T_0 \frac{1 + \alpha_n}{1 + \alpha_n + \alpha_T}$$

where  $n_0$  and  $T_0$  are the peaked density and temperature on the magnetic axis. The density and temperature profiles may then be modeled by expressions of the following nondimensional form:

$$n(\rho) = n_0(1 - \rho^2)^{\alpha_n} = \langle n \rangle (1 + \alpha_n)(1 - \rho^2)^{\alpha_n}$$

$$T(\rho) = T_0(1 - \rho^2)^{\alpha_T} = \langle T \rangle (1 + \alpha_T)(1 - \rho^2)^{\alpha_T}$$

The parameters  $\alpha_n$  and  $\alpha_T$  represent parabolic profile exponents, where  $\alpha_X = 0$  depicts a perfectly flat profile and larger values depict increasingly peaked parabolic profiles. The nominal values  $\alpha_n = 0.5$  and  $\alpha_T = 1.0$ , comparable with ITER assumptions, are used as default values. Actual profiles would have to be refined based on detailed MHD equilibrium and stability analysis to ensure that the pressure profile is consistent with the current density profile, which is not considered in STORAC.

The relatively flat density profile is consistent with expectations for operation in the H-mode regime, where density profiles tend to be very flat and even inverted [39]. Disregarding inverted profiles,  $0 < \alpha_n^{flat} < 0.75$  may be taken as a reasonable range. However, recent experience with frozen fuel pellets and neutral beam injection indicates very peaked density profiles in H-mode are possible. A significant problem with producing a fuel pellet containing  $^3\text{He}$  is that it does not solidify unless it is pressurized to about 30 atmospheres. It might be possible to encapsulate liquid  $^3\text{He}$  in a thin-walled polymetric shell overcoated with frozen deuterium, and inject such a pellet at velocities high enough to compensate for the increased ablation rate associated with high D- $^3\text{He}$  plasma temperatures [5]. Assuming a peaked density distribution can be formed and heated effectively, peaking factors of  $n_0/\langle n \rangle = 2.5$  to 4 are possible, corresponding to  $1.5 < \alpha_n^{peaked} < 3$  as a reasonable range. To sustain peaked density profiles given present pellet injector technology, however, a means of creating faster pellets will have to be developed.

The peaked temperature profile appears to be consistent with theoretical expectations. The temperature profile exponent,  $\alpha_T$ , may be derived in the following

way [39]. First, in resistive steady-state with classical resistivity,  $J \propto T^{3/2}$ . So,  $J_0/\langle J \rangle = 1 + \alpha_J = 1 + \frac{3}{2}\alpha_T$ . This then implies  $q_\psi(95\%)/q(0) = 1 + \frac{3}{2}\alpha_T$ . Taking  $q(0) = 1.0$  (e.g., with sawtooth oscillations), and  $q_\psi(95\%) \simeq 3.4$ , we have  $\alpha_T \simeq 1.6$ . For the second stability regime, assuming  $q(0) = 2.0$  and  $q_\psi(95\%) \simeq 3.4$ , we have  $\alpha_T \simeq 0.5$ . This derivation is not necessarily true for beam driven cases, as assumed for this study, so some corrections must be allowed. The temperature profile could be more peaked than this, e.g., with sawtooth stabilization or with highly peaked heating profiles. It could also be flatter due to naturally high elongations,  $\kappa \geq 2.5$ . Therefore, a mean value of  $\alpha_T = 1.0$  appears consistent with the previous considerations and a flat probability distribution  $0.5 < \alpha_T < 1.5$  is assumed as a reasonable range.

#### A.6 Steady-State Particle Balance

The steady-state densities of the various species present in a burning plasma are determined by a detailed particle balance calculation. In addition to the consumption and production of various species in a burning plasma, a realistic steady-state particle balance must consider the fueling of the plasma, the presence of impurity concentrations, the trapping fraction of the various energetic fusion products, and the diffusion loss of charged particles out of the plasma. Initial assumptions must define density and temperature parameters, an effective  ${}^3\text{He:D}$  fuel ratio, and effective steady-state impurity concentrations. Diffusion losses from the plasma are based on the calculated global energy confinement time  $\tau_E$ , and the required fuel injection rates are calculated to balance total losses and maintain plasma density. The final steady-state particle balance, however, is constrained by the effective density and beta limits of the plasma configuration.

The steady-state particle balance equations which describe the diffusion loss,

fuel injection, production and consumption of a given species are of the form

$$\frac{\partial n_f}{\partial t} = -\frac{n_f}{\tau_p^f} + S_f + \sum_{i,j} n_i n_j \delta_{ij} \langle \sigma v \rangle_{ij} \eta_f - \sum_i n_i n_f \langle \sigma v \rangle_{if}^b = 0$$

where  $i$  and  $j$  represent the appropriate species for reaction  $ij$  which produces species  $f$ . The term  $n_f/\tau_p^f$  is the diffusion loss rate and  $S_f$  is a source term representing the fuel injection rate for species  $f$ . The fusion reaction rates  $\langle \sigma v \rangle_{ij}$  which govern particle production and consumption represent the following five fusion reactions [7]:  $ij=dd1$  for  $D(D,P)T$ ,  $dd2$  for  $D(D,n)^3\text{He}$ ,  $dhe3$  for  $D(^3\text{He},P)\alpha$ ,  $dt$  for  $D(T,n)\alpha$ , and  $tt$  for  $T(T,2n)\alpha$ . For like particles,  $\delta_{ij} \simeq 1/2$  when  $i = j$ , otherwise  $\delta_{ij} \simeq 1$  when  $i \neq j$ . For D-T plasmas operating at 10-20 keV, the  $dd1$  and  $dd2$  reactions occur with nearly equal probability at a 50:50 ratio. For D- $^3\text{He}$  plasmas operating at 50-80 keV, however, the ratio 53:47 is a more accurate depiction of the  $dd1$  and  $dd2$  reaction rates, respectively.

The fractions of particles trapped on their first orbit are modelled by adjustable parameters  $\eta_f$ , where  $f$  represents 3.02 and 14.7 MeV protons (written as subscripts P3 and P14), 1.01 MeV tritons (T), 0.82 MeV  $^3\text{He}$  particles ( $^3\text{He}$ ) and the 3.5 and 3.7 MeV alpha particles ( $\alpha$ ) produced by the fusion reactions. The trapping fractions of fusion particle energy in the plasma depend on the magnitude of the plasma current [28]. Since the plasma current is generally much larger than 14/A MA, most of the 14.7 MeV protons can be confined and all of the slower particles are assumed to be confined. The default trapping fractions  $\eta_f$  are assumed to be 1, except  $\eta_{P14} = 0.9$  for the 14.7 MeV protons.

All particle confinement times are assumed to have the same value of  $\tau_p$ . If the energy confinement time  $\tau_E$  includes both convection and conduction power losses, then

$$\frac{1}{\tau_E} = \frac{1}{\tau_c} + \frac{C}{\tau_p}$$

where  $\tau_c$  is the confinement time associated with conductive power losses [19]. If we assume  $C=1$ , a default value that determines the power loss associated with the

outward flow of particles from the core plasma, and a ratio  $\tau_r = \tau_p/\tau_c = 2$ , which is at the low end of the experimental and theoretical indications, then the above equation may be rewritten as

$$\frac{1}{\tau_E} = \frac{2}{\tau_p} + \frac{1}{\tau_p} = \frac{3}{\tau_p}$$

or simply  $\tau_p/\tau_E \simeq 3$ , where the factor 3 may be varied as an input parameter. It is important to note here that this is a very simple approximation, and that global parameters such as the energy and particle confinement times do not adequately describe the physics of the D-<sup>3</sup>He and D-D-D burning plasmas [40].

The default value for the effective fuel ratio  $f_{3D}$  equal to  $n_3/n_D$  is 1.0, which assumes  $n_D = n_3$ . An important feature of D-<sup>3</sup>He fuel cycles is that the maximum value of the fusion power density achievable is virtually independent of  $f_{3D}$ , allowing optimization with respect to other design parameters [4]. A deuterium lean fuel mixture has the advantage of reducing the dd reactions and the production of tritium, thus reducing the tritium handling problem as well as producing fewer neutrons. A deuterium rich fuel mixture has the advantage of reducing the relative electron density and radiation losses. An optimum fuel mixture for tokamaks is estimated to be about 35% <sup>3</sup>He and 65% D [5]. A reasonable range for the fuel ratio is  $0.5 < f_{3D} < 2.0$ , which represents a realistic operating domain within D-<sup>3</sup>He ignition space [4].

A D-<sup>3</sup>He plasma is assumed to contain reasonable concentrations of representative low-Z (carbon, oxygen) and small amounts of high-Z (iron, tungsten, etc.) impurities. A low oxygen concentration is expected because tokamaks with long periods of operation and hot walls have less oxygen than those with cold walls or low power cases, and carbon concentrations drop at high densities ( $n_C \sim 1/n_e$ ). The iron concentration is typically very low because little or no Fe-bearing materials are expected to be used as a first wall, but may be considered representative of high-Z impurities which may be present. Experimental observations give the following



simple fits [35], normalized at  $\langle n_e \rangle = 0.7 \times 10^{20} \text{m}^{-3}$ , which are used as defaults:

$$n_C/n_e = [0.9 + 0.6(0.7e20/n_e)^{2.6}] \%$$

$$n_O/n_e = 0.1 \%$$

$$n_{Fe}/n_e = [0.05(0.7e20/n_e)^{2.3}] \%$$

Seven simultaneous equations may now be written which will solve for seven unknowns:  $n_P$ ,  $n_D$ ,  $n_T$ ,  $n_3$ ,  $n_\alpha$ ,  $S_D$ , and  $S_3$ . Particle balance equations for the five species, a charge balance equation (which includes a term for the neutral beam density,  $n_{beam}$ ), and the fuel ratio equation are required for solution of the steady-state particle balance. These equations are:

$$\frac{n_P}{\tau_p} = 0.47n_D^2 \langle \sigma v \rangle_{dd1} \eta_{P3} + n_D n_3 \langle \sigma v \rangle_{dhe3} \eta_{P14}$$

$$\frac{n_D}{\tau_p} = S_D - 0.47n_D^2 \langle \sigma v \rangle_{dd1} - 0.53n_D^2 \langle \sigma v \rangle_{dd2} - n_D n_3 \langle \sigma v \rangle_{dhe3} - n_D n_T \langle \sigma v \rangle_{dt}$$

$$\frac{n_T}{\tau_p} = S_T + 0.47n_D^2 \langle \sigma v \rangle_{dd1} \eta_T - n_D n_T \langle \sigma v \rangle_{dt} - n_T^2 \langle \sigma v \rangle_{tt}$$

$$\frac{n_3}{\tau_p} = S_3 + 0.53n_D^2 \langle \sigma v \rangle_{dd2} \eta_{He} - n_D n_3 \langle \sigma v \rangle_{dhe3}$$

$$\frac{n_\alpha}{\tau_p} = n_D n_3 \langle \sigma v \rangle_{dhe3} \eta_\alpha + n_D n_T \langle \sigma v \rangle_{dt} \eta_\alpha + n_T^2 \langle \sigma v \rangle_{tt}$$

$$n_e = (n_P + n_D + n_T + n_{beam}) + 2(n_3 + n_\alpha) + 6n_C + 8n_O + 26n_{Fe}$$

$$\frac{n_3}{n_D} = f_{3D}$$

The fusion reaction rates  $\langle \sigma v \rangle_{ij}$  (where  $\sigma$  is the reaction cross section,  $v$  is the relative speed of the reactants, and the brackets indicate averaging over the Maxwellian velocity distribution of the reacting species) are volume averaged using the density and temperature profiles where  $n_i = \langle n_i \rangle$ ,  $n_j = \langle n_j \rangle$ , and

$$\langle \sigma v \rangle_{ij}(\alpha_n, \alpha_T, \langle T \rangle) = 2(1 + \alpha_n)^2 \int_0^1 \rho(1 - \rho^2)^{2\alpha_n} (\overline{\sigma v})_{ij}[\langle T \rangle(1 + \alpha_T)(1 - \rho^2)^{\alpha_T}] d\rho$$

where  $(\overline{\sigma v})_{ij}$  is the temperature dependent Maxwellian reaction rate [41].

Disregarding the second and fourth equations for now, the other five equations are used to solve for  $n_P$ ,  $n_T$ ,  $n_3$  and  $n_\alpha$  in terms of  $n_D$ . Assuming tritium recycling, in which tritium diffusion losses are injected back into the plasma at an equal rate, allows for the substitution  $S_T = n_T/\tau_p$  in the third equation. No additional tritium fueling of the plasma is assumed. Recycling of tritium hardens the neutron spectrum and does not do much to improve the attainable power density, but does minimize the tritium storage requirement (with its inherent radioactivity and weapons proliferation risks). Letting  $n_3 = n_D f_{3D}$  and  $n_e - n_{beam} - 6n_C - 8n_O - 26n_{Fe} = C$ , a constant, the original seven equations are reduced to the following four equations with four unknowns:

$$\begin{aligned}\frac{n_P}{\tau_p} &= 0.47n_D^2 \langle \sigma v \rangle_{dd1} \eta_{P3} + n_D^2 f_{3D} \langle \sigma v \rangle_{dhe3} \eta_{P14} \\ 0 &= 0.47n_D^2 \langle \sigma v \rangle_{dd1} \eta_T - n_D n_T \langle \sigma v \rangle_{dt} - n_T^2 \langle \sigma v \rangle_{tt} \\ \frac{n_\alpha}{\tau_p} &= n_D^2 f_{3D} \langle \sigma v \rangle_{dhe3} \eta_\alpha + n_D n_T \langle \sigma v \rangle_{dt} \eta_\alpha + n_T^2 \langle \sigma v \rangle_{tt} \eta_\alpha \\ C - n_P - (1 + 2f_{3D})n_D - n_T - 2n_\alpha &= 0\end{aligned}$$

Now  $n_P$ ,  $n_T$  and  $n_\alpha$  are calculated in terms of  $n_D$  only, with all other terms representing constants.

$$\begin{aligned}n_P &= \tau_p (0.47 \langle \sigma v \rangle_{dd1} \eta_{P3} + f_{3D} \langle \sigma v \rangle_{dhe3} \eta_{P14}) n_D^2 \\ n_T &= \frac{-\langle \sigma v \rangle_{dt} + \sqrt{\langle \sigma v \rangle_{dt}^2 + 1.88 n_D^2 \langle \sigma v \rangle_{dd1} \langle \sigma v \rangle_{tt} \eta_T}}{2 \langle \sigma v \rangle_{tt}} \\ n_\alpha &= \tau_p (n_D^2 f_{3D} \langle \sigma v \rangle_{dhe3} \eta_\alpha + n_D n_T \langle \sigma v \rangle_{dt} \eta_\alpha + n_T^2 \langle \sigma v \rangle_{tt} \eta_\alpha)\end{aligned}$$

Note now

$$C - n_P - (1 + 2f_{3D})n_D - n_T - 2n_\alpha = 0$$

is a function of  $n_D$  only and may be solved numerically for the steady-state deuterium density in the plasma. STORAC solves for the zero of the function  $f(n_D)=0$  and returns the value for  $n_D$ . The other steady-state particle densities are then calculated

using the previously derived equations. The second and fourth equations of the original set are now used to calculate the source terms,  $S_D$  and  $S_3$ , representing the fuel injection rates required to maintain the steady-state particle balance.

### A.7 Density Limit

The density limit imposes an upper limit on the plasma edge density. A "weak" limit is usually assumed, implying that no *a priori* density limit is to be imposed. An optimistic estimate of what is achievable under best conditions is probably provided by the boundary of the accessible edge physics parameter space. Tentatively, the Borrass density limit for an ITER like device given by [35] is

$$n_e^{\text{crit}} \approx C [P_{\perp}^{0.53} B_0^{0.31} / (q_{\psi} R_0)^{0.22}]$$

where  $n_e^{\text{crit}} (10^{20} \text{m}^{-3})$  is the critical plasma density at the separatrix,  $q_{\psi} = q_{\psi}(95\%)$ ,  $P_{\perp} (\text{MW}/\text{m}^2)$  is the mean heat flux across the separatrix, and  $C \approx 1.8$  for ITER-like conditions. STORAC uses a modified Borrass model for the spherical tokamak of the form

$$n_{e,20}^{\text{crit}} \approx 0.1425 \times 10^{20} \frac{\langle n_e \rangle}{n_{e95}} [P_{\perp}^{0.57} B_t^{0.31} / (q R_0)^{0.1}]$$

where the factor  $0.1425 \times 10^{20}$  accounts for the density in the scrape-off layer relative to the average plasma density. The density limit may be exceeded, which has been observed experimentally in discharges with pellet injection or strong additional heating [36]. To allow for slightly higher densities during H-mode operation, the density limit constraint is modified by  $\sqrt{2}$  [27] and imposed as a default.

### A.8 Beta Limit

The plasma beta,  $\beta$ , is defined as the ratio of kinetic pressure to confining magnetic pressure and is a measure of the efficiency with which the magnetic field confines the plasma. The total volume average plasma beta is the sum of the thermal

plasma ( $\beta_{th}$ ), fast particle ( $\beta_{fast}$ ), and energetic beam ( $\beta_{beam}$ ) contributions. These components are:

$$\begin{aligned}\beta_{th} &= \frac{\langle n_e T_e + n_i T_i \rangle}{B^2/2\mu_0} \\ \beta_{fast} &= \frac{2n_f \langle E_{fast} \rangle / 3}{B^2/2\mu_0} \\ \beta_{beam} &= \frac{2n_{beam} E_{beam} / 3}{B^2/2\mu_0}\end{aligned}$$

where  $B$  is the total magnetic field in the plasma approximated as  $(B_0^2 + B_p^2)^{1/2}$ ,  $\mu_0$  is the permeability of free space ( $4\pi \times 10^{-7}$  H/m),  $\langle E_{fast} \rangle$  is the average fast particle energy approximated as  $0.30E_{fast}$  (about 1/3 of the fast particle's birth energy), and the beam density and energy are defined by current drive requirements.

The plasma beta can be limited by either the Troyon beta limit ( $\beta_f$ , appropriate for the first stability regime) or the  $\epsilon\beta_p$  limit ( $\beta_s$ , appropriate for the second stability regime), where

$$\beta_f \leq 10^{-8} \times g_f \frac{I_p(MA)}{a(m)B_t(T)}$$

and

$$\beta_s \leq g_s \left( \frac{B_p}{B} \right)^2 A$$

For steady-state operation, a Troyon coefficient  $3.0 < g_f < 3.3$  seems to represent the most likely region of operation, although the DIII-D tokamak has operated stably with  $g_f$  as high as 3.5 [39]. The default  $g_s$  value for the maximum  $\epsilon\beta_p$  is 0.6 for operation in the 1st stability regime and 1.0 for operation in the second stability regime.  $\epsilon$  is the inverse aspect ratio and the poloidal beta is

$$\beta_p = \frac{\langle n_e T_e + n_i T_i \rangle}{B_p^2/2\mu_0} = \beta \left( \frac{B}{B_p} \right)^2$$

Due to plasma paramagnetism effects and the definition of the total volume averaged plasma beta used in this model, beta values may exceed unity as  $\epsilon\beta_p$  values approach or exceed unity [27]. The  $\epsilon\beta_p$  limit is considered to be a more important constraint than the Troyon beta limit, but there is much speculation regarding how

high  $\epsilon\beta_p$  can safely go. However, requiring the bootstrap current to be less than the total plasma current for equilibrium (see A.4) may represent a type of beta limit. This was not included in any calculations for this study, but could be considered in future studies.

### A.9 Global Plasma Power Balance Equations

The general global plasma power balance equation for D-<sup>3</sup>He plasmas with electron temperature  $T_e$  and ion temperature  $T_i = T_D = T_{He}$  given by [28] is

$$\frac{d}{dt} \left[ \frac{3}{2} (n_D + n_3 + n_e/\gamma_i) K T_i \right] = P_F + P_{oh} + P_{aux} - P_{con} - P_{rad} - P_{ie}$$

where  $\gamma_i = T_i/T_e$  is the ion to electron temperature ratio,  $K$  is the Boltzmann constant,  $P_F$  is the fusion power density,  $P_{oh}$  is the ohmic heating power density,  $P_{aux}$  is the auxiliary heating power density,  $P_{con}$  is the conduction and convection loss term,  $P_{rad}$  is the bremsstrahlung and synchrotron radiation loss term, and  $P_{ie}$  is the equilibration power between ions and electrons when  $T_i$  and  $T_e$  are not equal. This study assumes  $T_i = T_e$ , so  $P_{ie} = 0$ . All background ions are assumed to be at the same local temperature,  $T_i(\rho)$ , and to have a common profile. In steady-state, the  $\frac{d}{dt}$  term equals zero, thus

$$P_F + P_{oh} + P_{aux} = P_{con} + P_{rad}$$

The global plasma power balance constraint equation used in STORAC, which requires an ignition margin to equal total power sources divided by total power losses, is

$$1 - \left( \frac{P_{con} + P_{rad-c}}{P_F + P_{oh} + P_{aux}} \right) \times IM \leq \epsilon$$

where  $\epsilon \simeq 0$  is an error tolerance, usually  $10^{-3}$  or  $10^{-4}$ . IM is the ignition margin, assumed to be 1 by default. Only the core radiation power loss ( $P_{rad-c}$ ) is included in the global power balance equation. The edge radiation is assumed to be lost to the divertor region.

The fusion power density (in  $MW/m^3$ ), calculated by summing over all fusion reactions, is:

$$P_F = [0.47n_D^2 \langle \sigma v \rangle_{dd1}(1.01\eta_T + 3.02\eta_{P3}) + 0.53n_D^2 \langle \sigma v \rangle_{dd2}(0.82\eta_{He}) + \\ n_D n_3 \langle \sigma v \rangle_{dhe3}(3.7\eta_\alpha + 14.7\eta_{P14}) + n_D n_T \langle \sigma v \rangle_{dt}(3.5\eta_\alpha) + \\ n_T^2 \langle \sigma v \rangle_{tt}(1.26\eta_\alpha)] \times 1.6 \times 10^{-13}$$

The ohmic heating power density is:

$$P_{oh} = [C_{oh}\gamma_{NC}(I_p/\kappa a^2)^2/t_{10}^{3/2}]/vol$$

where

$$C_{oh} \approx 9.33 \times 10^{-5} Z_{eff} [(1 + \alpha_n)/(1 + \alpha_n + \alpha_T)]^{3/2} (1 + 3\alpha_T/2)$$

and

$$\gamma_{NC} = 4.3 - 0.6A$$

is a neoclassical resistivity enhancement factor (ITER definition) [35]. Since ohmic heating at thermonuclear temperatures is a very slow process and there is no loop voltage for steady-state operation,  $P_{oh}$  for steady-state operation is negligible.

The auxiliary power density is a function of the injected power to the ions and electrons required for current drive and plasma heating. Neutral beam injection is used as the default method for current drive, so  $P_{aux}$  is a function of the neutral beam power required for noninductive current drive. The current drive subroutine in STORAC determines the neutral beam current drive efficiency, coulomb logarithm for ion-ion collisions, and the stopping cross-section for a hydrogen beam in a fusion plasma. The original equations used in STORAC calculate the neutral beam efficiency using modified fitting functions from the ITER neutral beam model [35]. These were further modified for a D- $^3\text{He}$  plasma background by replacing tritium with  $^3\text{He}$  where appropriate. The original  $T_{10}$  scalings ( $T_{10} = [T]/10\text{keV}$ ) were retained, which may not be appropriate for the higher operating temperatures of a

D-<sup>3</sup>He plasma. Although the neutral beam model is somewhat speculative, it is still useful for determining auxiliary power requirements and their estimated costs.

The conductive and convective losses (transport losses) are calculated using global energy confinement scalings. These scalings are usually empirical, and predict the global energy confinement time ( $\tau_E$ ) as a function of device parameters. The power density of the transport losses is

$$P_{con} = \frac{W_{th}}{\tau_E} = \frac{2.404 \times 10^{-22} (\langle n_e T_e \rangle + \langle n_i T_i \rangle)}{\tau_E} \times Vol$$

where  $W_{th}$  is the plasma thermal energy content. For a pure homogeneous plasma, this is simply  $W_{th} = 3nKT \times Vol$ .

The 1990 ITER H-mode power scaling was assumed for this study. It is

$$\tau_E = 0.64 f_L I_P^{0.87} P_{tot}^{-0.5} R_0^{1.82} a^{0.12} \kappa^{0.35} n_{20}^{0.09} B_0^{0.15} A_i^{0.5}$$

where  $P_{tot}$  is the total power injected into the plasma from outside including all heating and current drive methods and  $A_i$  is the average atomic mass number of the plasma ions. The parameter  $f_L$ , or H-factor, is a confinement time enhancement factor relative to L-mode. Improved confinement is observed particularly in machines with a divertor when the power input exceeds a certain threshold value, with  $1 < f_L < 4$  representing a reasonable range of values. At the end of each run, STORAC calculates  $f_L$  required to maintain power balance.

The radiation power term includes bremsstrahlung and synchrotron radiation calculated for the core and edge plasma. Only the core radiation power loss is included in the plasma power balance. The edge radiation is subtracted from the power flow to the divertor region. Bremsstrahlung (or braking) radiation in fusion plasmas is due to collisions between a Maxwellian sea of electrons with ions of charge  $Z_i$ . The electron-electron and electron-ion bremsstrahlung local power density given by [7] is

$$P_{br} = 5.355 \times 10^{-43} n_e^2 Z_{eff} T_e^{1/2} [1 + 1.55 \times 10^{-3} T_e + 7.15 \times 10^{-6} T_e^2]$$

$$+0.071Z_{eff}^2/T_e^{1/2} + 0.00414T_e/Z_{eff}]$$

which incorporates first-order e-i relativistic and spin corrections, e-e emission (non-relativistic), and a Born correction [7].  $Z_{eff}$  is the effective charge of the plasma ions, where  $Z_{eff} = \sum_j (n_j Z_j^2 / n_e)$ . The edge radiation power includes separate calculations for specified impurity density fractions and an assumption of coronal equilibrium. Synchrotron (or cyclotron) radiation is due to the acceleration of a charged particle moving perpendicular to a magnetic field as it executes a gyro-orbit, which results in emission of electromagnetic radiation. The synchrotron global power density given by [7] is

$$P_{sy} = 6.214 \times 10^{-23} n_e T_e B_0^2 \Phi_T$$

where the assumed Trubnikov absorption correction is

$$\Phi_T = \frac{5.198 \times 10^{-3}}{\Lambda^{1/2}} T_e^{1.5} \left( 1 + \frac{22.61}{AT_e^{1/2}} \right)^{1/2} (1 - R_{sy})^{1/2}$$

$$\Lambda^{1/2} = 7.78 \times 10^{-9} \left( \frac{n_e a}{B_0} \right)^{1/2}$$

The wall reflectivity  $R_{sy}$  is assumed to be 0.9, accounting for wall deterioration and penetrations of a smooth metallic wall. Corrections for plasma diamagnetism are approximated by substituting  $B_0(1 - \beta)^{1/2}$  for the vacuum field  $B_0$ . Technically, this diamagnetic correction is inappropriate when the plasma displays paramagnetic behavior, but synchrotron radiation is expected to be negligible at high beta regardless. The total radiation power is then the sum of the bremsstrahlung and synchrotron radiation terms.

If a separate power balance for ions and electrons is used, then the equilibration power between ions and electrons is

$$P_{ie} = 2.4 \times 10^{-41} C_{ie} \ln \Lambda_{ie} n_e^2 Z_{eff} \frac{(T_i - T_e)}{T_e^{1.5}}$$

where

$$C_{ie} = \frac{(1 + \alpha_n)^2}{(2\alpha_n - 0.5\alpha_T + 1)(1 + \alpha_T)^{1/2}}$$



is a volume averaged profile factor. Of course, if  $T_i = T_e$ , then  $P_{ie} = 0$ . An increase in the ratio of  $T_i/T_e$  will lead in most cases to increased fusion reaction power compared to the radiation power loss [7]. This potential enhancement of plasma performance, and the physics factors affecting the temperature ratio, would be worth investigating in future studies.

## APPENDIX B

### Reference Cases ST-1B and ST-2B

The reference cases used for this study have been designated ST-1B and ST-2B, respectively. Both cases assume an edge safety factor  $q_\psi = 5$ , which is a compromise between the physics advantages of high- $q$  operation and the engineering advantages of low- $q$  operation, as discussed in Chapter 3. The parametric investigation of  $\epsilon\beta_p$  values established a linkage between the 1st and 2nd stability regimes, allowing further parametric investigations to be made based on just the ST-2B reference case. The anticipated effects of specific parameter variations on reactor performance relative to either reference case are expected to be comparable.

Below is a brief review of the assumptions adopted for the ST-1B and ST-2B reference cases, as discussed in Chapter 2:

- Aspect ratio,  $R_0/a \geq 1.2$
- Plasma elongation,  $\kappa_e = 2.1(1.0 + 0.44\epsilon^{2.1})$
- Plasma triangularity,  $\delta_X = 0.53(1.0 + 0.77\epsilon^{3.0})$
- $\epsilon\beta_p = 0.6$  for ST-1B, 1.0 for ST-2B
- Central safety factor  $q(0)=1.0$  for ST-1B, 2.0 for ST-2B
- Temperature profile factor,  $\alpha_T = 1.0$
- Density profile factor,  $\alpha_n = 0.5$
- Effective fuel ratio,  $n_3/n_D = 1.0$
- Confinement time ratio,  $\tau_p/\tau_E = 3.0$
- 1990 ITER H-mode power scaling for  $\tau_E$
- Bootstrap current fraction,  $I_{bs}/I_P = 0.90$
- Centerpost current density,  $J_{cp} \leq 75 \text{ MA/m}^2$
- Thermal conversion efficiency,  $\eta_{th} = 0.40$
- Direct energy conversion efficiency,  $\eta_{dec} = 0.50$
- Net electric power output, 1000 MWe
- Plant operating life, 30 years
- Plant capacity factor, 0.75
- Level of safety assurance, LSA = 2

Parameter	ST-1B	ST-2B
Error of Constraint Equations:		
Beta	-1.58e-07	2.99e-06
Global power balance	-2.02e-07	3.79e-06
Beam ion density	1.84e-07	-3.92e-06
Field at coil	-4.06e-12	8.83e-09
Radial build	-7.11e-15	-2.83e-09
Centerpost temperature	2.00e-07	-1.32e-06
Particle confinement time	-2.47e-06	4.65e-05
Density limit	-2.62e-07	4.40e-06
Troyon beta limit	4.26e-14	1.42e-14
$\epsilon\beta_p$ limit	-8.53e-14	1.85e-13
Beam energy	-3.61e-09	-1.04e-08
Net electric power	2.06e-07	-2.94e-06
Average error of constraints	2.52e-06	4.73e-05
Plasma Geometry Parameters:		
Major radius, $R_0$ (m)	2.154	1.912
Minor radius, $a$ (m)	1.795	1.594
Aspect ratio, $A = R_0/a$	1.200	1.200
Elongation, X-point $\kappa_X$	2.665	2.665
Elongation, 95% surface $\kappa_{95}$	2.386	2.386
Triangularity, X-point $\delta_X$	0.766	0.766
Triangularity, 95% surface $\delta_{95}$	0.501	0.501
Plasma surface area, $S_P(m^2)$	247.2	194.9
Plasma volume, $V_P(m^3)$	297.4	208.2
Current and Field Parameters:		
Plasma current, $I_P$ (MA)	112.404	84.185
On-axis toroidal magnetic field, $B_0$ (T)	1.955	1.649
Average poloidal magnetic field, $B_p$ (T)	6.487	5.472
Total magnetic field, $B$ (T)	6.775	5.715
On-axis safety factor, $q_0$	1.000	2.000
Edge safety factor, $q_\psi$	5.000	5.000
95% surface safety factor, $q_{95}$	2.218	2.218

Parameter	ST-1B	ST-2B
Beta Parameters:		
Plasma beta, $\beta$	0.660	1.100
Poloidal beta, $\beta_p$	0.720	1.200
Fast particle beta, $\beta_{fast}$	9.52e-02	1.74e-01
Neutral beam beta, $\beta_{beam}$	6.32e-03	8.12e-03
Troyon coefficient, $g_f$	2.061	3.435
$\epsilon\beta_p$	0.600	1.000
Beta limit, $\beta_f$ and $\beta_s$	1.057	1.100
Temperature and Density Parameters:		
Temperature profile factor, $\alpha_T$	1.000	1.000
Density profile factor, $\alpha_n$	0.500	0.500
Electron temperature, $\langle T_e \rangle$ (keV)	59.877	62.937
Ion temperature, $\langle T_i \rangle$ (keV)	59.877	62.937
Electron n-temperature, $[T_e]$ (keV)	71.852	75.524
Electron density, $\langle n_e \rangle (10^{20} m^{-3})$	5.086	5.640
Ion density, $\langle n_i \rangle (10^{20} m^{-3})$	3.776	4.223
Deuterium density, $\langle n_D \rangle (10^{20} m^{-3})$	1.526	1.692
Helium-3 density, $\langle n_3 \rangle (10^{20} m^{-3})$	1.526	1.692
Tritium density, $\langle n_T \rangle (10^{18} m^{-3})$	1.433	1.682
High-Z impurity density, $\langle n_Z \rangle (10^{18} m^{-3})$	5.106	5.657
Alpha particle density, $\langle n_\alpha \rangle (10^{20} m^{-3})$	0.344	0.401
Proton density, $\langle n_P \rangle (10^{20} m^{-3})$	0.312	0.363
Effective charge, $Z_{eff}$	2.228	2.244
Mass-weighted $Z_{eff}$	0.711	0.718
Deuterium fuel rate, $S_D (10^{20} s^{-1} m^{-3})$	0.183	0.229
Helium-3 fuel rate, $S_3 (10^{20} s^{-1} m^{-3})$	0.174	0.217
Fusion Power Parameters:		
Charged fusion power, $P_F$ (MW)	2585	2348
Beam fusion power, $P_{F-Beam}$ (MW)	8.970	6.196
Neutron fusion power, $P_n$ (MW)	165.4	150.1
Neutron wall load ( $MW/m^2$ )	6.535	0.616
Fraction of power to electrons	0.306	0.287
Fraction of power to ions	0.694	0.713

Parameter	ST-1B	ST-2B
Plasma Power Balance Parameters:		
Ohmic heating power, $P_{oh}$ (W)	0.881	0.520
Bremsstrahlung radiation power, $P_{br}$ (MW)	1329	1191
Synchrotron radiation power, $P_{sy}$ (MW)	4.684	.0001
Wall reflectivity, $R_{sy}$	0.900	0.900
Edge radiation power, $P_{Line}$ (MW)	49.69	39.96
Electron transport power, $P_{tr,e}$ (MW)	748.8	682.1
Ion transport power, $P_{tr,i}$ (MW)	556.0	510.8
Injected power to electrons, $P_{inj-e}$ (MW)	26.72	17.61
Injected power to ions, $P_{inj-i}$ (MW)	26.12	18.48
Power to divertor, $P_{div}$	1255	1153
Divertor heat load ( $MW/m^2$ )	1.880	2.180
Divertor life (years)	2.120	1.830
ITER-H90P confinement-time multiplier, $\tau$	2.582	3.633
Global confinement time, $\tau_E$ (s)	3.487	3.124
Particle confinement time, $\tau_p$ (s)	10.46	9.371
Lawson parameter, $n\tau_E(10^{21}s/m^3)$	1.774	1.762
NBI Current-Drive Parameters:		
Steady-state power required (MW)	52.84	36.09
Heating power (MW)	3.375	1.002
Plasma Q-value, $Q_P = P_F/P_{CD}$	48.92	65.06
Bootstrap current fraction, $I_{bs}/I_P$	0.900	0.900
Non-inductive current fraction	0.100	0.100
Neutral beam efficiency, $\eta_{beam}$ (A/W)	0.227	0.240
Neutral beam gamma, $\gamma(10^{20}A/W - m^2)$	2.489	2.587
Neutral beam power, $P_{beam}$ (MW)	52.85	36.09
Neutral beam energy, $E_{beam}$ (MeV)	5.026	4.995
Neutral beam current, $I_{beam}$ (A)	10.51	7.226
Beam energy fraction to ions	0.494	0.512
Neutral beam shine through	2.48e-3	2.48e-3
Beam decay lengths to $R_0$	3.000	3.000

Parameter	ST-1B	ST-2B
Radial Build Parameters (m):		
Device centerline	0.000	0.000
Centerpost	0.299	0.259
First wall - inboard	0.319	0.279
Scrape off layer - inboard	0.359	0.319
Plasma centerline, $R_0$	2.154	1.912
Plasma edge	3.948	3.506
Scrape off layer - outboard	3.988	3.546
First wall - outboard	4.008	3.566
Shield - outboard	4.508	4.066
Gap	5.043	4.481
TF coil	5.342	4.740
Vertical Build Parameters (m):		
Plasma midplane	0.000	0.000
Plasma top	4.783	4.247
Scrape off layer	7.924	7.036
Divertor structure	8.024	7.136
Shield	8.524	7.636
Gap	8.687	7.799
TF coil	8.986	8.058
Port requirement for beams (m)	0.574	0.534
Port width (m)	1.592	1.439
Centerpost Parameters:		
Centerpost current density ( $MA/m^2$ )	75.00	75.00
Average resistivity ( $10^{-8}$ Ohm-m)	2.364	2.358
Resistive power loss (MW)	230.2	154.1
Nuclear heating (MW)	74.51	64.73
Centerpost coolant fraction	0.106	0.105
Coolant channel diameter (cm)	1.224	1.190
Coolant channel length (m)	17.37	15.60
Coolant flow speed (m/s)	20.00	20.00
Number of coolant tubes	800.3	628.8
Inlet coolant temperature ( $^{\circ}C$ )	40.00	40.00

Parameter	ST-1B	ST-2B
Centerpost Parameters, continued:		
Coolant temperature rise ( $^{\circ}\text{C}$ )	123.9	120.0
Average centerpost temperature ( $^{\circ}\text{C}$ )	116.6	115.2
Peak centerpost temperature ( $^{\circ}\text{C}$ )	180.1	176.7
Coolant inlet pressure (MPa)	4.801	4.451
Coolant pressure drop (MPa)	3.712	3.448
Pump power required (MW)	8.738	6.024
Centerpost volume ( $\text{m}^3$ )	15.38	10.35
Weight of centerpost ( $10^6$ kg)	0.122	0.083
TF Coil Parameters:		
Number of TF coil legs	16	16
Outer leg current density ( $\text{MA}/\text{m}^2$ )	4.369	4.799
Coil resistance ( $10^{-6}$ Ohm)	2.391	3.123
Resistive power loss (MW)	66.2	48.6
TF coil current (MA)	21.06	15.77
Peak field at TF coil, $B_c$ (T)	14.09	12.19
Ripple at plasma edge (%)	1.50	1.50
Stored energy per coil (GJ)	0.136	0.069
Vertical force - inner leg (MN)	4.307	2.438
Radial stress (MPa)	118.0	88.25
Coil volume ( $\text{m}^3$ )	8.679	5.271
Weight of outer legs ( $10^6$ kg)	0.989	0.601
TF Power Supply Parameters:		
Bus current density ( $\text{MA}/\text{m}^2$ )	1.250	1.250
Maximum impedance (Ohm)	4.207e-05	5.507e-05
Bus resistance (Ohm)	3.799e-06	5.073e-06
Bus length - all coils (m)	160.0	160.0
Resistive power loss (MW)	6.6	4.9
Peak voltage/coil (V)	3.46	3.39
Peak power (MW)	30.30	20.75

Parameter	ST-1B	ST-2B
PF Coil Parameters:		
Number of PF coil groups	2	2
Circuit 1,2 radius from $R_0$ (m)	0.78	0.69
Circuit 1,2 distance from midplane (m)	$\pm 8.02$	$\pm 7.14$
Circuit 1,2 field at coil (T)	27.5	23.5
Circuit 1,2 current (MA)	45.14	33.81
Circuit 1,2 current density ( $MA/m^2$ )	5.624	0.673
Circuit 3,4 radius from $R_0$ (m)	5.84	5.24
Circuit 3,4 distance from midplane (m)	$\pm 2.15$	$\pm 1.91$
Circuit 3,4 field at coil (T)	27.5	23.5
Circuit 3,4 current (MA)	-44.96	-33.67
Circuit 3,4 current density ( $MA/m^2$ )	3.949	3.772
Bus length - all circuits (m)	314.5	310.6
Resistive power loss (MW)	0.31	0.31
Maximum PF coil voltage (kV)	5.0	5.0
Outer Shield Parameters:		
Shield thickness (m)	0.50	0.50
Shield volume ( $m^3$ )	190.8	154.9
Weight of shield ( $10^6$ kg)	1.116	0.906
Nuclear heating (MW)	1523	1366
Reactor Power Parameters:		
Charged fusion power (MW)	2585	2348
Neutron fusion power (MW)	165	150
Neutron power multiplier	1.270	1.270
Injector wall plug power (MW)	105.7	72.2
Vacuum heat (MW)	0.50	0.50
Tritium process heat (MW)	1.00	1.00
TF coil resistive power (MW)	303.0	207.5
Coolant pump power (MW)	8.7	6.0
Power loss to holes (MW)	224.8	201.2
Primary heat (MW)	2151	1942
Secondary heat (MW)	59.1	45.2



Parameter	ST-1B	ST-2B
Reactor Parameters, continued:		
Thermal conversion efficiency (%)	0.40	0.40
DEC conversion efficiency (%)	0.50	0.50
Gross electric power (MWe)	1488	1353
Net electric power output (MWe)	1000	1000
BOP recirculating power fraction	0.047	0.050
Total recirculating power fraction	0.330	0.260
Cost of electricity (mill/kWh)	88.90	73.68
Cost Accounts Output (\$M):		
211 Site and facilities	10.00	10.00
212 Reactor building	66.84	59.88
213 Other buildings	90.78	85.49
21 Total	167.62	155.37
2211 First wall	33.31	26.41
2213 Shield	59.16	48.04
2215 Divertor/DEC	48.57	38.30
221 Total	420.27	238.82
2221 TF magnet assemblies	112.90	69.76
2222 PF magnet assemblies	285.13	160.81
222 Total	398.02	230.57
223 Total, current drive system	303.83	220.07
224 Total, vacuum system	73.94	69.42
2251 TF power supplies	178.02	134.12
2252 PF power supplies	32.33	25.93
225 Total	210.35	160.05
226 Total, heat transport system	199.04	180.91
227 Total, fuel handling system	259.22	251.43
228 Total, instrumentation and control	182.88	177.38
229 Total, maintenance equipment	151.35	146.80
22 Total	2198.92	1675.43
23 Turbine plant equipment	391.31	359.60
24 Electric plant equipment	116.94	109.44
25 Miscellaneous plant equipment	61.96	57.98
26 Heat rejection system	84.16	76.01

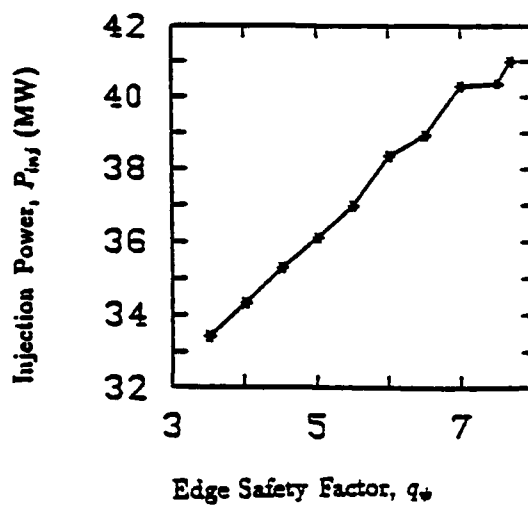
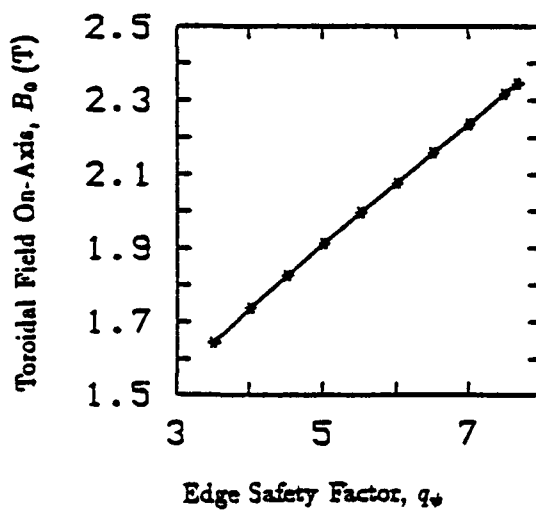
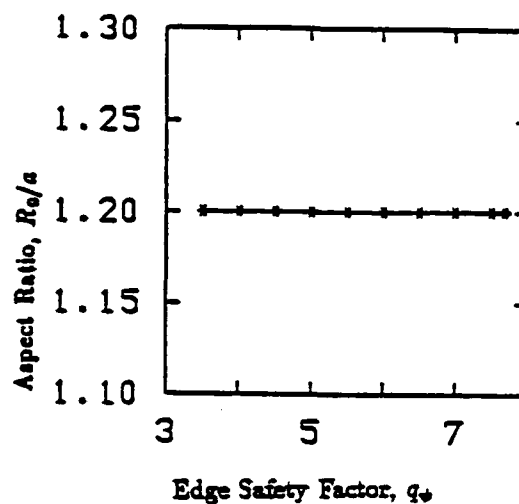
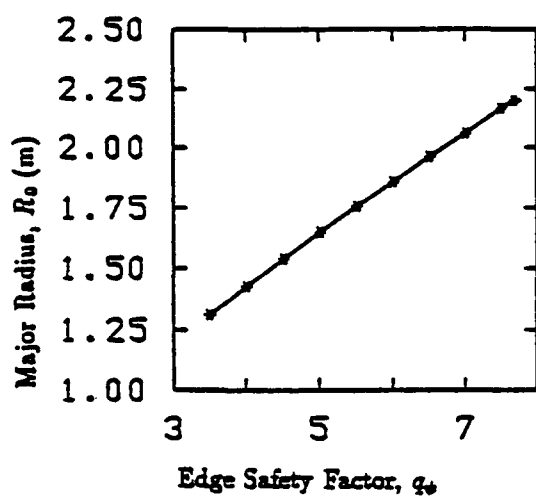
Parameter	ST-1B	ST-2B
Cost Accounts Output, continued (\$M):		
2 Total plant direct cost	3020.89	2433.84
Indirect costs	847.66	682.94
Contingency costs	669.26	539.20
Interest during construction	788.56	635.32
Total capital cost	5326.37	4291.30
Miscellaneous Parameters:		
Intercoil structure mass ( $10^6$ kg)	1.298	0.650
PF coil support mass ( $10^6$ kg)	7.679	3.396
General support mass ( $10^6$ kg)	0.030	0.021
Total structure mass ( $10^6$ kg)	9.007	4.067
Reactor building volume ( $10^3 m^3$ )	73.98	61.97

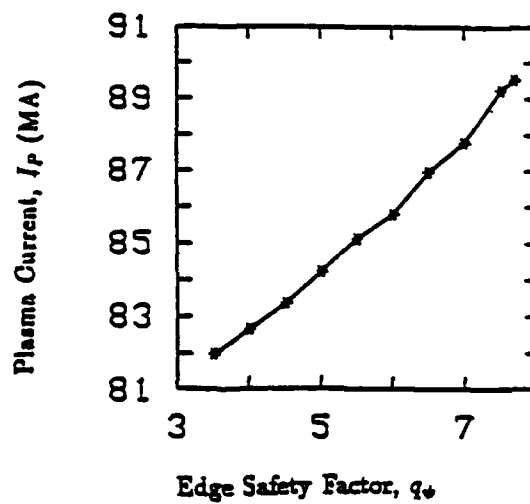
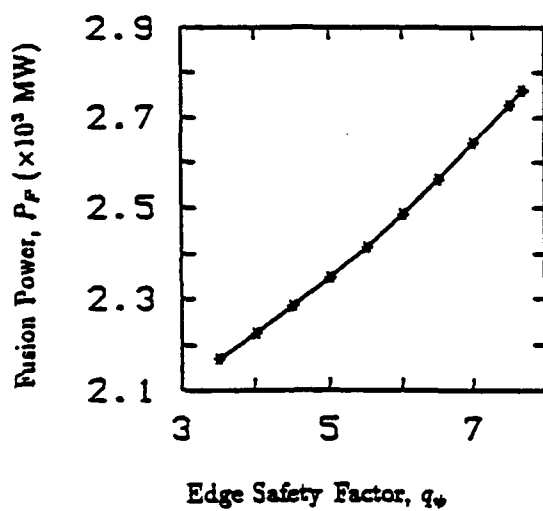
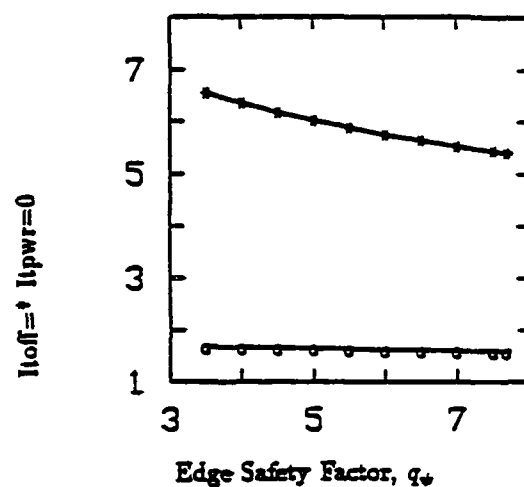
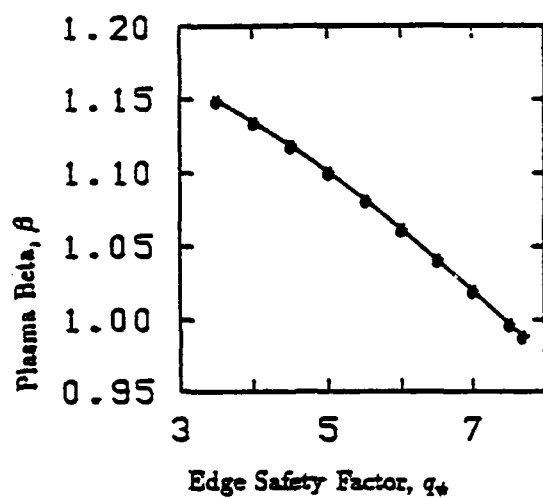
## APPENDIX C

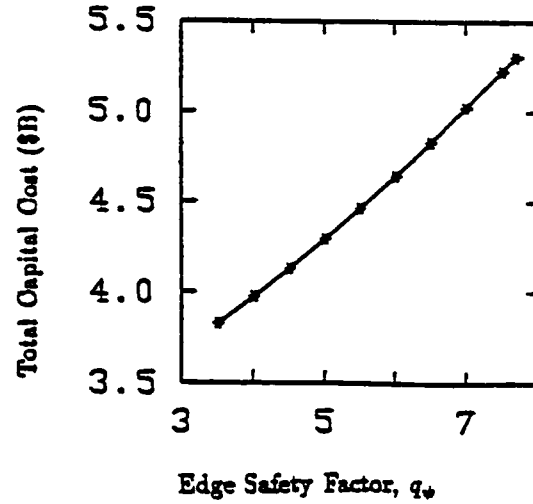
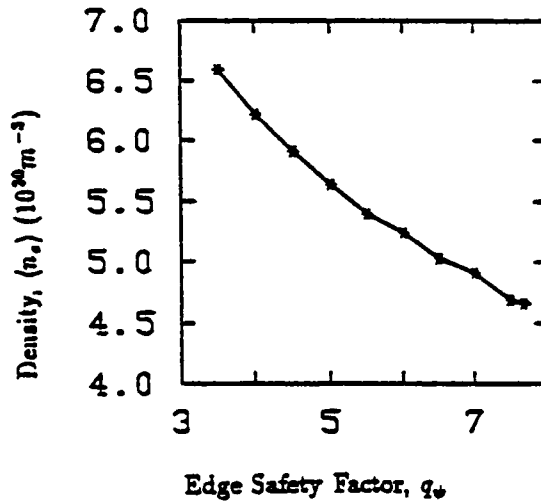
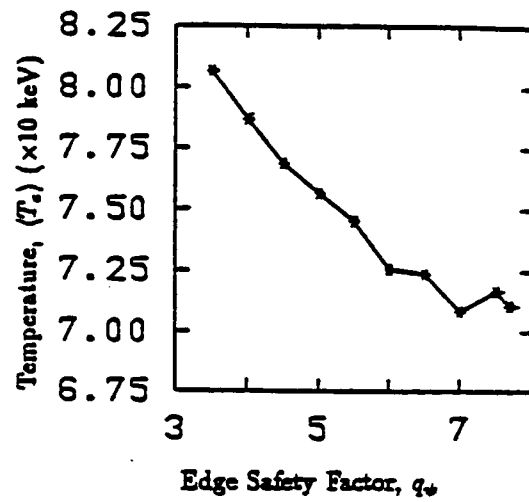
### Edge Safety Factor Scan of ST-2A

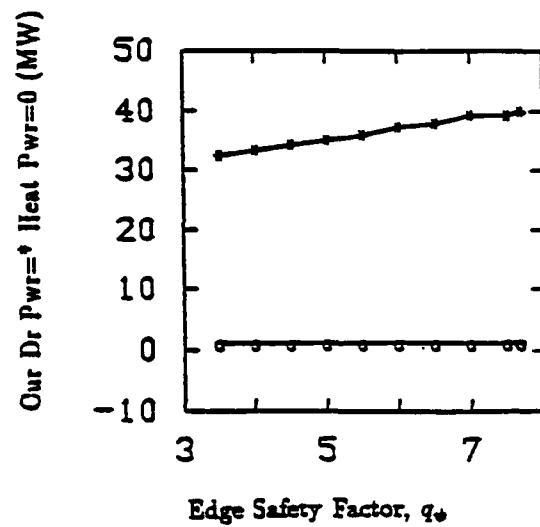
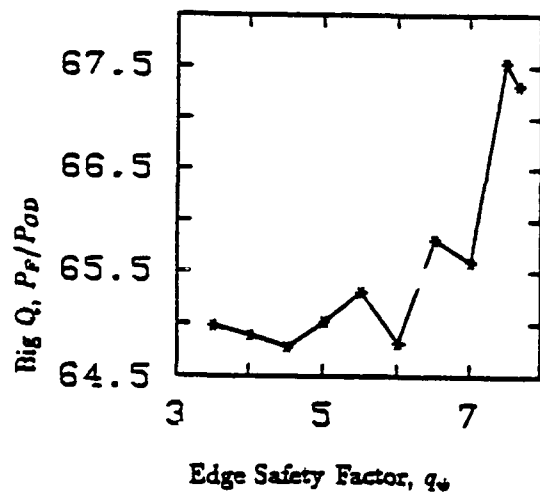
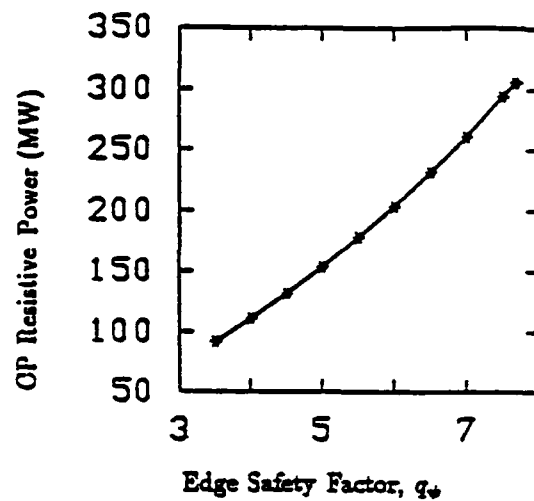
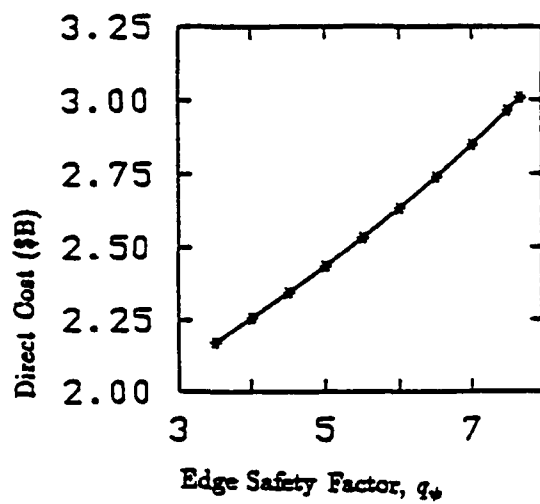
This appendix contains all the output plots generated by STORAC for the edge safety factor scan of the ST-2A 2nd stability reference case as  $q_\psi$  was varied from 7.68 to 3.5. These are representative of the plots generated from the plot files of every STORAC run which uses the scan option. The scan routine stores in an array many of the output quantities calculated in the optimization process, and prints them into a separate file which may be read by a plotting routine.

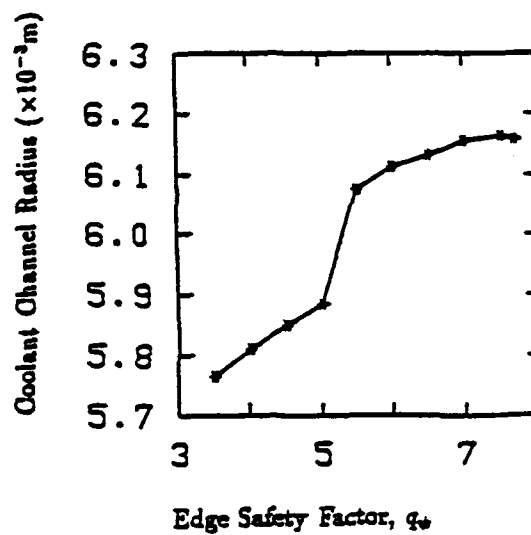
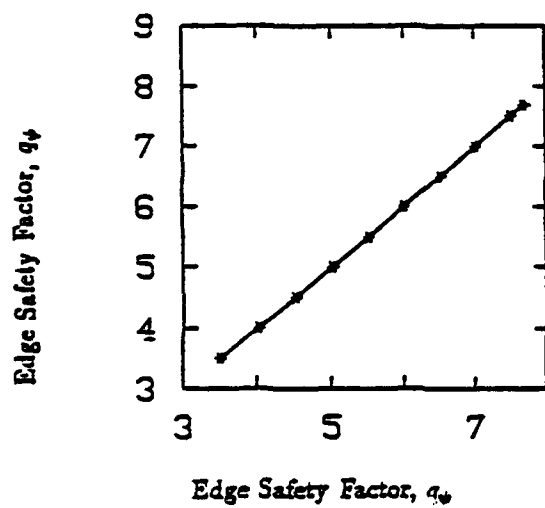
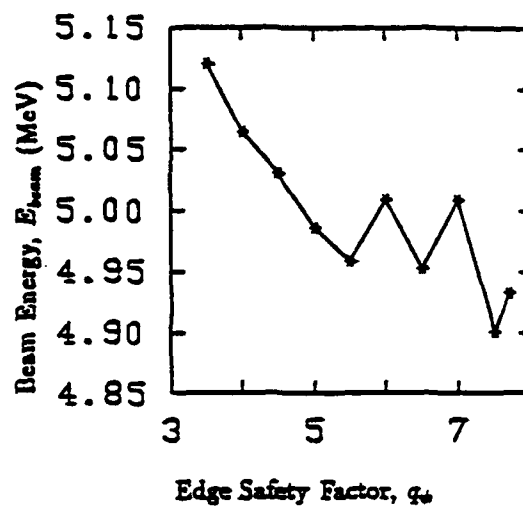
Systems codes are often used to perform scans in order to determine the sensitivity of results to different input assumptions. STORAC is capable of performing up to 10 successive calculations for a prescribed variable, where each calculation iterates from the previous solution. The "smoothness" of a given plot depends on the residual error of the previous solution and the step-size of the scan variable. If either the residual error or the step-size is too large, successive iterations can produce poor solutions or fail to execute. If the poor solution has a residual error in the range of  $10^{-2} - 10^{-3}$ , then successive iterations could still produce successful optimizations rather than get worse. For example, the "dent" in the curve in Figure 3.18 at  $J_{cp} = 75 MA/m^2$  (ironically, the assumed value for the reference cases) shows how the scan can recover from a bad iteration and produce an otherwise smooth curve.



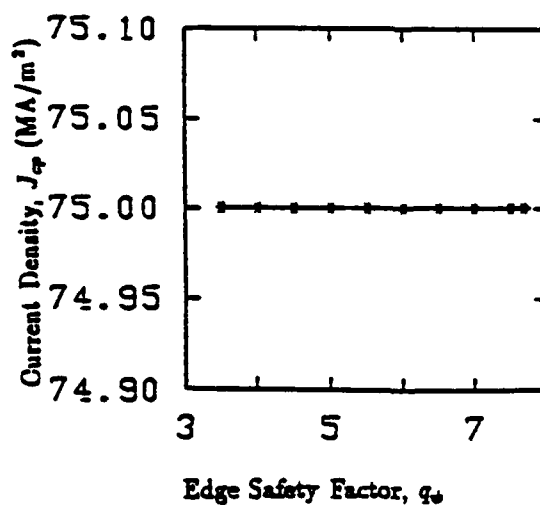
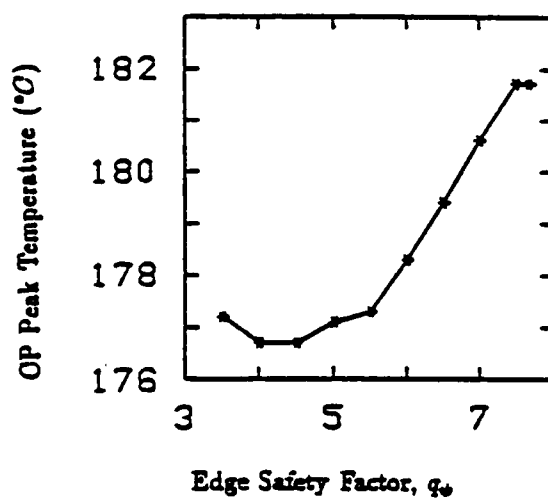
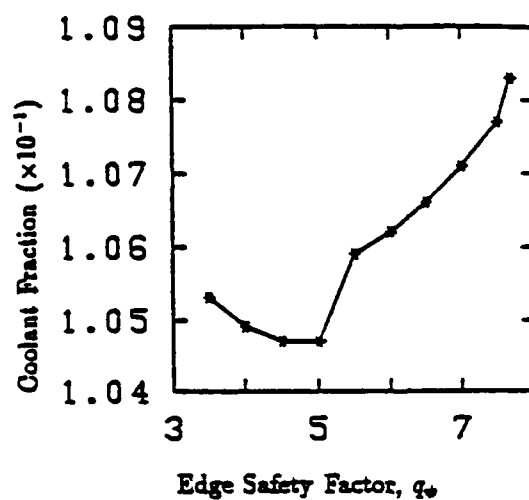
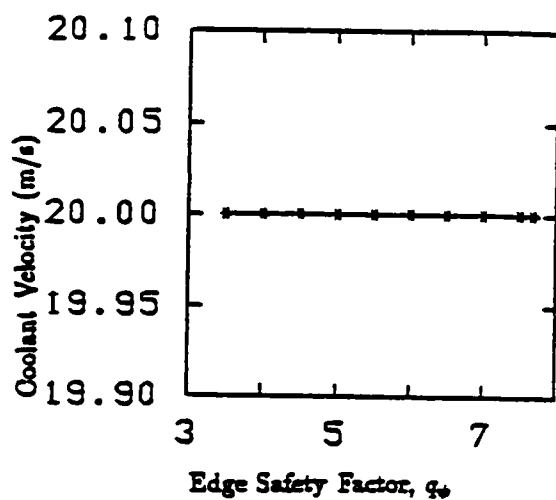


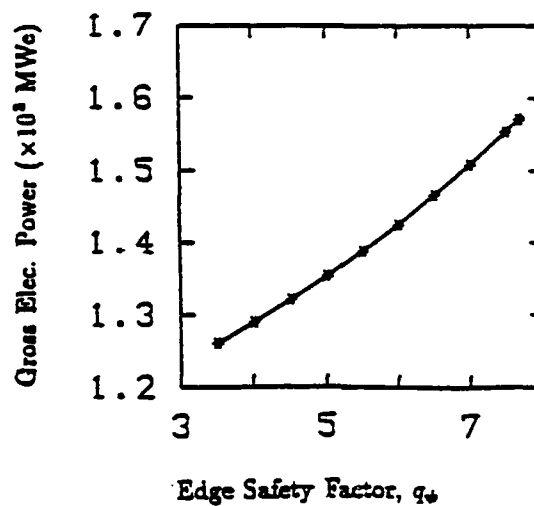
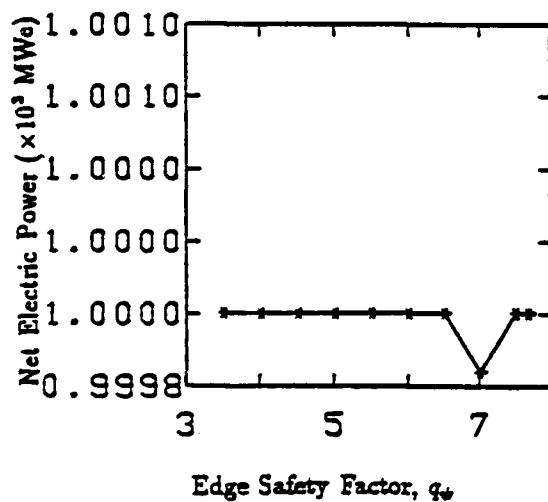
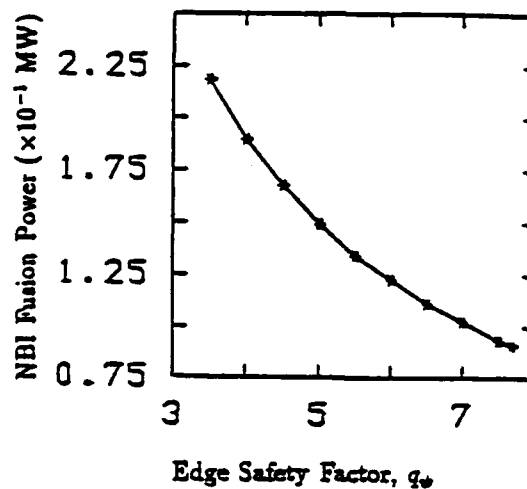
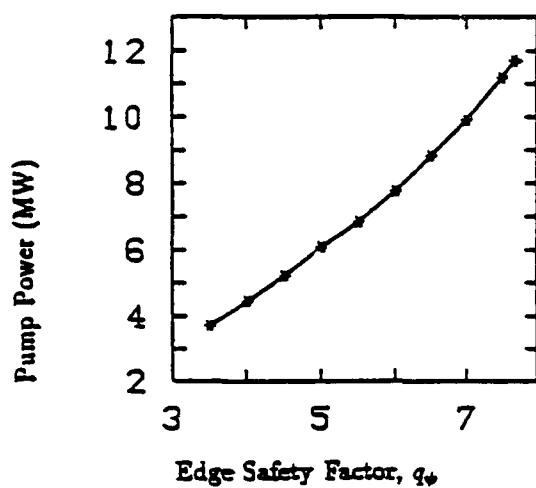


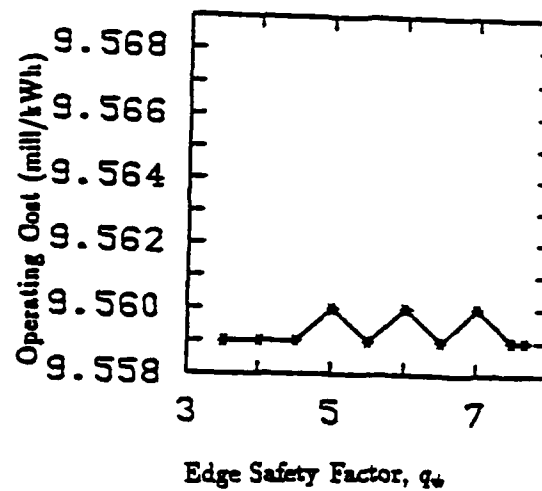
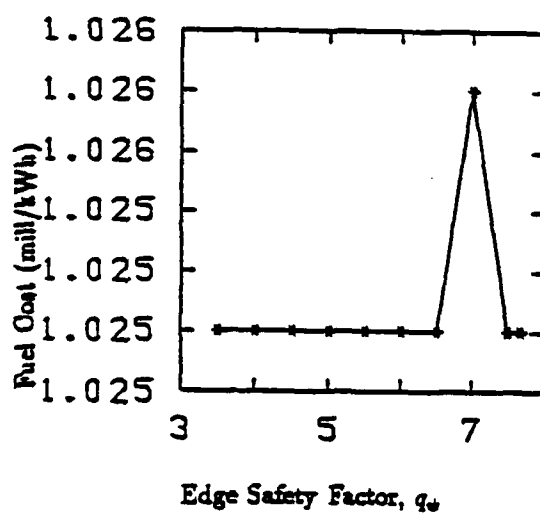
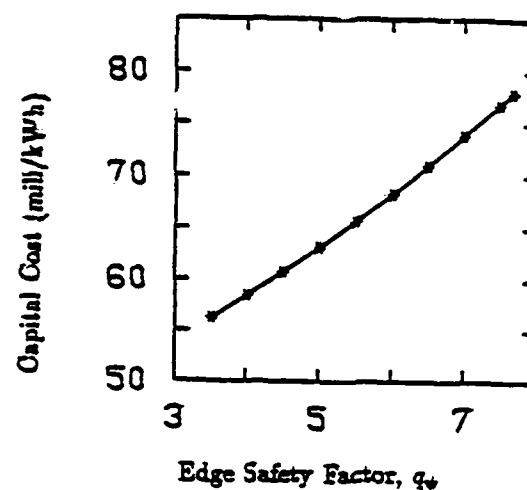
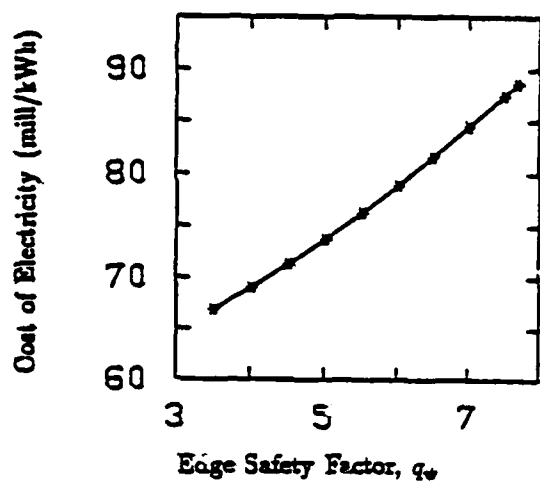


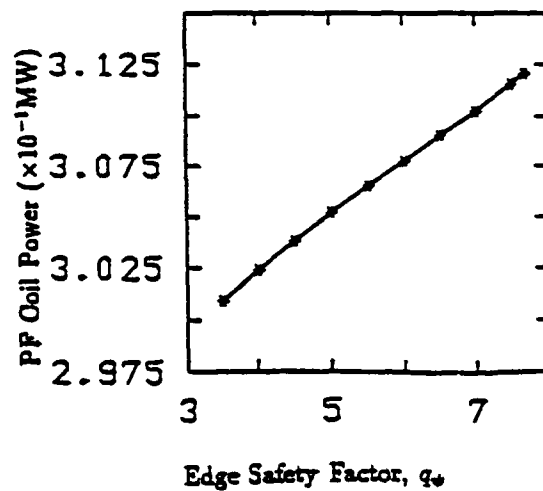
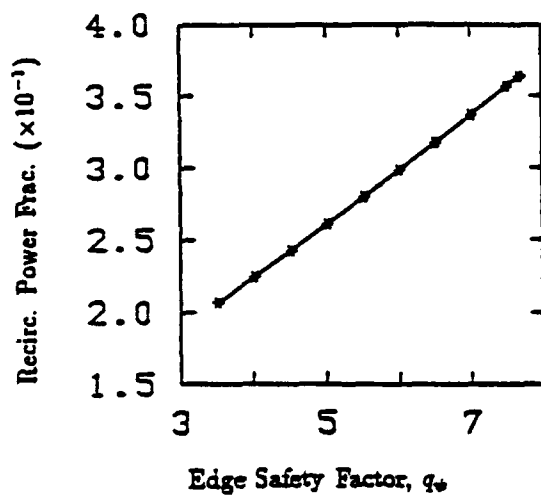
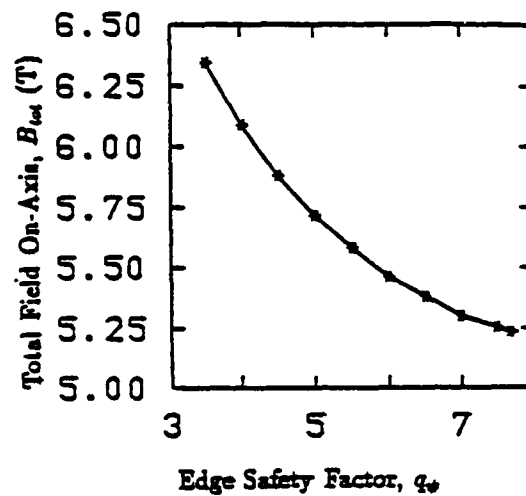
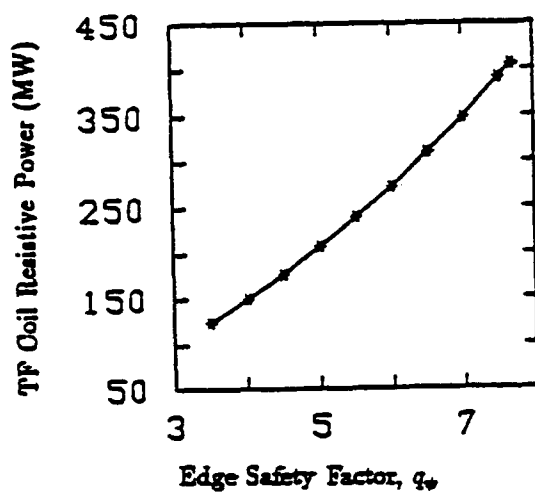


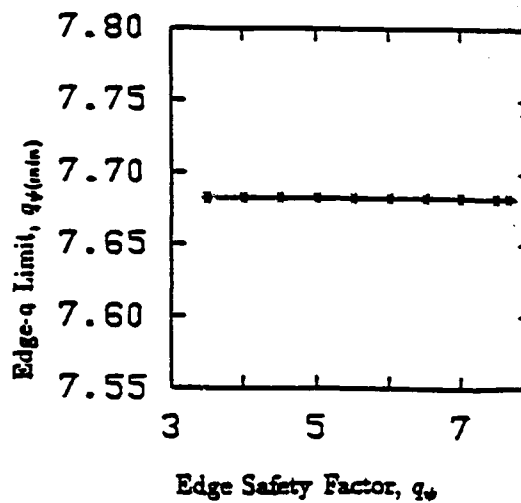
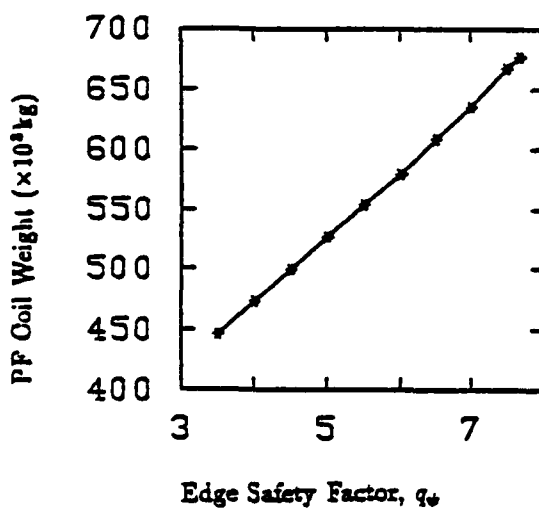
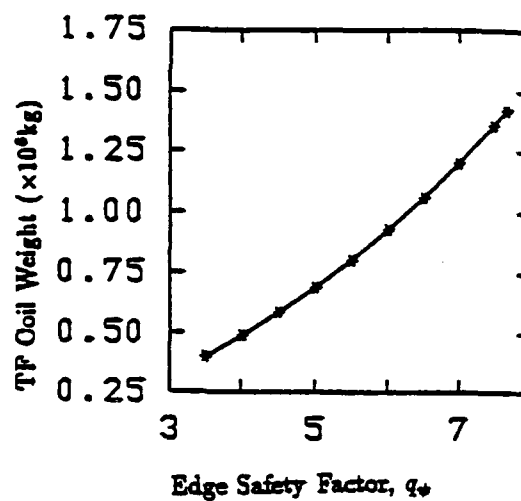
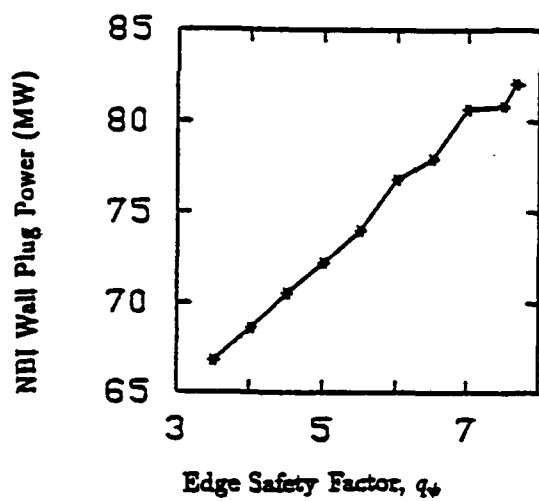


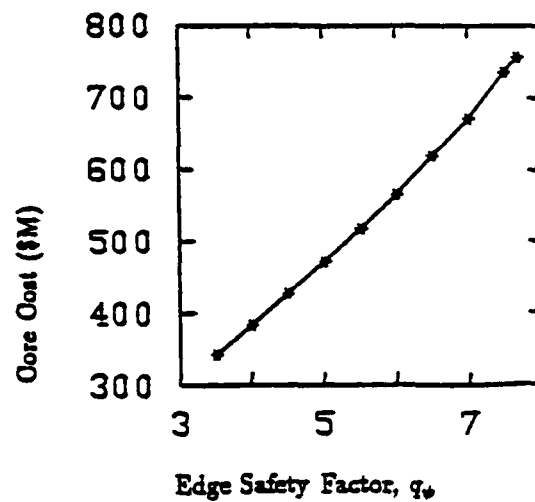
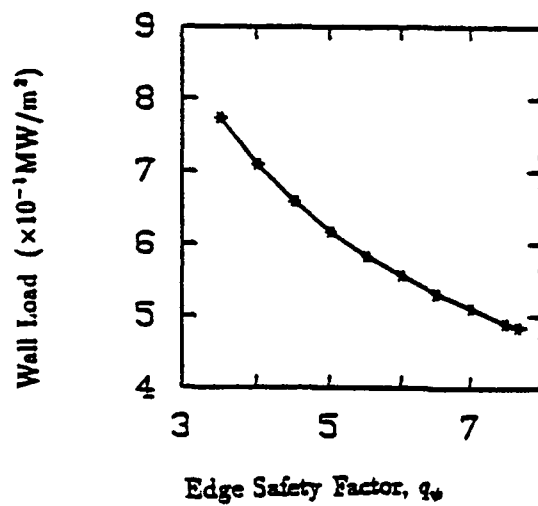
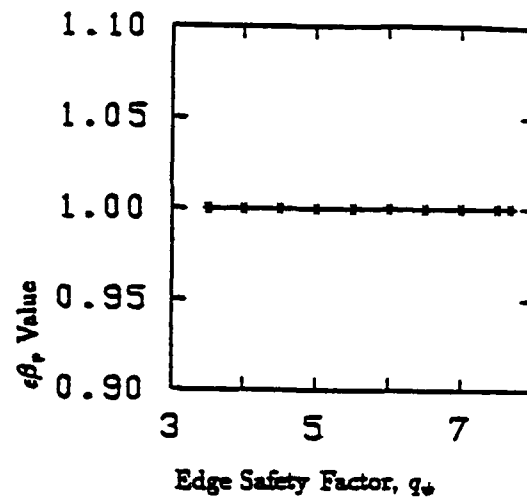
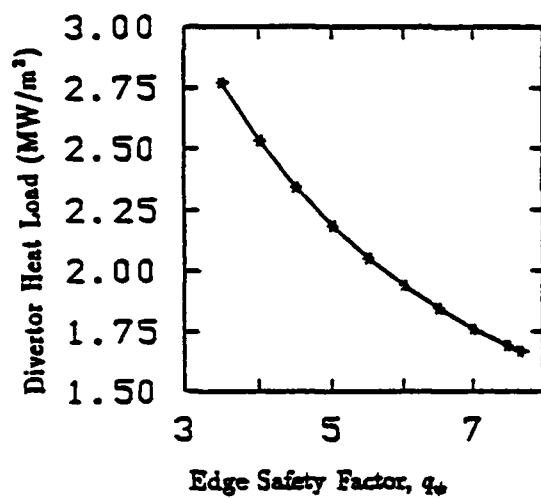












## LITERATURE CITED

- [1] J.P. Holdren et al. "Exploring the Competitive Potential of Magnetic Fusion Energy: The Interaction of Economics with Safety and Environmental Characteristics". *Fusion Technology*, 13:7, 1988.
- [2] R.W. Conn et al. "Economic, Safety and Environmental Prospects of Fusion Reactors". *Nuclear Fusion*, 30:1919, 1990.
- [3] A.E.Dabiri. "An Overview of D-<sup>3</sup>He Fusion Reactors". *Nucl. Instr. and Meth.*, A271:71, 1988.
- [4] W. Kernbichler et al. "D-<sup>3</sup>He Fuel Cycles for Neutron Lean Reactors". *Fusion Technology*, 15:1142, 1989.
- [5] G.A. Emmert et al. "Possibilities for Breakeven and Ignition of D-<sup>3</sup>He Fusion Fuel in a Near Term Tokamak". *Nuclear Fusion*, 29:1427, 1989.
- [6] J.F. Santarius et al. "Energy Conversion Options for ARIES-III - A Conceptual D-<sup>3</sup>He Tokamak Reactor". In *IEEE 19th Symposium on Fusion Engineering*, Knoxville, TN, October 1989.
- [7] J.R. McNally, Jr. "Physics of Fusion Fuel Cycles". *Nuclear Technology/Fusion*, 2:9, 1982.
- [8] L.J. Wittenberg, J.F. Santarius, and G.L. Kulcinski. "Lunar Source of <sup>3</sup>He for Commercial Fusion Power". *Fusion Technology*, 10:167, 1986.
- [9] M. Kikuchi. "Steady State Tokamak Reactor Based on the Bootstrap Current". *Nuclear Fusion*, 30:265, 1990.
- [10] R.S. Devoto et al. "Projections for a Steady-State Tokamak Reactor Based on the International Thermonuclear Experimental Reactor". *Fusion Technology*, 19:251, 1991.
- [11] B.B. Kadomtsev, F.S. Troyon, and M.L. Watkins. "Tokamaks". *Nuclear Fusion*, 30:1675, 1990.
- [12] M.S. Chance, S.C. Jardin, and T.H. Stix. "Ballooning Mode Stability of Bean-Shaped Cross Sections for High Beta Tokamak Plasmas". *Physical Review Letters*, 51:1963, 1983.
- [13] Y-K.M. Peng. *Spherical Torus, Compact Fusion at Low Field*, ORNL/FEDC-84/7. Technical Report, Oak Ridge National Laboratory, 1985.

- [14] J.D. Galambos, D.J. Strickler, Y-K.M. Peng, and R.L. Reid. "Plasma Elongation Studies for ITER-Like Tokamaks". *Fusion Technology*, 15:483, 1989.
- [15] D.J. Strickler et al. *Equilibrium Modeling of the TFCX Poloidal Field Coil System, ORNL/FEDC-83/10*. Technical Report, Oak Ridge National Laboratory, 1984.
- [16] Y-K.M. Peng and D.J. Strickler. *Features of Spherical Torus Plasmas, ORNL/FEDC-85/6*. Technical Report, Oak Ridge National Laboratory, 1985.
- [17] Y-K.M. Peng et al. "Spherical Torus: An Approach to Compact Fusion at Low Field - Initial Ignition Assessments". *Fusion Technology*, 8:338, 1985.
- [18] Y-K.M. Peng and J.B. Hicks. "Engineering Feasibility of Tight Aspect Ratio Tokamak (Spherical Torus) Reactors". In *16th Symposium on Fusion Technology*, London, September 1990.
- [19] J.D. Galambos and Y-K.M. Peng. "Ignition and Burn Criteria for D-<sup>3</sup>He Tokamak and Spherical Torus Reactors". *Fusion Technology*, 19:31, 1991.
- [20] R.T.C. Smith et al. "START (Small Tight Aspect Ratio Tokamak)". In *16th Symposium on Fusion Technology*, London, September 1990.
- [21] A.Sykes et al. "First Results from the START Experiment". 1991. Draft Report.
- [22] "Quantifying the Concepts and the Potential of the Steady-State Spherical Tokamak (TST) and the Neutron Spherical Tokamak (NST)". 1990. Oak Ridge National Laboratory Proposal.
- [23] R.L. Reid et al. *ETR/ITER Systems Code, ORNL/FEDC-87/7*. Technical Report, Oak Ridge National Laboratory, 1988.
- [24] G.W. Shuy, A.E. Dabiri, and H. Gurol. "Conceptual Design of a Deuterium-<sup>3</sup>He Fueled Tandem Mirror Reactor Satellite/Breeder System". *Fusion Technology*, 9:459, 1986.
- [25] S. Thompson. "Systems Code Cost Accounting", FEDC-M-88-SE-004. 1988. Oak Ridge National Laboratory Memorandum.
- [26] R.L. Crane, K.E. Hillstrom, and M. Minkoff. "Solution of the General Nonlinear Programming Problem with Subroutine VMCON", ANL-80-64. Technical Report, Argonne National Laboratory, 1980.
- [27] Private communication with J.D. Galambos and Y-K.M. Peng, Oak Ridge National Laboratory.



- [28] O. Mitarai et al. "Saddle Point Ignition Condition for D-<sup>3</sup>He Tokamak Fusion Reactor". *Fusion Technology*, 19:234, 1991.
- [29] ARIES-III Parametric/Systems Calculations (Version 8.1, April 1991) obtained through private communication with C. Bathke, Los Alamos National Laboratory.
- [30] R.A. Krakowski. "Progress in Commercial Magnetic Fusion Energy Reactor Designs". *Fusion Technology*, 20:121, 1991.
- [31] W. Kramer. "Critical Safety Issues in the Design of Fusion Machines". In *16th Symposium on Fusion Technology*, London, September 1990.
- [32] J.F. Santarius et al. "A High Efficiency D-<sup>3</sup>He Tandem Mirror Fusion Reactor". In *IEEE 12th Symposium on Fusion Engineering*, Monterey, CA, October 1987.
- [33] V.K. Rohatgi and T. Vijayan. "Technical Issues in Fusion Reactors - A Review". *Fusion Technology*, 16:287, 1989.
- [34] E.E. Bloom. "Structural Materials for Fusion Reactors". *Nuclear Fusion*, 30:1879, 1990.
- [35] N.A. Uckan et al. *International Thermonuclear Experimental Reactor Design Information Document, ITER-TN-PH-0-5*. Technical Report, IAEA, Vienna, 1990.
- [36] J. Johner. "Thermonuclear Ignition in the Next-Generation Tokamaks". *Fusion Technology*, 19:515, 1991.
- [37] R.J. Bickerton, J.W. Conner, and J.B. Taylor. "Diffusion Driven Plasma Currents and Bootstrap Tokamak". *Nature of Physical Science*, 229:110, 1971.
- [38] K. Miyamoto. *Plasma Physics for Nuclear Fusion*, chapter 8. Massachusetts Institute of Technology, revised english language edition, 1989.
- [39] D.P. Stotler, R.J. Goldston, and The CIT Team. "Ignition Probabilities for Compact Ignition Tokamak Design Points". *Fusion Technology*, 20:7, 1991.
- [40] B. Coppi and L.E. Sugiyama. *Questions in Advanced Fuel Fusion, Report PTP-88/6*. Technical Report, Massachusetts Institute of Technology, 1988.
- [41] G.H. Miley, H. Towner, and N. Ivich. *Nucl. Eng. Report C000-2218-17*. Technical Report, U. of Illinois, 1974.